AFRL-SR-BL-TR-98

0220

REPORT DOCUMENTATION PAGE

Public reporting burden for this collection of information is estimated to average 1 hour per response gathering and maintaining the data needed, and completing and reviewing the collection of informati collection of information, including suggestions for reducing this burden, to Washington Headquarter Davis Highway, Suite 1204, Arlington, VA 22202-4302, and to the Office of Management and Budg

3

data sources, aspect of this 215 Jefferson 0503.

1. AGENCY USE ONLY *(Leave blank)*	2. REPORT DATE	3. REPORT TYPE AND DATES COVERED
		Final Technical 03/01/97 -08/31/97

4. TITLE AND SUBTITLE
Influence of Loading Frequency on the Fatigue Behavior of Fiber-Reinforced Ceramic Composites

5. FUNDING NUMBERS
F49620-95-1-0206

6. AUTHOR(S)
John W. Holmes

7. PERFORMING ORGANIZATION NAME(S) AND ADDRESS(ES)
Ceramic Composites Research Laboratory
The University of Michigan
Ann Arbor, MI 48109

8. PERFORMING ORGANIZATION REPORT NUMBER

9. SPONSORING/MONITORING AGENCY NAME(S) AND ADDRESS(ES)
AFOSR/NA
110 Duncan Ave, Suite B115
Bolling AFB, DC 20332-8080

10. SPONSORING/MONITORING AGENCY REPORT NUMBER

11. SUPPLEMENTARY NOTES

12a. DISTRIBUTION AVAILABILITY STATEMENT
Approved for public release, Disbribution unlimited

12b. DISTRIBUTION CODE

19980311 091

13. ABSTRACT *(Maximum 200 words)*

The AFOSR funded two year project (which expires March 1, 1997) addresses the effect of loading frequency and frictional heating on the ambient temperature fatigue life of continuous fiber ceramic matrix composites (CFCMCs). The project, which involves mechanics modeling, mechanical testing and microscopy, examined several composite systems and has provided details concerning the damage mechanisms that occur during high frequency fatigue. The currentresearch effort on high-frequency fatigue has been performed at the Cermaic Composites Research laboratory, in the Mechanical Engineering and applied Mechanics Department at the University of Michigan. 1. "Soft" matrix composites with strong interface bonding were shown to provide superior resistance to high frequency fatigue damage. 2. thick fiber coatings were more effective in reducing the amount of fiber wear and damage which occur during high frequency fatigue. 3. The effect of laminate stacking sequence has a profound effect on high frequency fatigue behavior of CFCMCs. 4. Surface roughness in Nicalon fibers can be determined using Atomic force Microscoopy (AFM). 5. Elongated crystalline grains and asmall volume fraction of whiskers in the matrix can improve the high frequency fatigue behavior of CFCMCs. 6. Loading rate was found to significantly effect monotonic tensile behavior of CFCMCs.

14. SUBJECT TERMS

15. NUMBER OF PAGES
87

16. PRICE CODE

17. SECURITY CLASSIFICATION OF REPORT	18. SECURITY CLASSIFICATION OF THIS PAGE	19. SECURITY CLASSIFICATION OF ABSTRACT	20. LIMITATION OF ABSTRACT
UNCLASSIFIED	UNCLASSIFIED	UNCLASSIFIED	UL

DTIC QUALITY INSPECTED 3

JAN 20 1998

INFLUENCE OF LOADING FREQUENCY ON THE FATIGUE BEHAVIOR OF FIBER - REINFORCED CERAMIC COMPOSITES

Final Technical Report
Contract # F49620-95-1-0206

John W. Holmes*
Principle Investigator

Ceramic Composites Research Laboratory
The University of Michigan
Ann Arbor, MI 48109

Submitted to

Dr. Alexander Pechenik
Program Manager
Directorate of Chemistry and Materials Science
Air Force Office of Scientific Research
Bolling Air Force Base, DC

March 1, 1997

*Department of Mechanical Engineering and Applied Mechanics
+ Department of Materials Science and Engineering

DTIC QUALITY INSPECTED 3

Table of Contents

I. Overview of Collaborations and Research Results

II. Dissemination of Research Results

III. High Frequency Fatigue Behavior of Woven Continuous Fiber Reinforced Polymer-Derived Matrix Composites with a strong fiber/matrix interface

IV. Effect of Interfacial Coating Thickness on the High Frequency Fatigue Behavior of Woven Continuous Fiber Reinforced SiC Matrix Composites with a weak fiber/matrix interface

V. Effect of Laminate Stacking Sequence on the High Frequency Fatigue Behavior of SCS-6 Fiber Reinforced Si_3N_4 Composites

VI. Surface Roughness Characterization of Continuous Ceramic Fibers by Atomic Force Microscopy (AFM).

Overview of Collaborations and Research Results

The AFOSR funded two year project (which expires March 1, 1997) addresses the effect of loading frequency and frictional heating on the ambient temperature fatigue life of continuous fiber ceramic matrix composites (CFCMCs). The project, which involves mechanics modeling, mechanical testing and microscopy, examined several composite systems and has provided details concerning the damage mechanisms that occur during high frequency fatigue.

The current research effort on high-frequency fatigue has been performed at the Ceramic Composites Research Laboratory, in the Mechanical Engineering and Applied Mechanics Department at the University of Michigan. The team consisted of a combination of materials and solid mechanics researchers: Professor John W. Holmes, Professor James Barber, and Ph.D. candidates Nikhilesh Chawla and Yahya Tur. All members of this group have been active in the area of fatigue deformation of continuous fiber-reinforced ceramic matrix composites.

As part of the 2-year AFOSR funded project, collaborative research efforts were established with industrial counterparts and national laboratories:

- Dow Corning Corp. (with Andy Szweda). Nicalon/Si-C-O-N specimens were donated by Dow Corning and tested at the University of Michigan.

- Oak Ridge National Laboratory (with Rick A. Lowden). Nicalon/SiC specimens were donated by ORNL and tested at the University of Michigan.

- High Temperature Materials Laboratory, Oak Ridge National Laboratory (with Matt K. Ferber and Edgar Lara-Curzio). User Agreement to perform single fiber pushout experiments on fatigued specimens.

- NASA-Lewis (with Jeff Eldridge). Room and elevated temperature fiber pushout experiments of pristine and fatigued specimens are in progress.

- Riso National Laboratory (with Bent F. Sørensen). Studies of the influence of loading rate on the monotonic tensile behavior of CFCMCs and the mechanisms that cause fatigue failure in CFCMCs.

In addition to the numerous collaborations listed above, a significant amount of progress has been made in a variety of areas related to high frequency fatigue of CFCMCs, resulting in six peer-reviewed publications (one additional paper is under review), seven presentations (two of them were invited), and a best graduate student paper award.

Several key findings were made, the most important of which were:

1. "Soft" matrix composites with strong interface bonding were shown to provide superior resistance to high frequency fatigue damage.

2. Thick fiber coatings were more effective in reducing the amount of fiber wear and damage which occur during high frequency fatigue.

3. The effect of laminate stacking sequence has a profound effect on high frequency fatigue behavior of CFCMCs.

4. Surface roughness in Nicalon fibers can be determined using Atomic Force Microscopy (AFM).

5. Elongated crystalline grains and a small volume fraction of whiskers in the matrix can improve the high frequency fatigue behavior of CFCMCs.

6. Loading rate was found to significantly effect monotonic tensile behavior of CFCMCs.

The research effort in 1997 will focus on developing new insights into the mechanisms responsible for the degradation in the fatigue life of fiber-reinforced ceramics subjected to high frequency loading at elevated temperatures. This will mark the first research program that addresses the combined effects of creep-fatigue and high frequency cyclic loading interactions on fatigue damage mechanisms and fatigue life.

II. Dissemination of Research Results

A list of publications, presentations, and awards that were a direct result of AFOSR funding for this project are listed below. Authors' names directly involved with this project are underlined.

Peer-Reviewed Publications

1. N. Chawla, J.W. Holmes and J.F. Mansfield, "Surface Roughness Characterization of Nicalon and HI-Nicalon Ceramic Fibers by Atomic Force Microscopy," *Mater. Charac.*, (1995) 35 199.

2. N. Chawla, J.W. Holmes, and R.A. Lowden, "The Role of Interfacial Coatings on the High Frequency Fatigue Behavior of Continuous Fiber Ceramic Matrix Composites," *Scripta Mater.*, (1996), in press.

3. N. Chawla, J.W. Holmes, Y.K. Tur, J.R. Barber, and A. Szweda, "The High Frequency Fatigue Behavior of a Woven Fiber Fabric Reinforced Polymer-Derived Ceramic Matrix Composite," May 1996, submitted to *J. Am. Ceram. Soc.*

4. N. Chawla and J.W. Holmes, "High Frequency Fatigue of Continuous Fiber Ceramic Matrix Composites," in **Processing and Design of High Temperature Materials** (N.S. Stoloff and R. Jones, eds.), TMS, Warrendale, PA (1996), in press.

5. J.W. Holmes, N. Chawla, M. Steen, and J. Valles, "High Temperature Fatigue Behavior of Continuous Fiber Ceramic Matrix Composites (INVITED)," submitted to *Mater. Sci. & Eng.*, (1996), in press.

6. B. F. Sørensen and J. W. Holmes, "Effect of Loading Rate on the Monotonic Tensile Behavior of a Continuous Fiber-Reinforced Glass-Ceramic Composite," *J. Am. Ceram. Soc.*, (1996) 79 313.

Presentations

1. N. Chawla and J.W. Holmes, "High Frequency Fatigue of Continuous Fiber Reinforced Ceramic Matrix Composites," **AFOSR Review**, Hueston Woods, OH, May 1996.

2. N. Chawla and J.W. Holmes (INVITED), "High Frequency Fatigue of Continuous Fiber Reinforced Ceramic Matrix Composites," **Conference on Processing and Design of High Temperature Materials**, Davos, Switzerland, May 1996.

3. N. Chawla and J.W. Holmes, "High Frequency Fatigue of Continuous Fiber Reinforced Ceramic Matrix Composites," **Dow Corning Corp.**, May 1996.

4. N. Chawla, J.W. Holmes, and A. Szweda "The High Frequency Fatigue Behavior of Woven Nicalon Fiber Reinforced Si-C-O-N Matrix Composites," **ASTM Symposium on Thermal and Mechanical Test Methods**, Cocoa Beach, FL, January 1996.

5. B. F. Sørensen and J.W. Holmes (INVITED), "Fatigue of Ceramic Matrix Composites: Review of Mechanisms and Models," **Petten Research Center, The Netherlands**, September 1995.

6. B. F. Sørensen, J.W. Holmes and P. Brondsted, "Effect of Environment and Loading Rate on Fatigue Damage in Ceramic Matrix Composites," **Conference on High Temperature Ceramic Matrix Composites**, Santa Barbara, CA, August 1995.

7. J. W. Holmes, N. Chawla, M. Steen and J. Valles, "Mechanisms of Fatigue Damage in Ceramic Matrix Composites," **Petten Research Center, The Netherlands**, September 1996.

Awards

Nikhilesh Chawla won the ASM International Graduate Student paper competition for 1996 for his entry entitled "Effect of Laminate Stacking Sequence on the High Frequency Fatigue Behavior of SCS-6/Si_3N_4 Ceramic Matrix Composites." The award, a first for the MSE Dept. at University of Michigan, consists of a certificate, a $500 honorarium, and $250 in expense money to attend the annual meeting of ASM/TMS to be held October of 1996 to receive the award. Nikhilesh is the first student from the University of Michigan to win this award.

III. High Frequency Fatigue Behavior of Woven Continuous Fiber Reinforced Polymer-Derived Ceramic Matrix Composites

N. Chawla, Y.K. Tur, J.W. Holmes, J.R. Barber, and A. Szweda

I. Introduction

In CFCMCs with weak bonding between the fibers and matrix, energy dissipation by frictional sliding occurs during cyclic loading [1]. This energy dissipation may result in a substantial temperature increase in the composite due to the repeated frictional sliding between fiber and matrix at the fiber/matrix interface. Temperature increases during fatigue have also been observed in thermoplastic polymer matrix composites, although in polymers the viscoelastic nature of the matrix is the primary mechanism responsible for heating [2]. The temperature associated with frictional sliding in CFCCs has been documented in hot-pressed Nicalon/CAS II composites and chemical vapor infiltrated C/SiC [3,4]. At a frequency of 85 Hz and R ratio of 0.04 in C/SiC, a temperature rise of 50 K was observed. Large temperature increases have also been observed by Koch and Grathwohl [5] in 100 Hz fatigue of Tyranno/C/SiC composites.

The effect of loading frequency on the high frequency fatigue behavior of a Nicalon/CAS II glass matrix composite showed that, unlike monolithic ceramics, fatigue life of this composite decreased rapidly with loading frequency [3]. During fatigue, wear occurs along debonded fiber/matrix interfaces. By lubricating the interface, it was shown that dramatic increases in the fatigue life of this composite system could be attained [6]. It is believed that by producing a damage-tolerant CFCC with a strong fiber/matrix bonding, fatigue properties can be enhanced due to inhibition of fiber/matrix sliding.

Increasingly, the emphasis of processing research in the CMC area has shifted to fabricating less expensive composites with small amounts of residual porosity. Polymer infiltration and pyrolysis (PIP) is an attractive processing route because of its relatively low cost. Moreover, this approach allows near

net-shape molding and fabrication technology that is able to produce nearly fully-dense composites [7-10]. In PIP, the fibers are infiltrated with an organic polymer. The polymer is heated to fairly high temperatures and pyrolyzed to form a ceramic matrix. Due to the relatively low yield of polymer to ceramic, several infiltrations are used to densify the composite. A large amount of shrinkage and cracking in the matrix occurs during the pyrolysis process; particulate fillers are added to the polymer to reduce shrinkage and to stiffen the matrix material in the composite [11].

In this study, the fatigue behavior of an eight harness satin weave Nicalon fiber reinforced Si-C-O-N matrix composite made by PIP was investigated. Two matrix variations were tested: one composite had a BN filler and another a SiC filler. The fibers were coated with a proprietary B-containing coating that created a strong bond between the fibers and matrix. A debond stress of about 1500 MPa was obtained from fiber pushout tests [12]. Contrary to the widespread view that a weak fiber/matrix interface is needed for optimum monotonic and fatigue properties in CMCs, it will be shown that the strong interface in Nicalon/Si-C-O-N composites can provide both high monotonic toughness and excellent fatigue life.

The monotonic and high frequency fatigue behavior was investigated at room temperature. The temperature rise in test specimens due to frictional heating, and the stiffness reduction during the fatigue tests were monitored to characterize the damage state of the composite. Scanning electron microscopy was used to identify microstructural damage that took place during fatigue.

II. Experimental Procedure

As mentioned in the introduction, the Nicalon/Si-C-O-N composites were processed by PIP. The woven eight harness satin fiber fabric was coated with a proprietary B-containing interface, stacked and infiltrated. The volume fraction of fibers in the composite was nominally 40%. The composites were infiltrated with a mixture of polymer and filler particles during the first infiltration, while 9-

10 subsequent infiltrations were made with polymer only. Table 1 shows the density and percent porosity of the BN and SiC filler composites.

Testing was conducted using an MTS High Frequency servohydraulic load frame. Alignment of the load train was conducted by the specifications delineated in the provisional ASTM standard for monotonic tensile testing of continuous fiber ceramic composites [13]. At a load of 1 kN (equivalent to less than 500 microstrain) the amount of bending in the specimen was less than 5% of the tensile uniaxial strain. Experiments were conducted at a minimum stress of 10 MPa and a loading frequency of 100 Hz (100 cycles per second). A water-cooled chamber was used to maintain a constant temperature around the specimen during the experiments. Temperature measurements of the specimen were conducted using an infrared pyrometer and a high frequency extensometer was used to measure strain. The edge-loaded specimens were machined to 111 mm length, with a 33 mm gauge length. Details of the testing and gripping procedures are given elsewhere [3,4].

III. Results and Discussion

As-received microstructure of the composites. Filler composition profoundly affected the degree of processing-related cracking in the matrix. The matrix with BN filler was relatively crack free, as shown in Fig. 1(a). The addition of SiC to the matrix, however, was not as effective in containing shrinkage during pyrolysis which resulted in cracks through fiber bundles, shown in Fig. 1(b). The filler network obtained during filler-controlled pyrolysis, described in the introduction, was observed in the microstructure of both composites, Fig. 2.

Monotonic tensile behavior. Figure 3 shows monotonic tensile curves for the two composites. The composite with BN filler had a higher strength, but in the linearly elastic region of the material, a lower stiffness was observed compared to the composite with the SiC filler. Clearly, the addition of the SiC

Density and Percent Porosity of Nicalon/Si-C-O-N matrix Composites

	Density (g/cm^3)	Open porosity (%)
Nicalon/Si-C-O-N, BN filler	2.107	5.17
Nicalon/Si-C-O-N, SiC filler	2.215	5.08

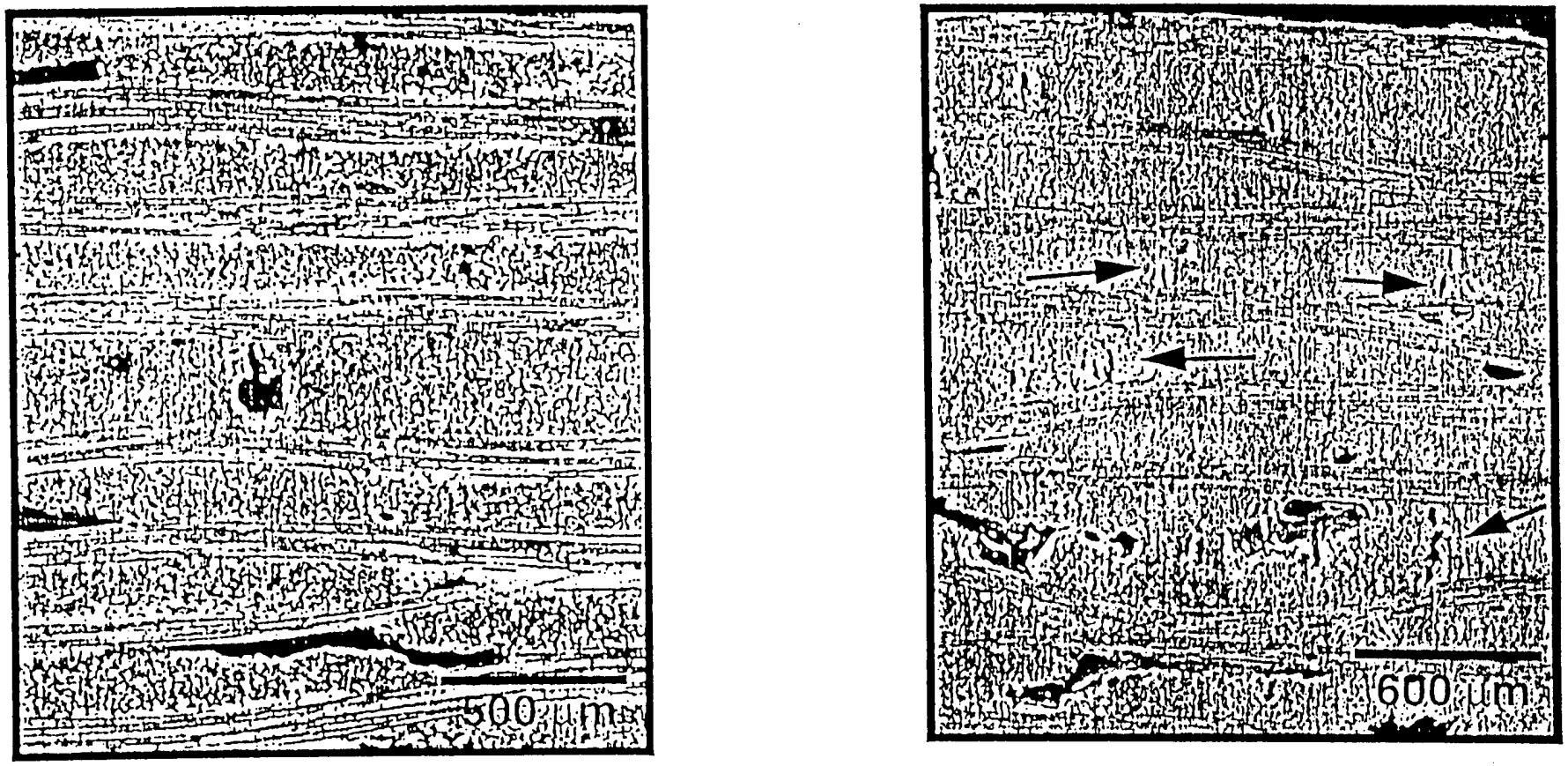

(a) (b)

Fig. 1. As-processed matrix with (a) BN filler which is relatively crack free, and (b) SiC filler, not as effective in containing shrinkage during pyrolysis resulting in cracks through the fiber bundles.

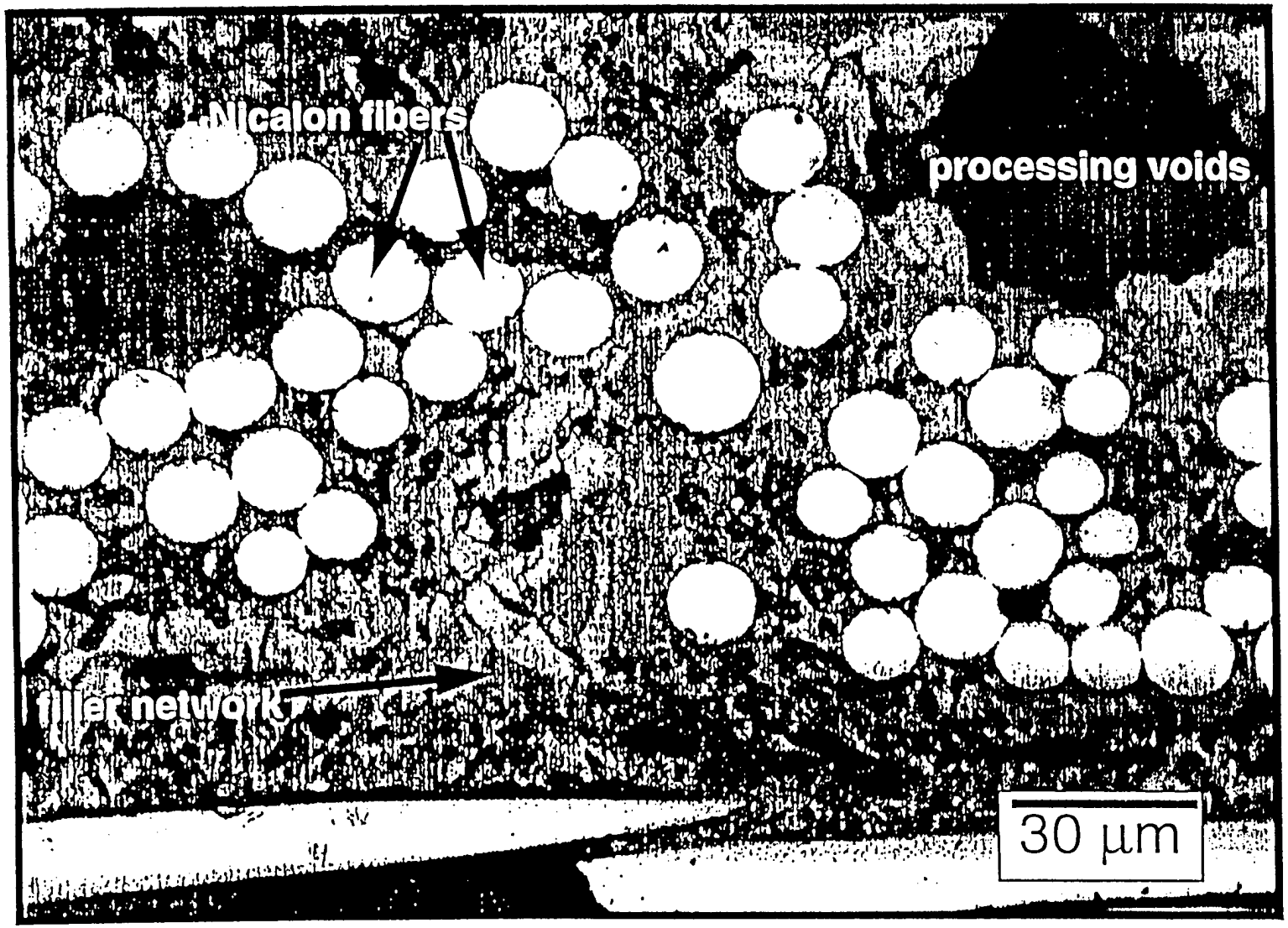

Fig. 2. Optical micrograph of filler network obtained during filler-controlled pyrolysis in BN and SiC filler composites.

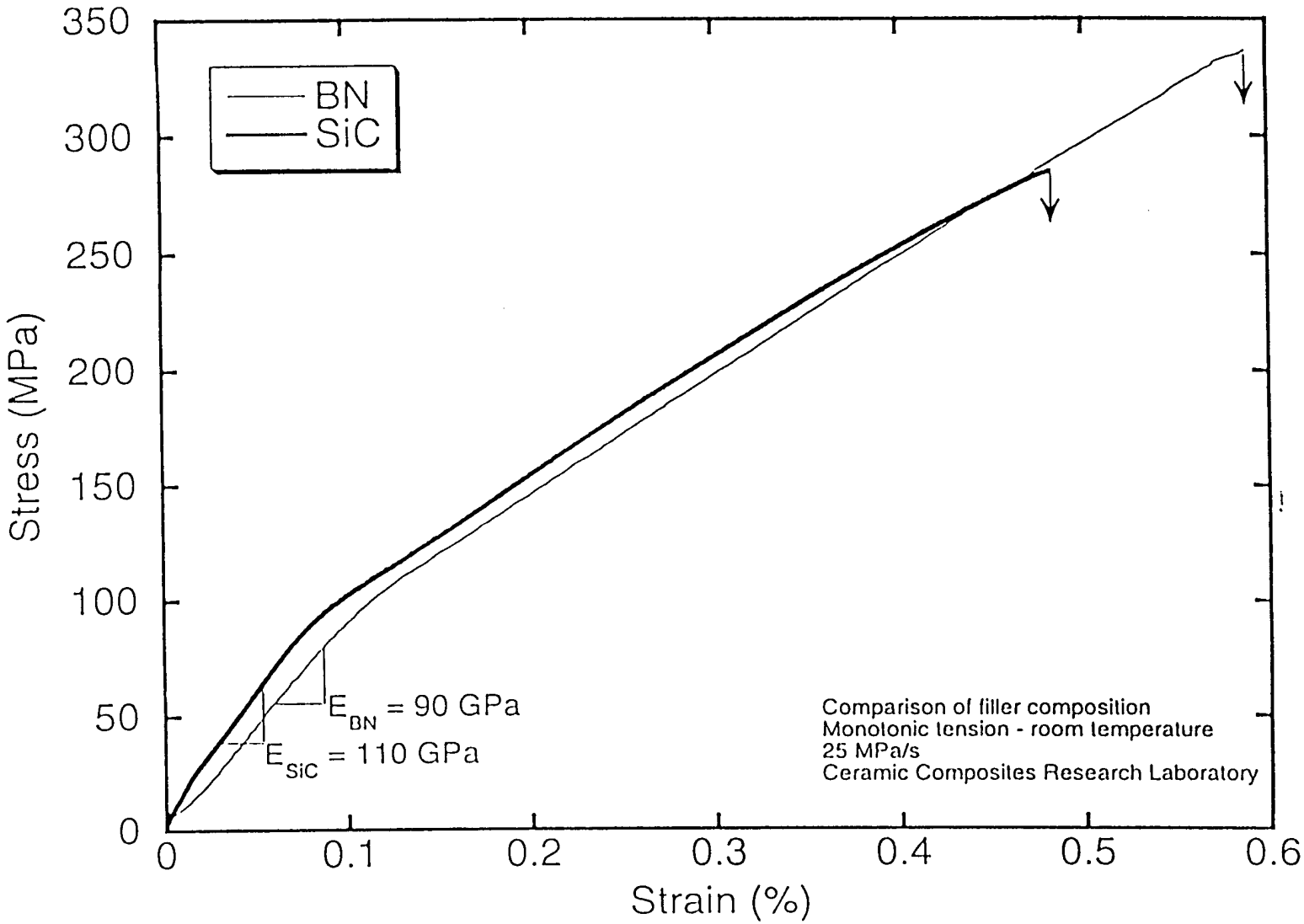

Figure 3. Monotonic tensile curves for BN and SiC filler composites.

filler increased the modulus of the matrix and therefore the modulus of the composite was also increased. Although the reinforcement volume fraction and architecture in both composites was the same, the SiC composite had a lower strength. This is attributed to processing cracks in the fiber bundles of the SiC filler composite which lowered the overall strength of the composite.

Because the fiber was very strongly bonded to the matrix, the well-documented mechanisms of matrix cracking, followed by fiber debonding and crack deflection, and finally fiber pullout, did not apply in these composites. Instead, due to the woven nature of this material, the occurrence of a distinct proportional limit in the monotonic curves is attributed to localized matrix crack and debonding between longitudinal and transverse fiber bundles at the cross-over points in the woven fabric. The precise nature of these mechanisms is described in the next section which deals with fatigue behavior of these composites.

Fatigue life. The stress-cycles (S-N) curve for the composites is shown in Fig. 4. At high cycles (10^5 and above), a clustering of failures in the two materials was seen, i.e., the life of the two materials in the high cycle regime was about the same. It is interesting to note that slightly below the monotonic strength (e.g., 20 MPa below σ_{uts}) the fatigue life of the composite was about 10^4 cycles.

Lara-Curzio et al. [14] have studied a similar material at lower frequencies (1 Hz) and due to longer test duration at 1 Hz, determined that no failures at 10^6 cycles was a satisfactory endurance limit. In this study, endurance limits of the composite were taken at 10^7 cycles, but failures were observed at lives as high as 7×10^6 cycles. The S-N curve obtained in this study is very similar to that of Lara-Curzio et al. [14], indicating that there is no significant effect of frequency on fatigue life of this composite. One reason for this may be the strong interfacial bonding between fiber and matrix, such that fiber/matrix wear during fatigue is inhibited. In composites with a weak

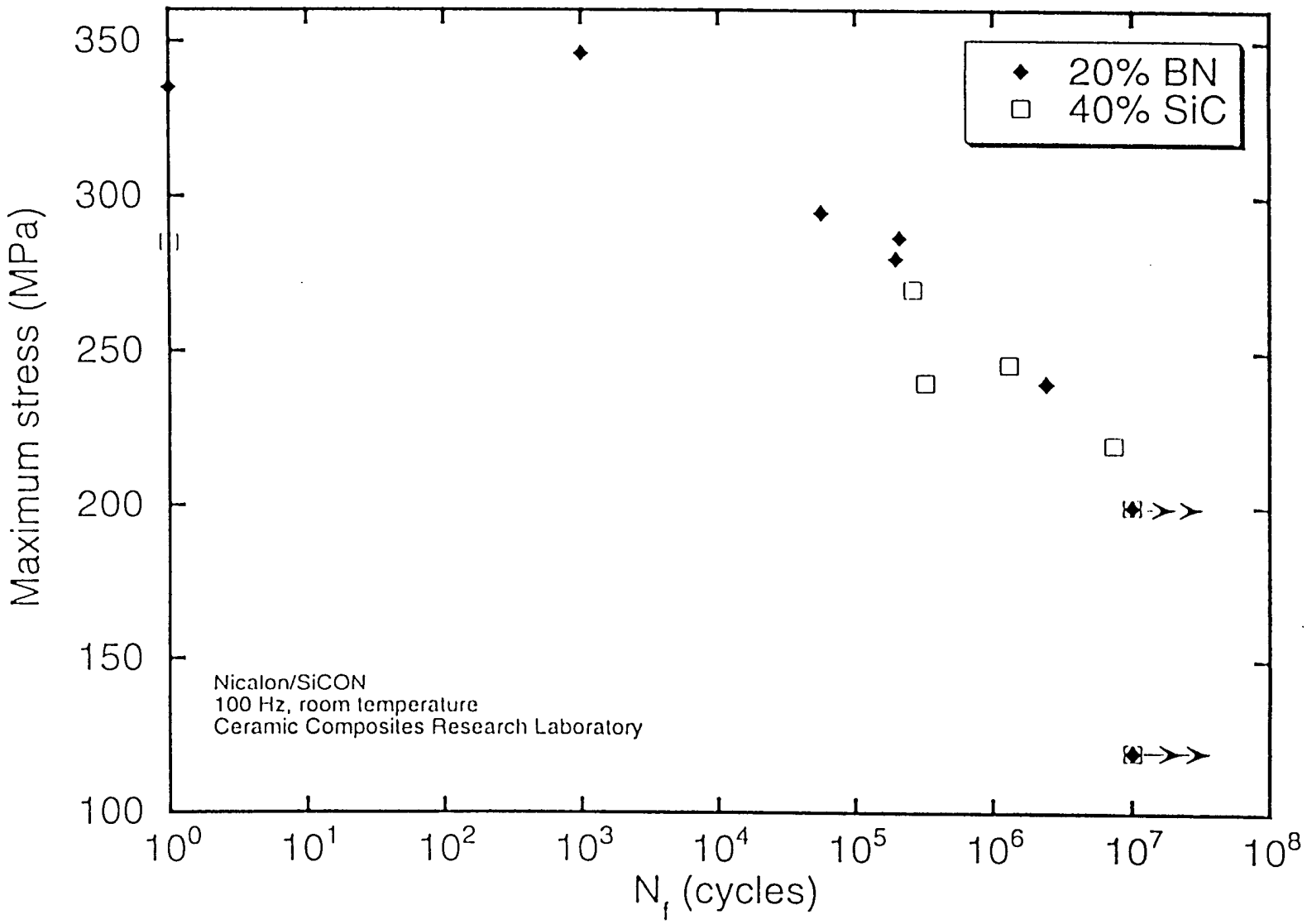

Figure 4. Stress-cycles (S-N) curve for the composites tested in fatigue at a frequency of 100 Hz. The minimum stress in all tests was 10 MPa.

fiber/matrix bond, wear rates at the interface are much faster at higher frequencies resulting in more premature failures. Since there seems to be no effect of frequency in this composite system, testing at higher frequencies is a more attractive way of testing the composite for higher lifetimes in a shorter amount of time.

Damage mechanisms. To explain the damage mechanisms, we must first turn to the strong interfacial bond between fiber and matrix in this composite system. Due to the strong nature of bonding, any matrix microcracks are arrested by fibers or the cracks propagate through the fibers, without debonding or crack deflection at the fiber/matrix interface. Fiber cracking will only occur, of course, if stresses are high enough for fiber fracture and these are observed in this study of Nicalon/Si-C-O-N. Petitpas et al. [15] showed that in [0/90] carbon fiber reinforced plastic (CFRP) progressive debonding along transverse and longitudinal ply junctions led to an increased stress concentration in the fibers, increasing the probability of fiber fracture.

A decrease in the tangent modulus can be attributed to two major mechanisms: debonding of the longitudinal and transverse bundles which results in debonding of the plies, and fiber failure. The wavy parts of the bundles are prone to debonding due to strain mismatch between plies. These regions may debond if the stresses exceed the bond strength between bundles. With a higher applied stress, the debonded region increases. Figure 5 shows severe cracking of a transverse bundle that crosses over a longitudinal bundle in specimen that was fatigued. Similar cracking at crossover points between longitudinal and transverse bundles during fatigue of woven carbon fiber reinforced plastics (CFRP) has also been observed [16].

Thus, the damage evolution process is envisioned to occur as follows. Due to strain mismatches between transverse and longitudinal bundles, matrix microcracking occurs at the contact points between the two types of bundles. This damage occurs at low stresses, with pronounced damage occurring at the proportional limit stress. Stress relief in the transverse bundle may also occur

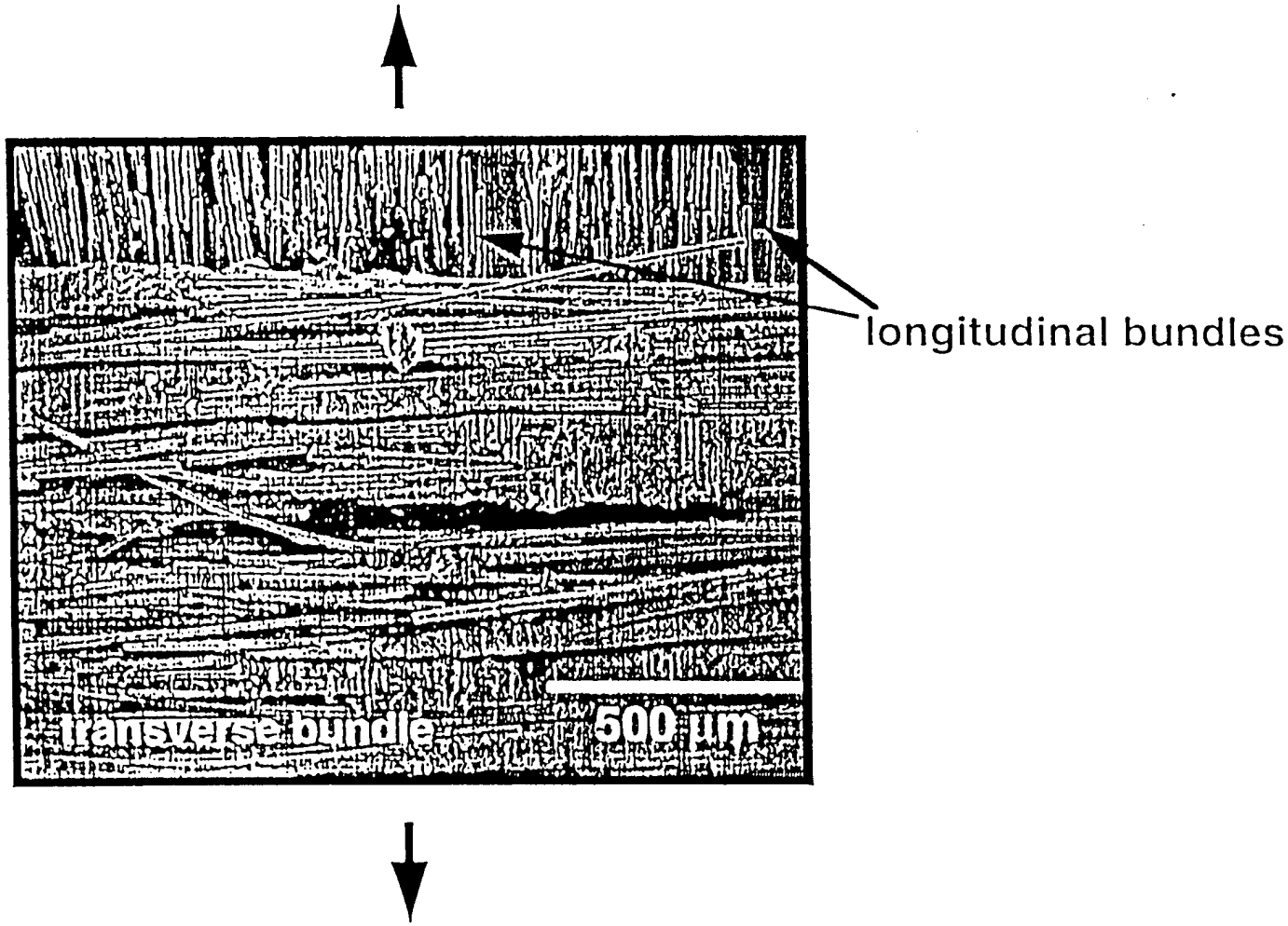

Figure 5. Severe cracking of a transverse bundle that crosses over a longitudinal bundle in a specimen that was fatigued.

through the formation of microscopic matrix cracks or cracks emanating from processing pores.

In the composite with the BN filler, with an increase in damage, the localized debonded sites and cracks resulted in interlaminar cracking and failure as shown in Fig. 6. Furthermore, linkage of delaminated plies occurs between transverse bundles that reside between the two adjacent delaminations, Fig. 7. Interlaminar failure during compressive fatigue in woven CFCCs has also been reported in C/SiC composites [17, 18].

Stress-strain hysteresis and modulus reduction. From stress-strain hysteresis measurements and modulus reduction data, it was determined that the majority of damage in the composite during fatigue occurred during initial loading. Damage was quantified by defining a normalized damage parameter D_E, which is given by [19, 20]:

$$D_E = 1 - E/E_o \qquad (1)$$

where E_o is the initial modulus, taken from the linearly elastic portion of the loading curve, and E is the modulus at a given number of cycles. Figure 8 shows that in both composites the majority of damage occurred in the first cycle. A similar observation has been reported for 1 Hz fatigue of the same composite system [14]. The higher the initial loading stress (also the cycling stress), the higher the degree of damage. Subsequent cyclic damage after the first cycle was rather limited. At a stress level slightly above the proportional limit the modulus decrease after the first cycle was more gradual, reaching a saturation point around 10^6 cycles. It should be noted that in this and other systems a modulus reduction has been observed in cyclic tests at stresses even below the proportional limit [21]. One can infer from this, that given a sufficiently large number of cycles, the composite may fail even at a stress below the proportional limit.

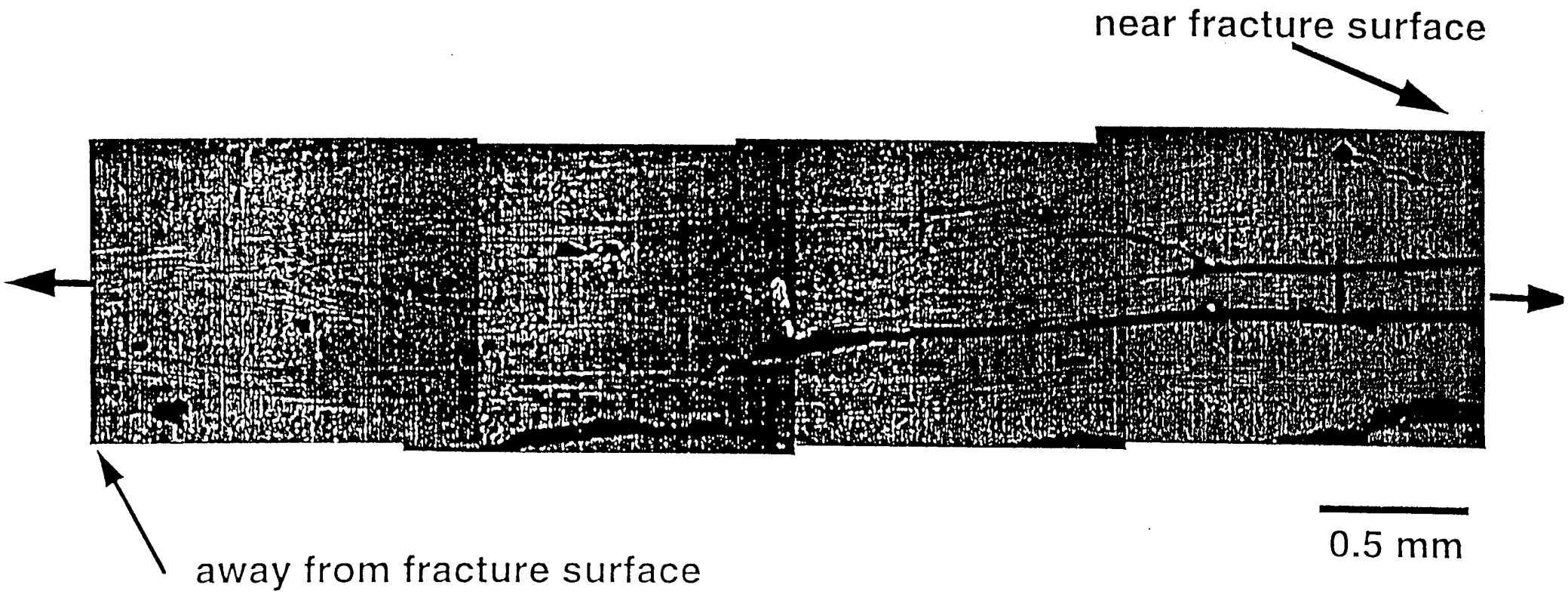

Figure 6. SEM micrograph of interlaminar cracking and failure during fatigue, resulting from the linkage of localized debonded sites at cross-over points between longitudinal and transverse bundles.

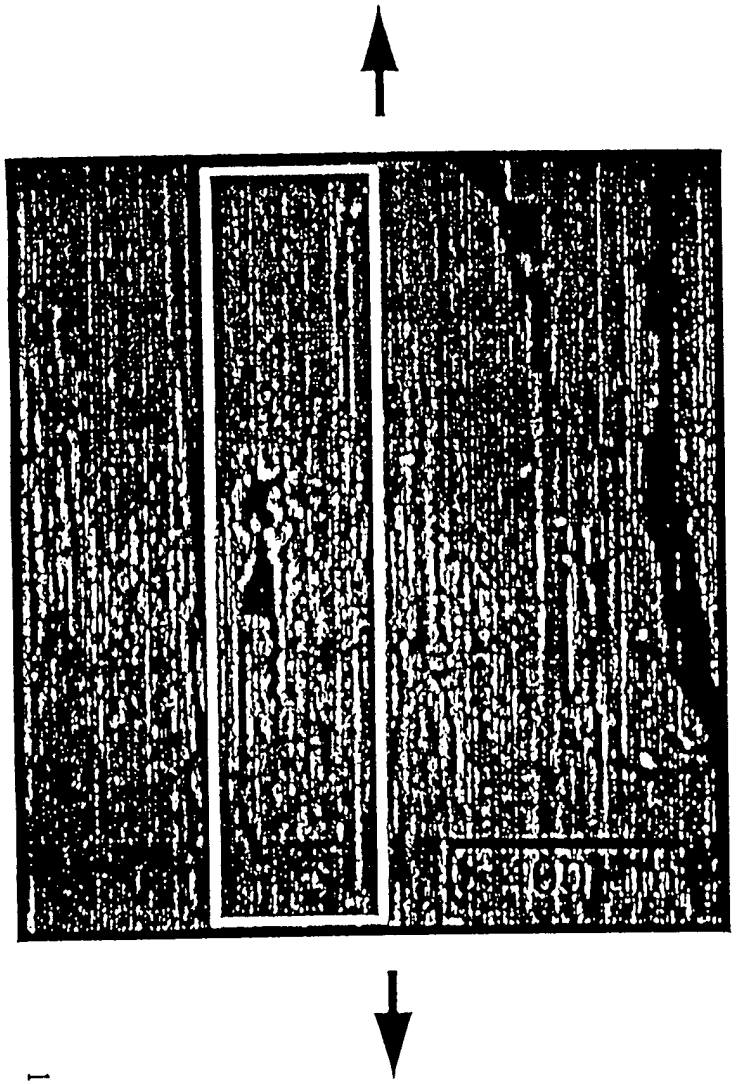

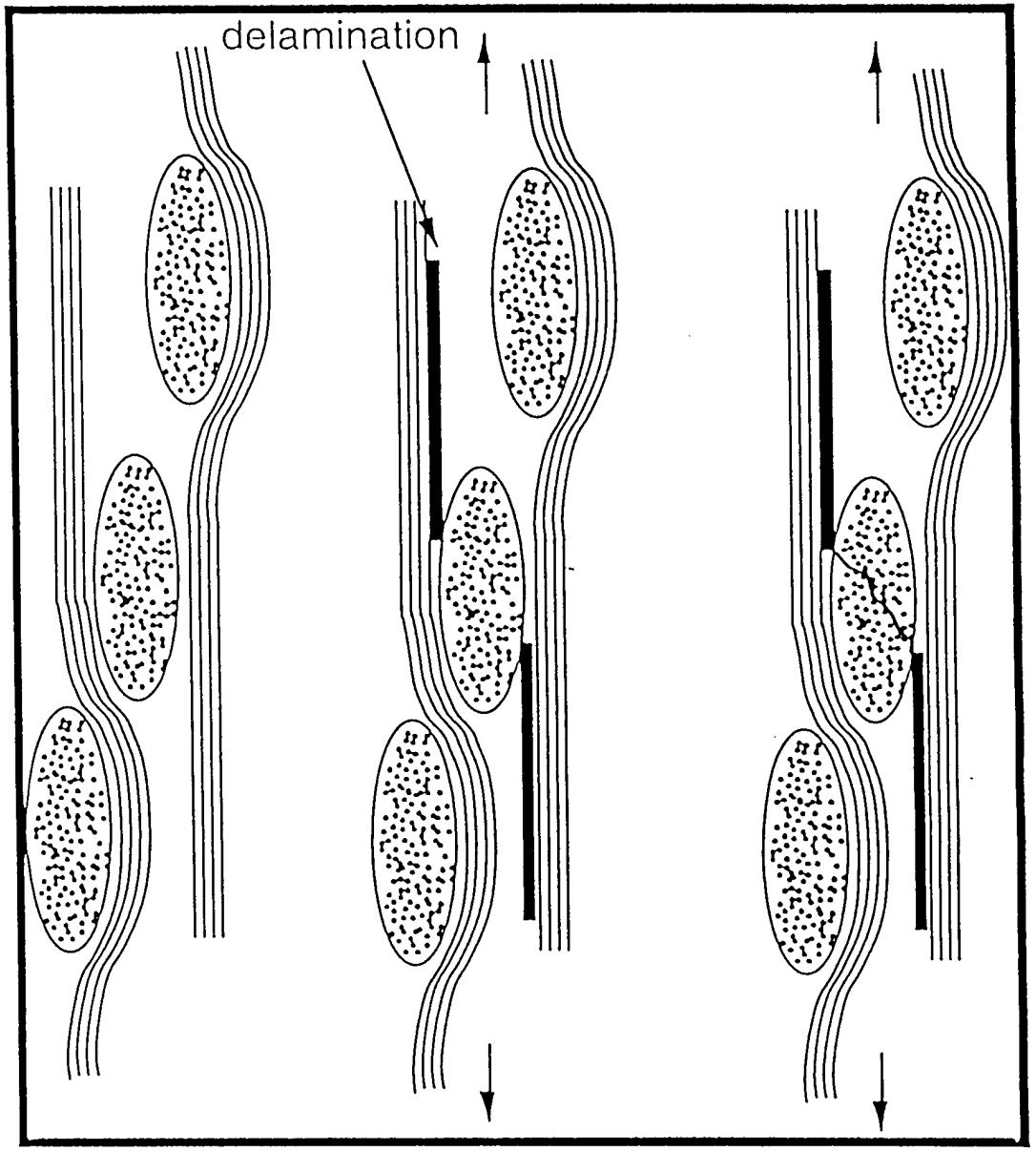

Figure 7. SEM micrograph showing linkage between two delamination cracks.

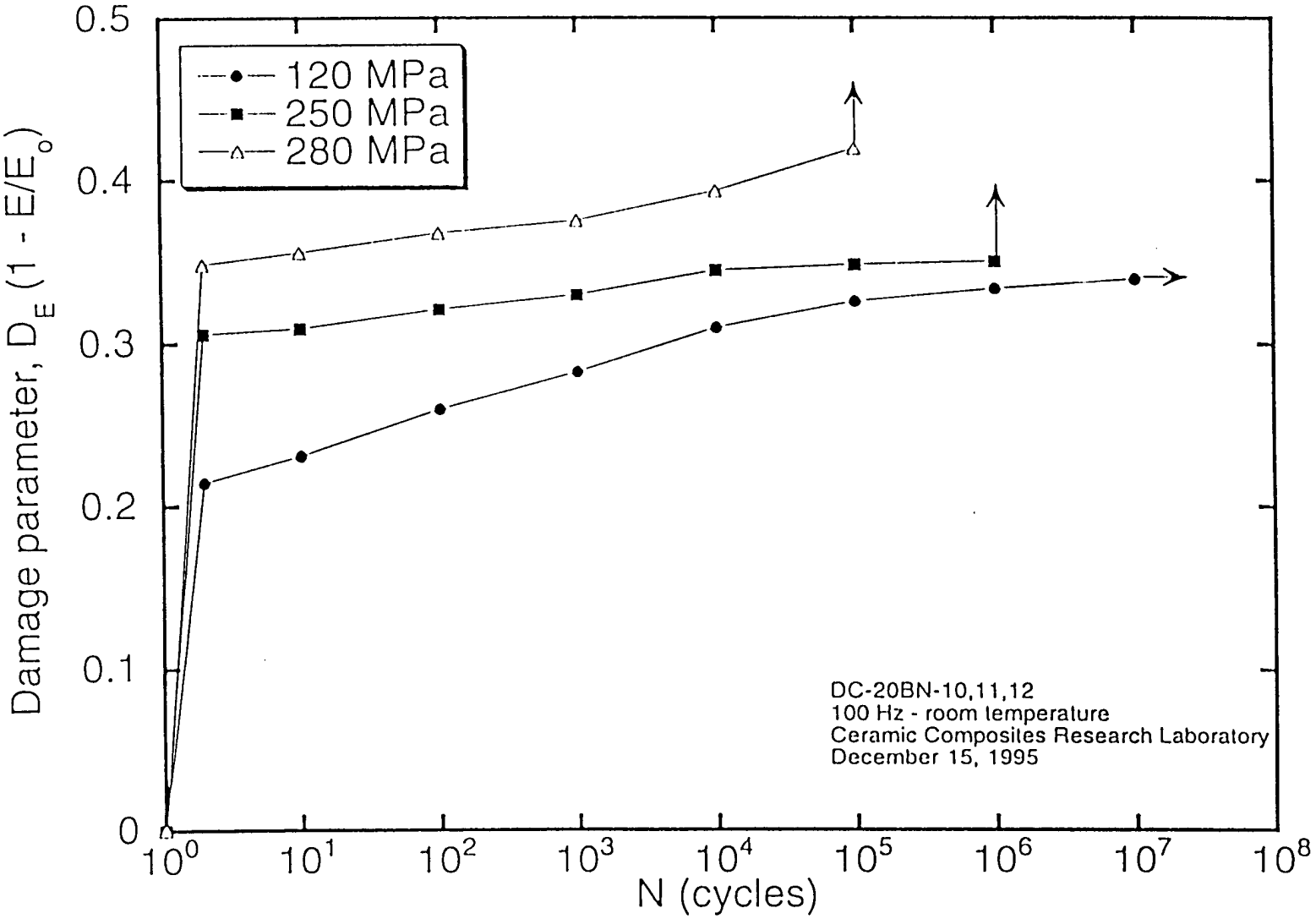

(a)

Figure 8(a). Damage versus cycles in BN filler composite and (b) SiC filler composite. In both composites the majority of damage occurred in e first cycle.

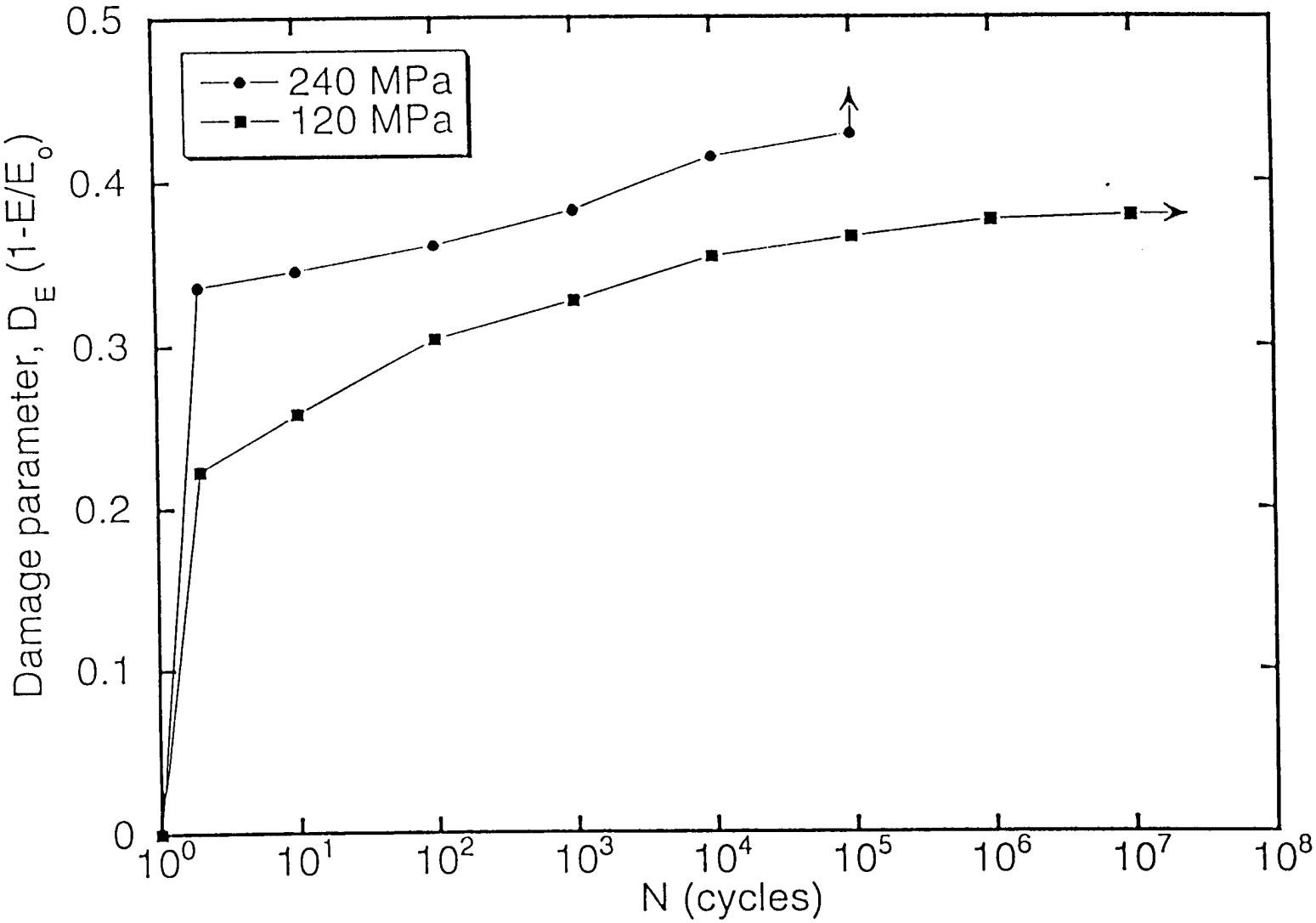

(b)

Figure 8. Contd.

The irreversible damage that occurred in the first cycle or loading ramp can be attributed to debonding and microcracking at crossing points of longitudinal and transverse bundles, as described above. This damage mechanism is in distinct contrast with the fatigue behavior of unidirectional Nicalon/CAS, for example, where the fiber/matrix bonding is quite weak (debond stress of about 400 MPa, and τ between 8-10 MPa) [22]. Hysteresis loops in the latter system show an S-shaped behavior [1,23] which is characterized by changes in interfacial shear stress at the fiber matrix interface during loading and unloading. Furthermore, in Nicalon/CAS an increase in modulus is observed at high cycles which is attributed to an increase in interfacial shear stress. In the present system, no S-shape was observed in the hysteresis loops and the amount of permanent strain was negligible, leading us to believe that fiber sliding was not a factor, Fig. 9. Rather, the relative motion of bundles in the weave would seem to be responsible for hysteresis.

Frictional heating behavior. A significant increase in temperature in both composites was observed during high frequency fatigue. A transient stage was observed where the specimen began to heat up until an equilibrium was achieved with the surrounding environment. Once the specimen reaches an equilibrium temperature any increase in temperature can be attributed to incremental damage. As can be seen in Fig. 10, the transient stage is almost instantaneous. This is followed by a region where the temperature remains fairly constant, indicating a plateau in the damage level of the composite. In the last portion of the life of the composite an increase is temperature is observed followed by failure. The length of the plateau region is highly dependent on the applied stress. At 120 MPa the plateau region continued until fatigue runout of the material. At 240 MPa the plateau region is longer than that at 280 MPa where it is almost absent, i.e, the temperature exhibits a continuous increase from the onset of equilibrium. Thus, in addition to providing a quantitative

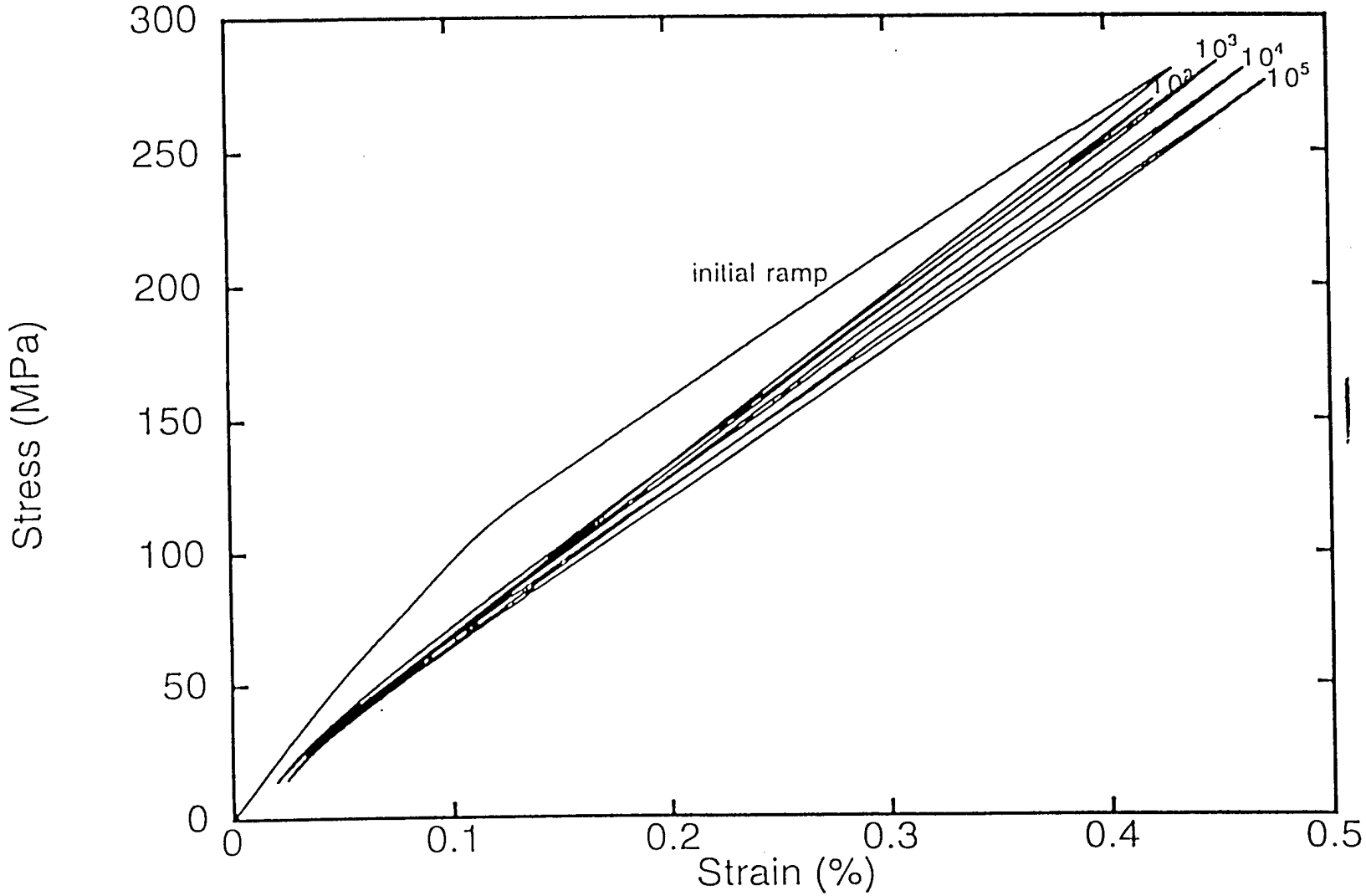

Figure 9. Stress-strain hysteresis in Nicalon/Si-C-O-N with BN filler. Note the absence of an S-shaped loop (normally associated with fiber sliding) and a negligible amount of permanent strain.

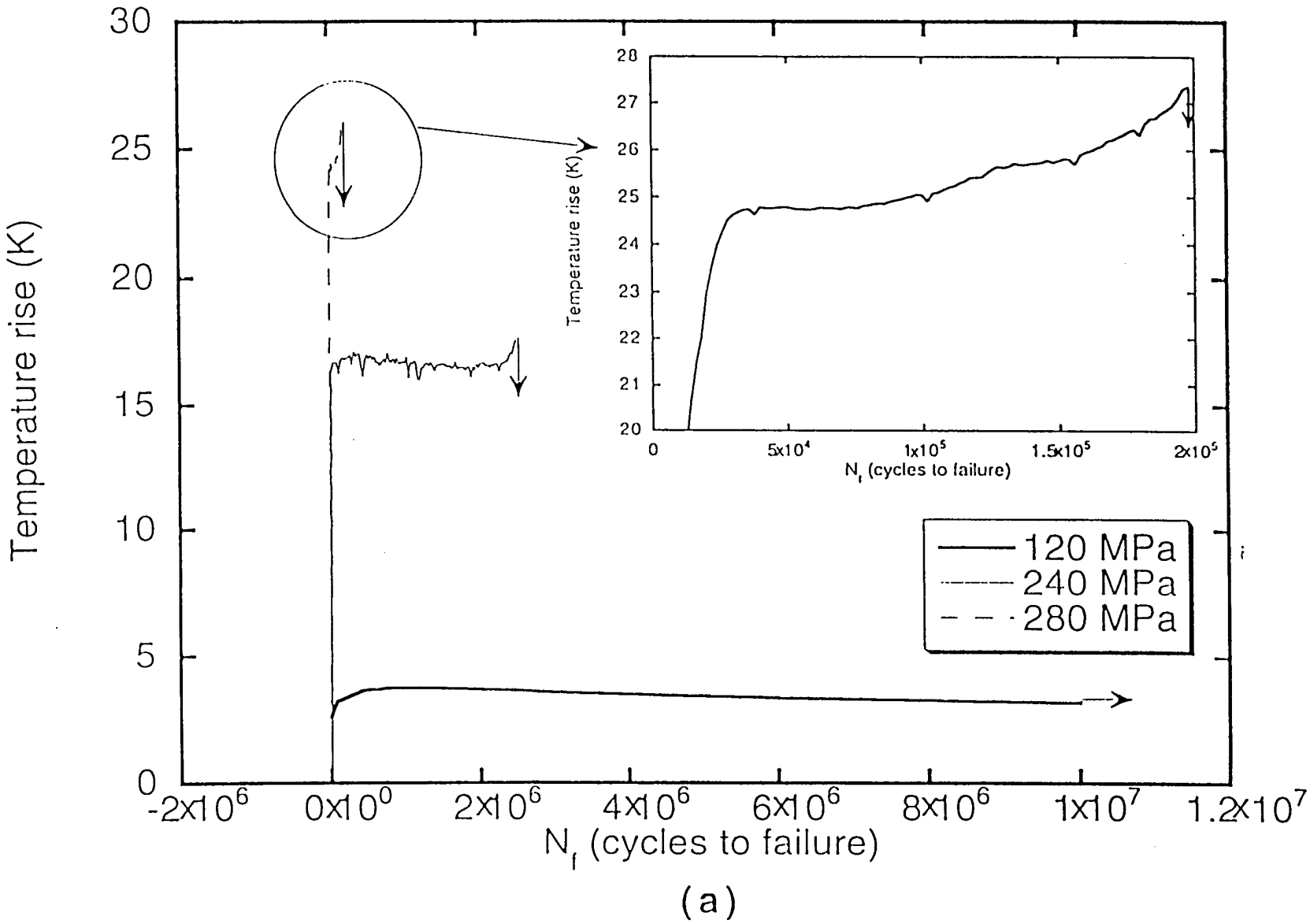

Figure 10. Temperature rise versus cycles in (a) BN filler and (b) SiC filler composite. A slight increase in temperature with increasing cycles was observed after stabilization, which continued to increase until failure of the composite.

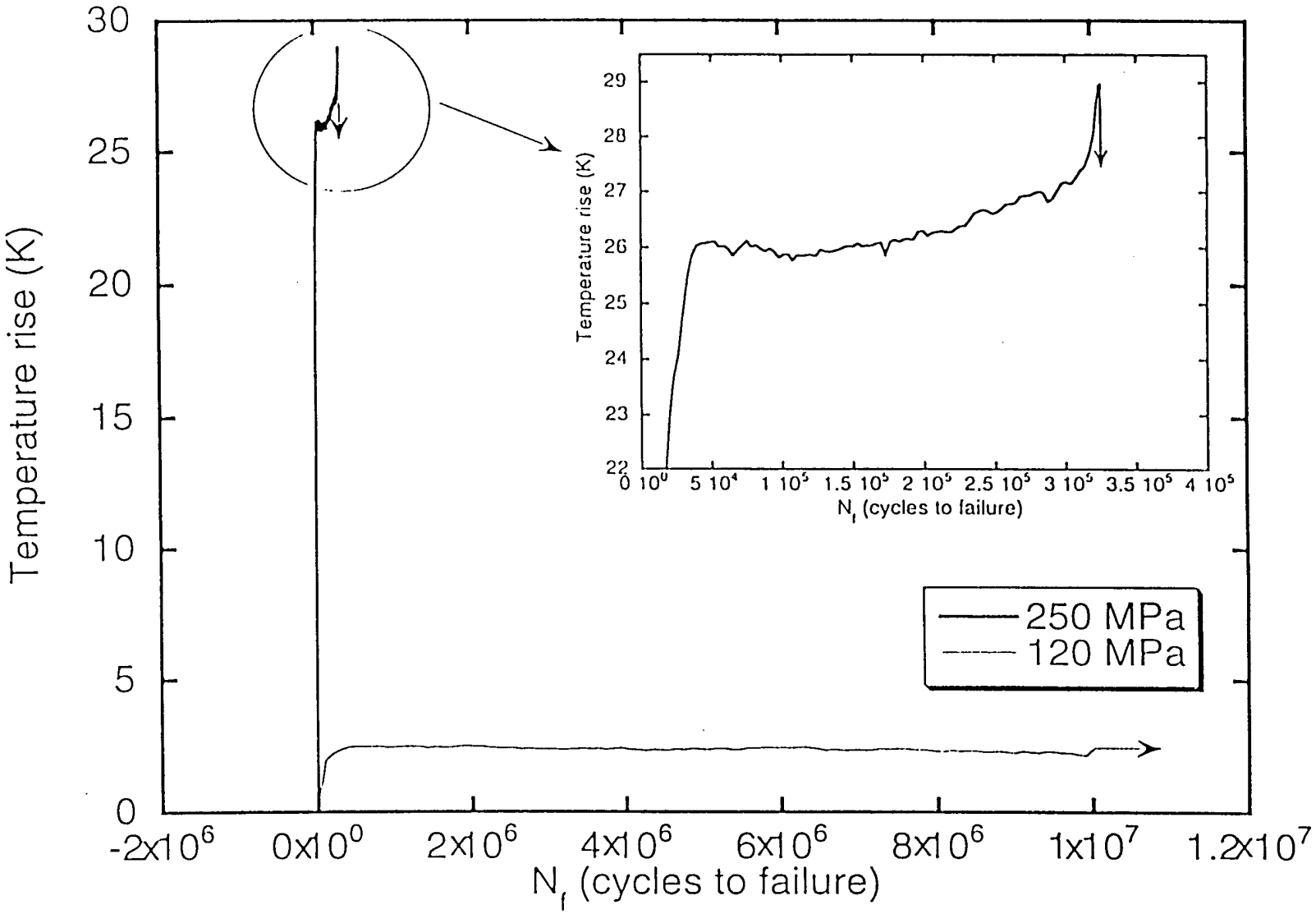

(b)

Figure 10 (Contd.).

estimate of the energy dissipation in the composite, temperature rise can be used as a damage parameter.

Heating arose from laminate and ply delamination and the accompanying friction between two surfaces during fatigue. Once debonding between bundles occurred, the fiber bundle itself was fatigued in the longitudinal direction, and since the fiber was not allowed to slide to dissipate energy, any localized matrix cracks propagated through the fibers, Fig. 11. This localized fiber cracking during the fatigue process was responsible for slight decreases in modulus of the composite after the first cycle.

The degree of debonding between bundles was dependent on the applied stress. If the stress level was high enough, most of the bundle debonding occurred in the first cycle, as shown by the large increase in damage parameter, Fig. 8. At stresses close to the proportional limit, the damage accumulation was more gradual, indicating progressive debonding of the fiber bundles until a saturation in damage occurred.

It is instructive to once again compare the behavior of Nicalon/Si-C-O-N with that of unidirectional Nicalon/CAS with a weak fiber/matrix interface [3]. In the latter system the magnitude of heating is quite large due to frictional sliding at the fiber/matrix interface, where a large number of small diameter fibers are allowed to slide and dissipate heat during fatigue. Also, a bell-shaped temperature curve is observed [5]. This is attributed to easy slip in the beginning of fatigue (lower τ) and higher temperature rise, followed by restricted slip in the latter parts of the test (higher τ) and lower temperature. In the present study, fiber sliding is not a damage mechanism so the magnitude of heating is lower and there is a constant increase in temperature during the test until final fatigue failure of the composite occurs.

Residual strength. Samples that survived 10^7 cycles at 200 MPa were tested monotonically to determine the effect of fatigue on the residual strength of

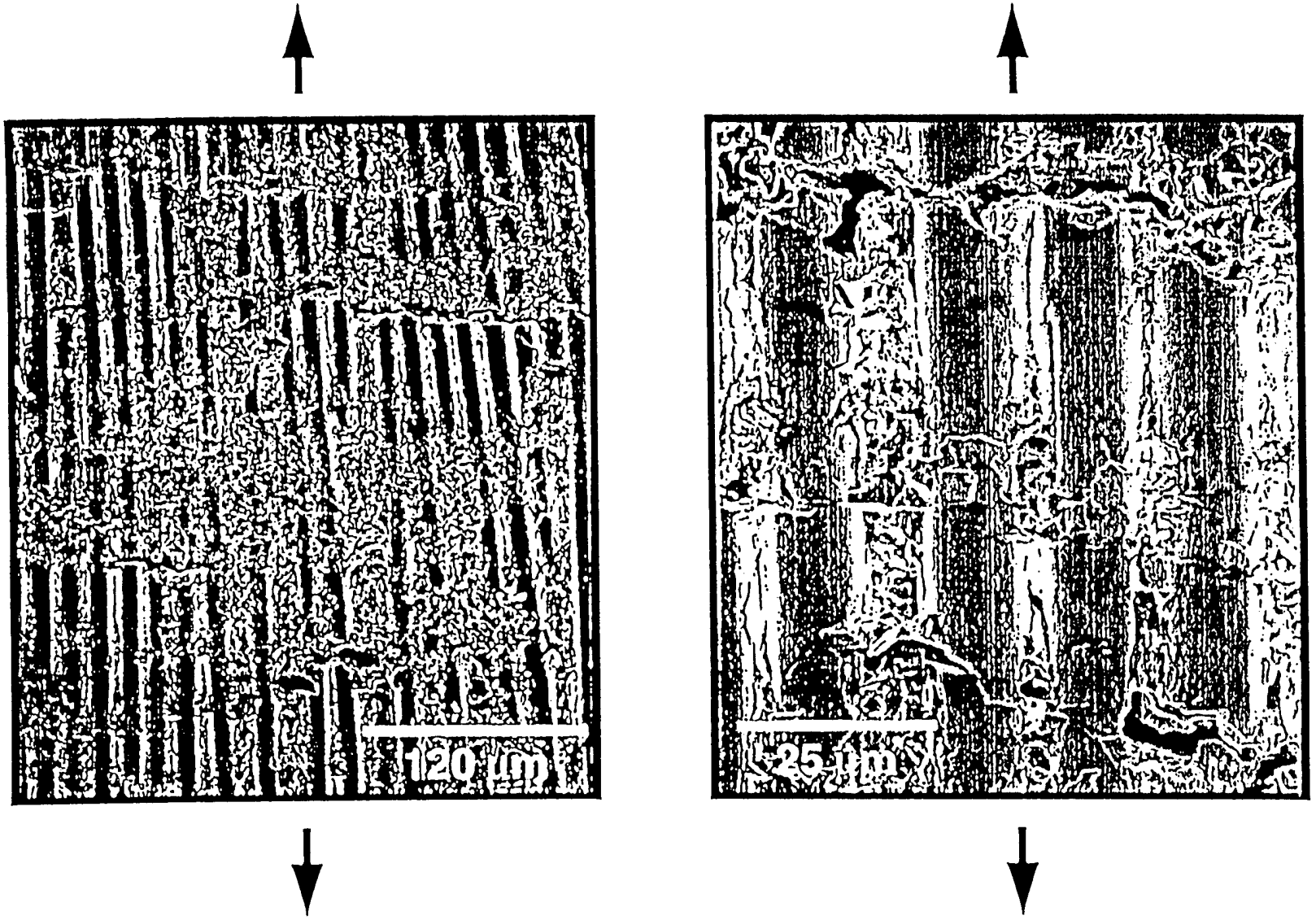

Figure 11. SEM micrographs of localized fiber fracture during fatigue.

the composite. The behavior of the composites also provided some insight into the damage mechanisms in the composite during fatigue.

Figure 12 shows the strength of the virgin material and residual strength of the BN filler composite after fatigue. The fatigued specimen had a very small amount of accumulated strain and the ultimate strength of the composite was higher than that of the virgin material. Furthermore, the stress-strain curve for the fatigued specimen was linear up to the applied maximum fatigue stress. The increase in strength is similar to that observed in a woven C/SiC composite investigated by Shuler et al. [4]. Similar to C/SiC, the mechanism responsible for higher strength after fatigue in Nicalon/Si-C-O-N is the alignment of the weave during fatigue. The matrix with BN filler was very compliant, so with relief of strain mismatches between bundles during fatigue the longitudinal bundles were allowed to stretch while the transverse bundles aligned themselves, Fig. 13. This process was believed to be aided by a Poisson-type effect during loading. With stretching of the weave, a higher strain to failure could be achieved, i.e., more load-carrying capability for the fibers which control the strength of the composite.

In the SiC filler composite, the residual strength of the composite after fatigue was about the same as that of the virgin material, Fig. 14. Because of the large clamping force of the matrix onto the fibers (from shrinkage of the polymer during conversion to ceramic) and subsequent cracks formed during processing, stretching of the weave and increases in strength were not observed in the composite. Furthermore, fracture in the SiC filler composite resulted in a planar fracture surface, with no sign of interlaminar shear, Fig. 15. Since fiber fracture likely did not take place at 200 MPa, the strength of the SiC composite remained the same as that of the virgin material.

IV. Conclusions

Several conclusions were obtained from this study of the high frequency fatigue behavior of Nicalon/Si-C-O-N matrix composites:

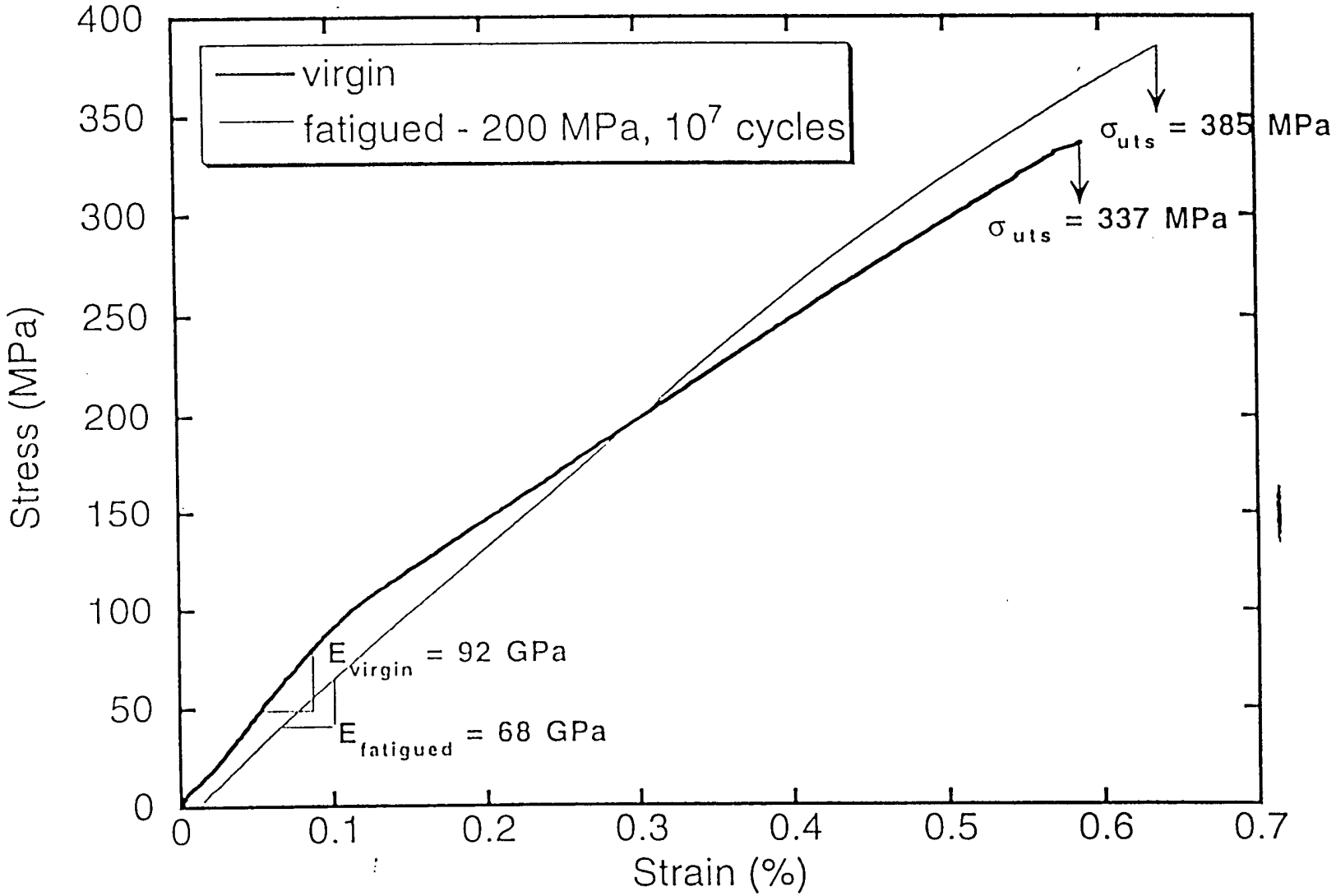

Figure 12. Residual strength after fatigue versus virgin material strength in the BN filler composite. Notice higher strength BN filler composite due to straightening and aligning processes of the fiber fabric during the fatigue process.

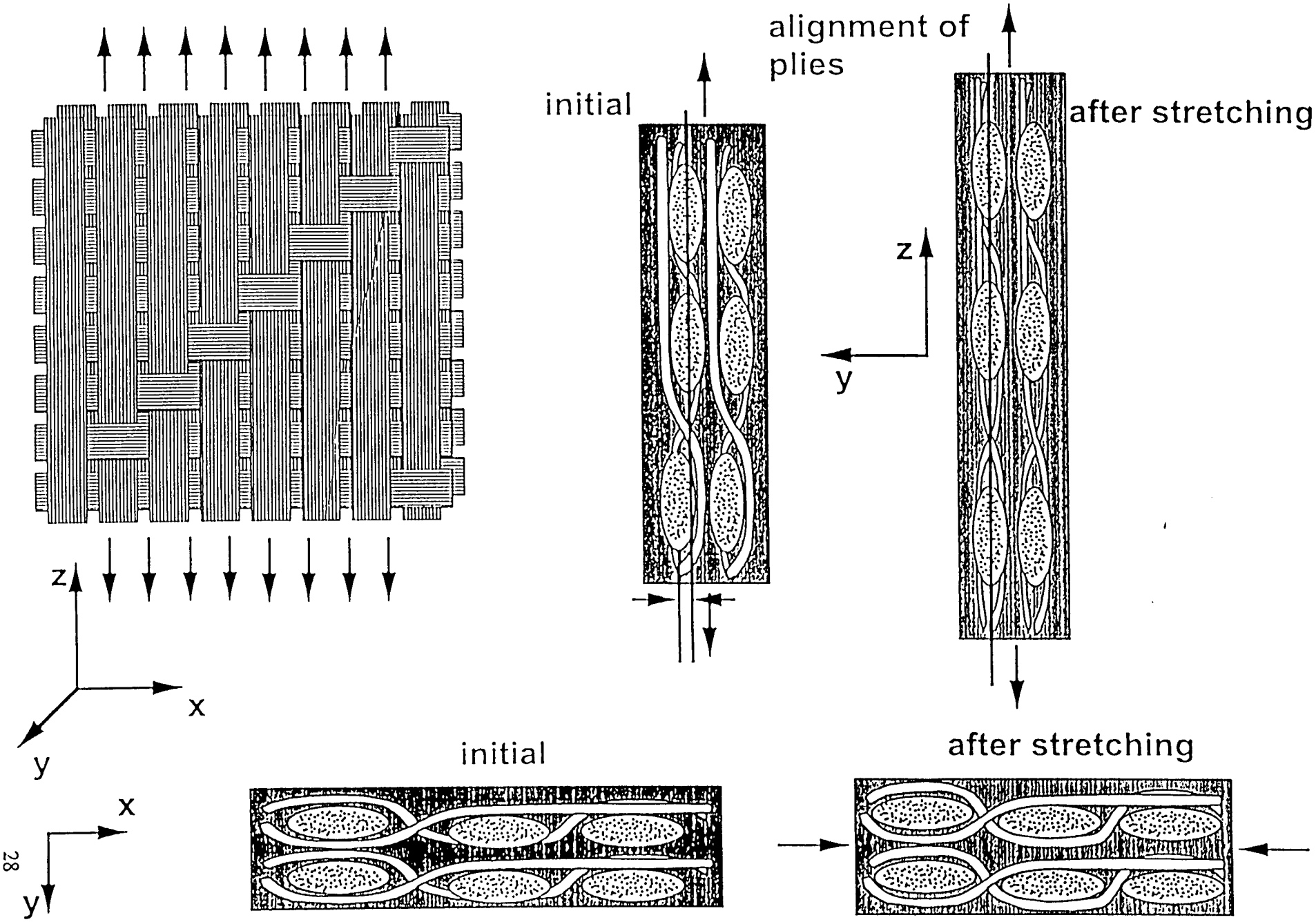

Figure 13. Schematic of the stretching of the weave and realignment of transverse fiber bundles which occurs during fatigue of Nicalon/Si-C-O-N with a BN filler.

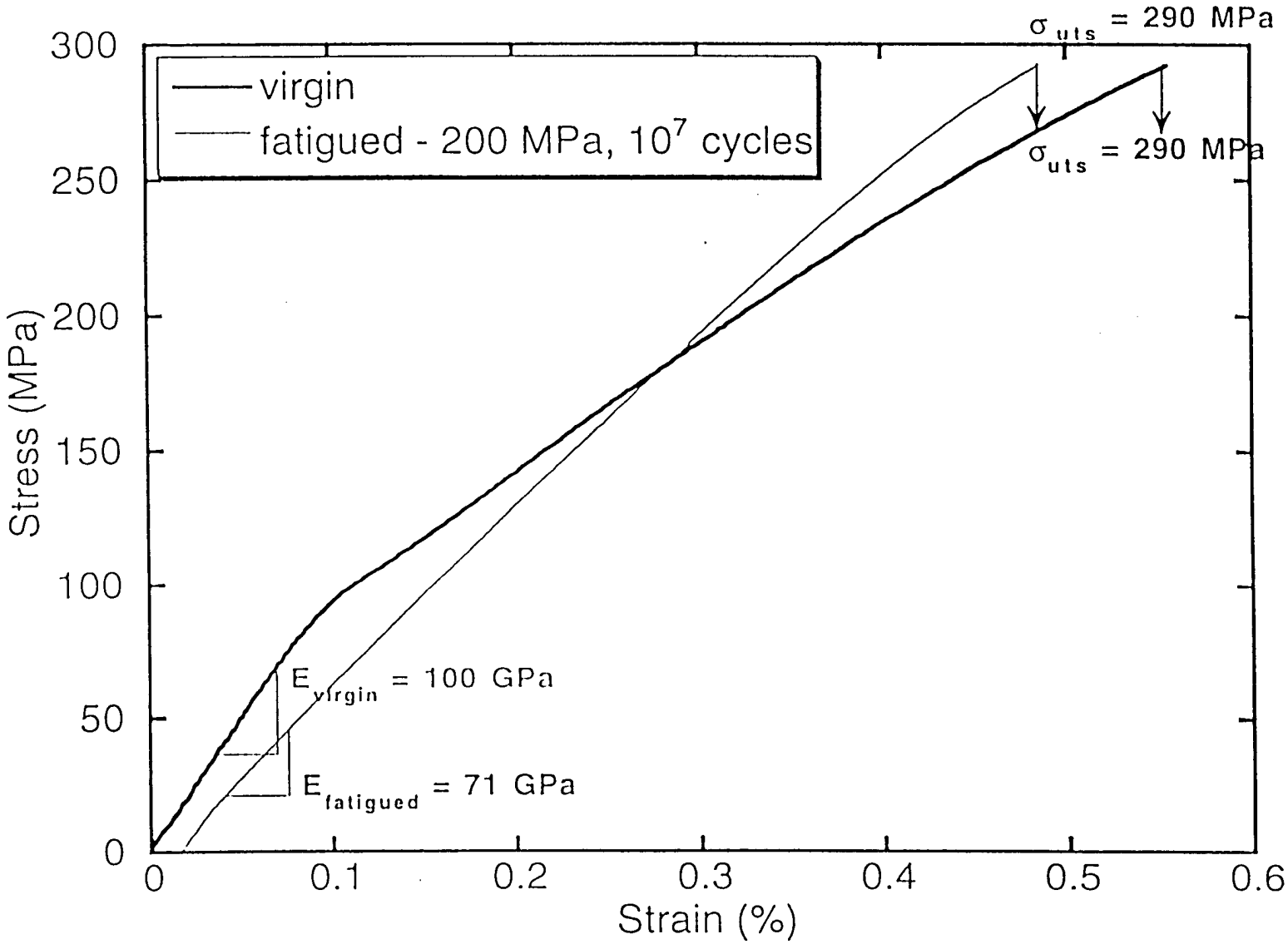

Figure. 14. Residual strength after fatigue versus virgin material strength in the SiC filler composite. Strengths between fatigued and virgin materials are similar due to the absence of weave-aligning processes.

interlaminar damage is not present. The higher magnification micrograph shows cracks from processing.

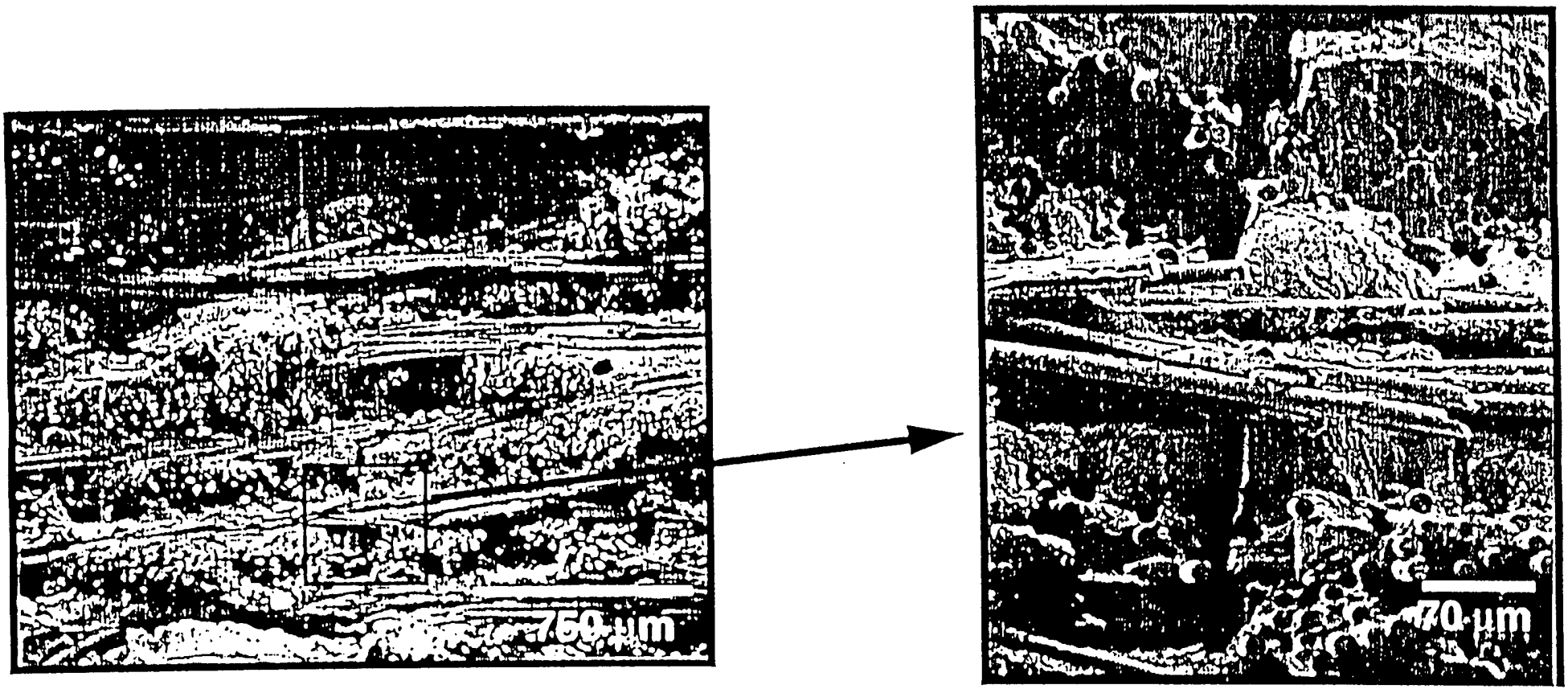

Figure 15. Fracture surface of the SiC filler composite showing planar fracture with little pullout. The higher stiffness of the matrix creates large residual clamping stresses on the fibers does not allow the weave to be stretched, so

- A strong interface between fiber and matrix hinders interfacial sliding and the amount of frictional heating during fatigue. Thus, the temperature rise observed in these composites was considerably less than that in composites with weak fiber/matrix interfaces.

- Since interface sliding is not a factor in this composite system, frequency does not seem to play a role in the fatigue life of the composite.

- Microstructural observations indicated that damage during fatigue occurred between cross-over points of longitudinal and transverse fiber bundles, which are postulated to occur due to strain mismatches between the bundles. By debonding these sites and relieving stress concentrations, alignment of the weave occurred in the BN filler composite resulting in higher post-fatigue strengths in that composite.

- Since clamping stresses on the fibers were higher in the SiC filler composite (arising from shrinkage during conversion from polymer to ceramic), weave stretching mechanisms were thought to be inhibited and thus, no increase in strength after fatigue was observed.

- The largest amount of damage during fatigue occurred during the first cycle, especially at or above the proportional limit of the composite, where the bulk of transverse-longitudinal ply debonding took place.

V. References

1. T. Kotil, J.W. Holmes, and M. Comninou, "Origin of Hysteresis Observed During Fatigue of Ceramic-Matrix Composites," *J. Am. Ceram. Soc.*, **73** 1879 (1990).

2. E. Dan-Jumbo, S.G. Zhou, and C.T. Sun, "Load-Frequency Effect on Fatigue Life of IMP6/APC-2 Thermoplastic Composite Laminates," p. 113 in Advances in Thermoplastic Composite Materials, ASTM STP 1044. Edited by G.M. Newaz. American Society for Testing Materials, Philadelphia, 1989.

3. J.W. Holmes and C. Cho, "Experimental Observations of Frictional Heating in Fiber-Reinforced Ceramics," *J. Am. Ceram. Soc.*, **75** [4] 929 (1992).

4. S.F. Shuler, J.W. Holmes, X. Wu, and D. Roach, "Influence of Loading Frequency of the Room-Temperature Fatigue of a Carbon-Fiber/SiC-Matrix Composite," *J. Am. Ceram. Soc.*, **76** 2327 (1993).

5. D. Koch and G. Grathwohl, "Tensile Fatigue Testing of SiC-SiC Composites," p. 217 in *Composites Testing and Standardization ECCM-CTS*, EACM, Bordeaux, France, 1992.

6. B.F. Sorensen and J.W. Holmes, "Improvement in the Fatigue Life of Fiber-Reinforced Ceramic by use of Interfacial Lubrication," *Scripta Met. et. Mater.*, **32** 1393 (1995).

7. R. Lundberg, R. Pompe, R. Carlsson, "Fibre Reinforced Silicon Nitride Composites," *Comp. Sci. Tech.*, **37** 165 (1990).

8. F. Sirieix, P. Goursat, A. Lemcote, and A. Dauger, "Pyrolysis of polysilazanes: relations between the architecture of the precursors and the microstructure of the ceramics," *Comp. Sci. Tech.*, **37** 7 (1990).

9. K. Sato, H. Morozumi, A. Tezuka, O. Funayama, and T. Isoda, "Interface and Mechanical Properties of Ceramic Fiber Reinforced Silicon Nitride Composites Prepared by a Preceramic Polymer Impregnation Method," p. 199 in *High Temperature Ceramic-Matrix Composites II*, (Santa Barbara, CA, February, 1995). Edited by A.G. Evans and F.W. Zok. American Ceramic Society, Westerville, OH, 1995.

10. M.F. Gonon, G. Fantozzi, M. Murat, and J.P. Disson, "Association of the CVI Process and of the Use of Polysilazane Precursor for the Elaboration of Ceramic Matrix Composites Reinforced by Contunous Fibers," *J. Eur. Ceram. Soc.*, **15** 185 (1995).

11. P. Greil, "Active-Filler-Controlled Pyrolysis of Preceramic Polymers," *J. Am. Ceram. Soc.*, 78 835 (1995).

12. E. Lara-Curzio, private communication.

13. ASTM Standard for Monotonic Tensile Strength Testing of Continuous Fiber Advanced Ceramics with Solid Rectangular Cross-Section Specimens at Elevated Temperatures, ASTM Subcommittee C28.07 on Ceramic Matrix Composites, Rev. 1.5, June 1994.

14. E. Lara-Curzio, M.K. Ferber, R. Boisvert, and A. Szweda, "The High Temperature Tensile Fatigue Behavior of a Polymer-Derived Ceramic Matrix Composite," *Ceram. Eng. Sci. Proc.*, 16 341 (1995).

15. E. Petitpas, M. Renault, and D. Valentin, "Fatigue Damage Mechanisms in (0/90)s Composite Laminate," *J. Mater. Sci. Lett.*, 8 1029 (1989).

16. P.T. Curtis, "The Fatigue Behaviour of Fibrous Composite Materials," *J. Strain. Anal.*, 24 235 (1989).

17. Z.G. Wang, C. Laird, Z. Hashin, B.W. Rosen, C.-F. Yen, "Mechanical Behaviour of a Cross-Weave Ceramic Matrix Composite - Part I, Tensile and Compressive Loading," *J. Mater. Sci.*, 26 4751 (1991).

18. Z.G. Wang, C. Laird, Z. Hashin, B.W. Rosen, C.-F. Yen, "Mechanical Behaviour of a Cross-Weave Ceramic Matrix Composite - Part II, Repeated Loading," *J. Mater. Sci.*, 26 4751 (1991).

19. P. Karandikar and T.-W. Chou, "Damage Development and Moduli Reductions in Nicalon-Calcium aluminosilicate Composites under StaticFatigue and Cyclic Fatigue," *J. Am. Ceram. Soc.*, 76 1720 (1993).

20. Z.R. Xu, K.K. Chawla, A. Wolfenden, A. Neuman, G.M. Liggett, and N. Chawla, "Stiffness loss and density decrease due to thermal cycling in an alumina fiber/magnesium alloy composite," *Mater. Sci. & Eng. A*, A203 75 (1995).

21. N. Chawla and J.W. Holmes, unpublished work.

22. E. Lara-Curzio and M.K. Ferber, "A Methodology for the Determination of the Interfacial Properties of Brittle Matrix Composites," *J. Mater. Sci.*, (1995).

23. D. Koch and G. Grathwohl, "S-Curve-Behavior and Temperature Increase of Ceramic Matrix Composites During Fatigue Testing," in *High Temperature Ceramic-Matrix Composites II*, (Santa Barbara, CA, February, 1995). Edited by A.G. Evans and F.W. Zok. American Ceramic Society, Westerville, OH, 1995.

IV. Effect of Interfacial Coating Thickness on the High Frequency Fatigue Behavior of Woven Continuous Fiber Reinforced SiC Matrix Composites with a Weak Fiber/Matrix Interface

N. Chawla, J.W. Holmes, and R.A. Lowden

I. Introduction

A significant number of researchers have shown that, under monotonic loading, a weak fiber/matrix interface is desirable in obtaining toughness and graceful failure in CFCCs [1-3]. Such an interface is usually accomplished by the insertion of a thin coating (typically 0.1-1 μm thick) such as C or BN, which is compliant enough to relieve residual clamping stresses from processing, and whose structure consists of several weakly bonded basal planes. These planes in the coating promote such mechanisms as fiber debonding, crack deflection, and finally fiber pullout from the matrix - all of which serve to dissipate energy during fracture and provide toughness in the composite. Recently, however, it has been shown that while a weak fiber/matrix interface is desirable from a monotonic loading standpoint, it is quite detrimental during fatigue - especially at high loading frequencies [4-6]. Holmes et al. [5] showed that in a unidirectional Nicalon/CAS composite with a weak interface, increasing loading frequency caused a significant decrease in fatigue life. Due to repeated frictional sliding of fibers, a significant amount of heat is generated by the specimen, and a large temperature rise is observed. In fact, Sorensen and Holmes [7] have shown that immersing specimens in oil, in order to create a "lubricating" layer at the fiber/matrix interface, can dramatically improve the fatigue life of the composite. this improvement may be attributed to a fundamental change in t and/or a significant decrease in fiber damage provided by the lubricating layer.

Following this observation of Sorensen and Holmes [7], we have hypothesized that thicker interfacial coatings may improve the fatigue life of CFCCs. To this end, Nicalon/SiC composites were examined, with a carbon

coating of 0.33 and 1.1 μm. The samples were identical in nature, except for the interfacial coating thickness.

II. Materials and Experimental Procedure

Nicalon/C/SiC composites were fabricated by chemical vapor infiltration (B.F. Goodrich Co., Los Angeles, CA). Details of the CVI fabrication process are given elsewhere [8]. The fibers were woven into a plain-weave fabric and coated with chemically vapor deposited (CVD), pyrolitic carbon. The composite had 10 plies per 0.25 cm and a nominal fiber volume fraction of 40%. Specimens were machined to an edge-loaded configuration, and tested in an isothermal chamber where specimen temperature measurements were taken. Specimens were tested at loading frequencies of 100 and 350 Hz.

III. Results and Discussion

Under monotonic loading, Fig. 1, both composites exhibited similar strength. The higher strain to failure observed in 1.1 μm coated material may be attributed to the lower magnitude of residual compressive stresses on the fibers in the composite. With a thicker layer of the compliant C interface, the residual stresses on the fiber are decreased. Thus, with lower residual clamping stresses, a greater amount of pullout was observed. The similarity in strength of the two composites is to be expected since the strength is controlled by the fiber architecture and volume fraction of the fibers, which were the same for both composites.

During fatigue significant differences in temperature rise and degradation in modulus were observed between the two materials. Substantial damage in terms of modulus (averaged from stress-strain hysteresis loops) was observed, with most of the damage occurring during the first cycle, Fig. 2. At a constant stress, the level of damage was not significantly dependent on frequency, Fig. 3.

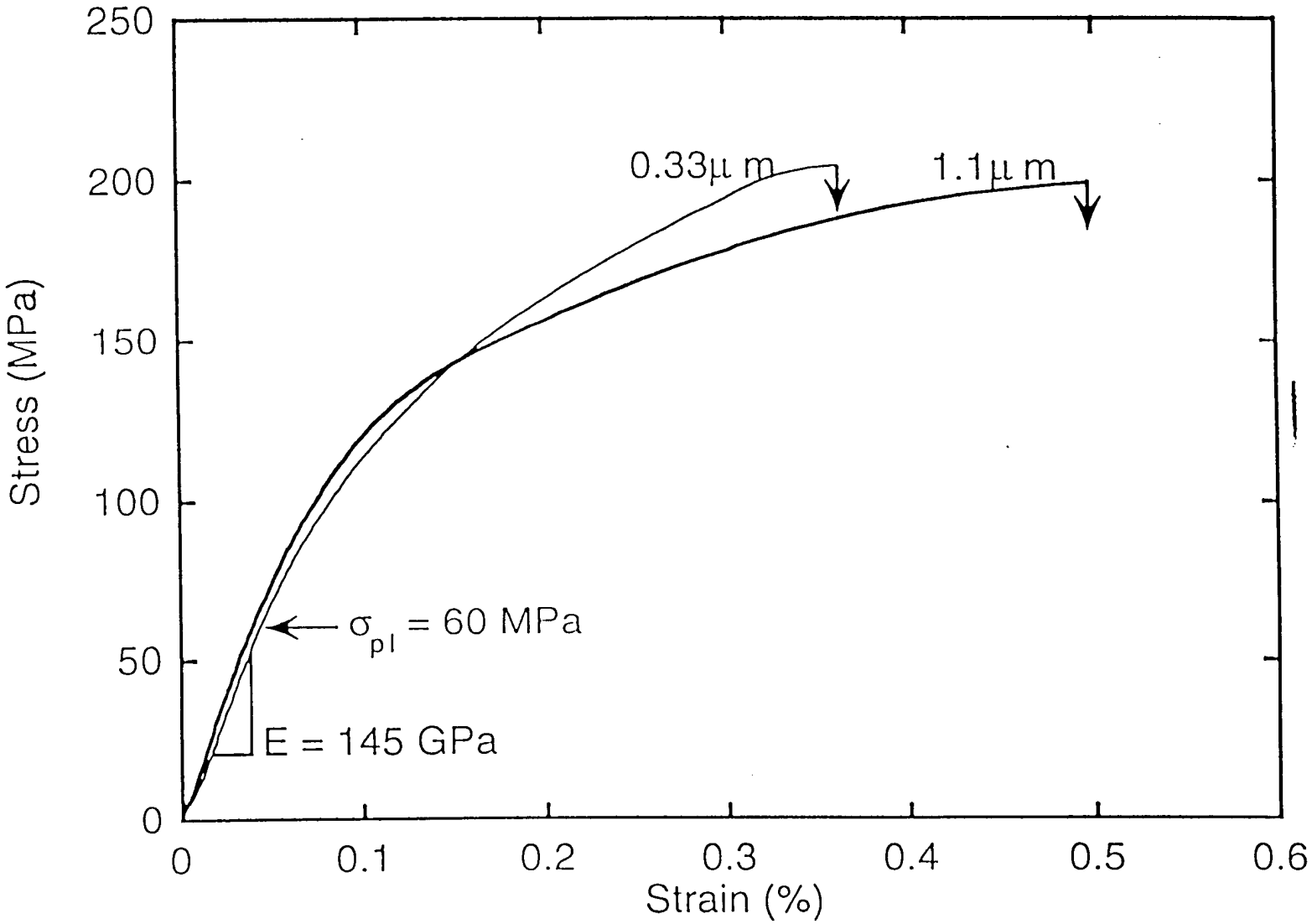

Figure 1. Monotonic tension curves for Nicalon reinforced SiC matrix composites with varying carbon coating thickness.

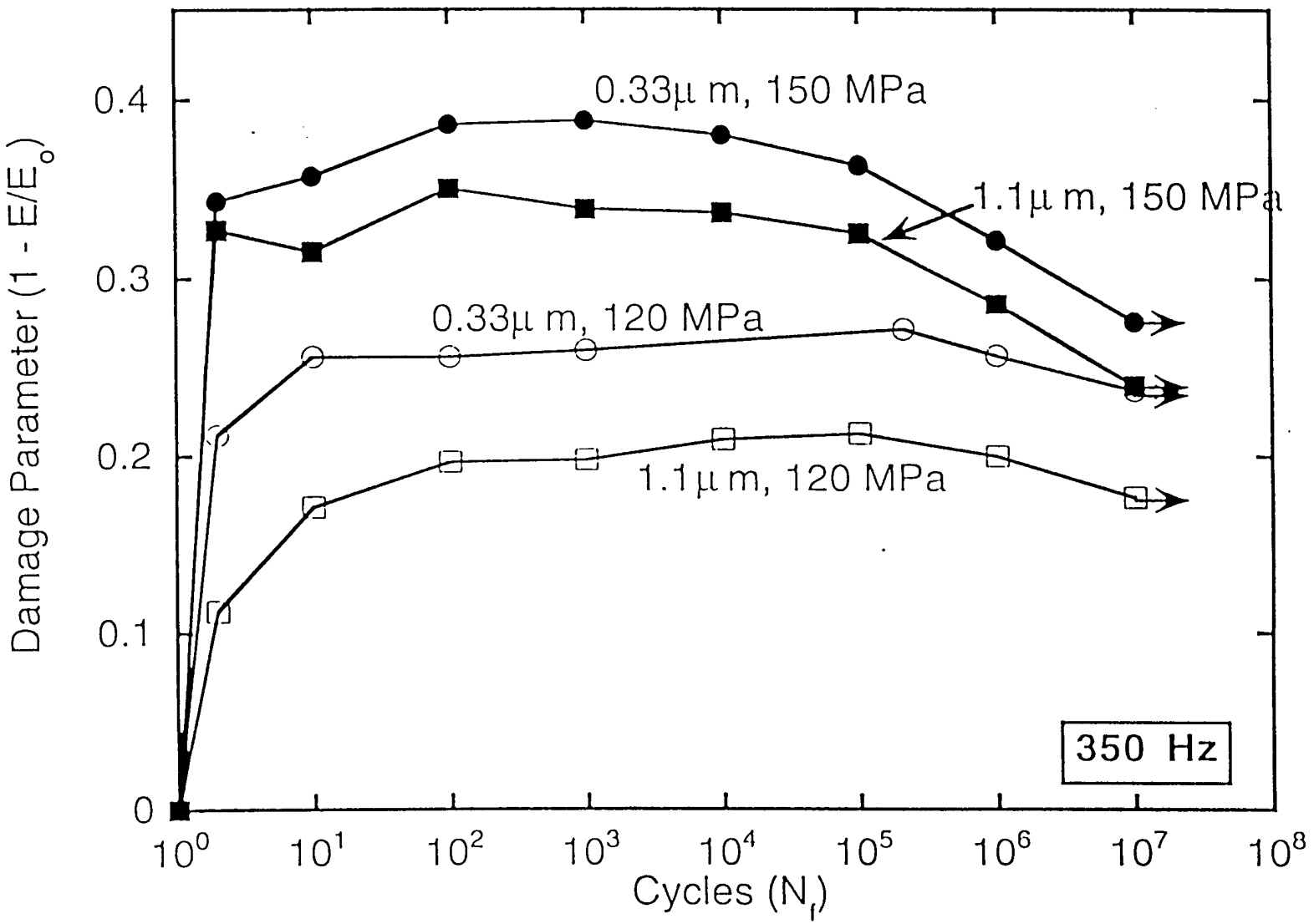

Figure 2. Effect of applied stress on the damage evolution, D_E (1-E/E$_o$), in Nicalon/C/SiC composites.

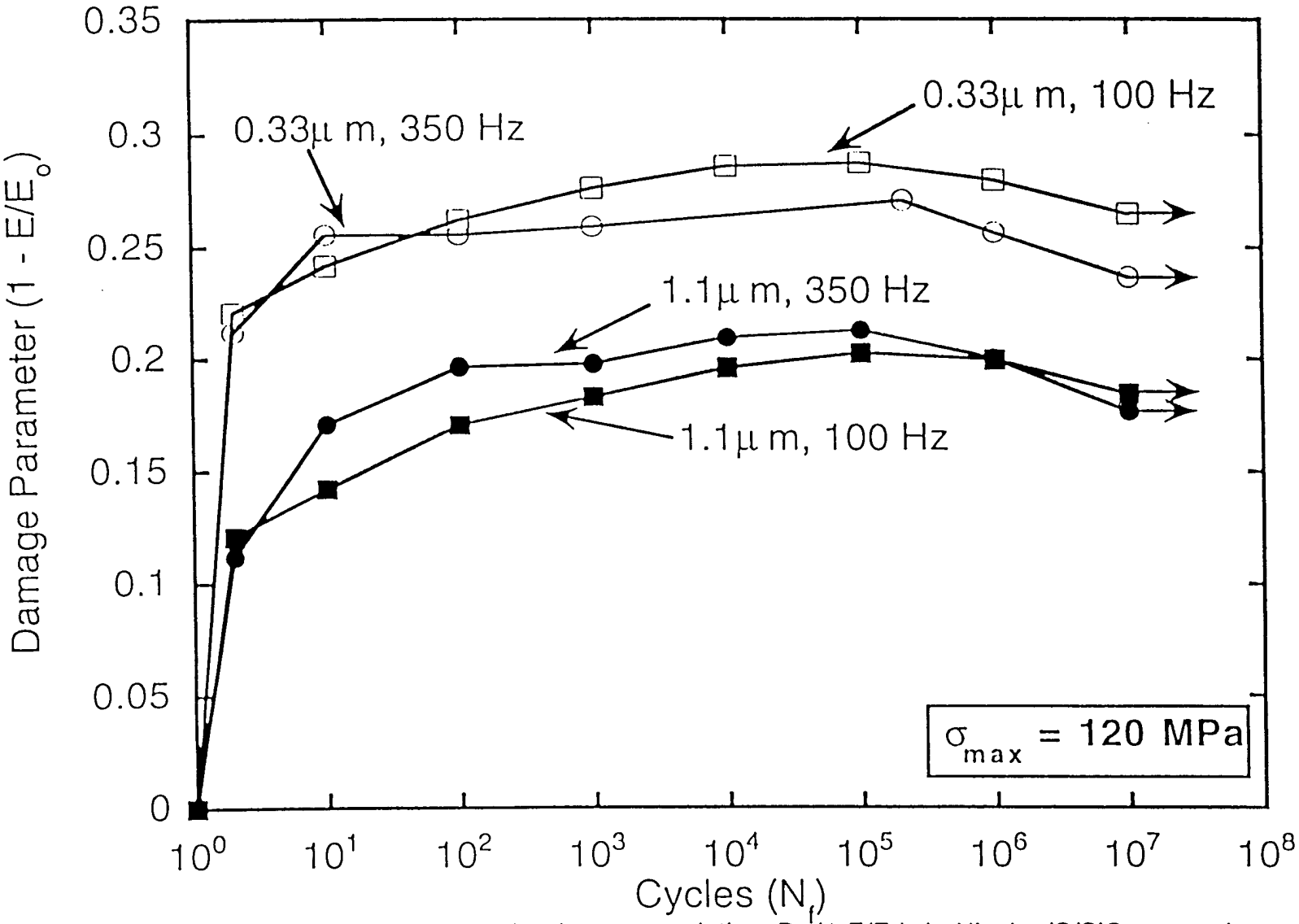

Figure 3. Effect of frequency on the damage evolution, D_E (1-E/E$_o$), in Nicalon/C/SiC composites.

At a given frequency, however, higher stresses induced more damage in both composites, Fig. 2. The large amount of damage that occurred in the first cycle, a phenomenon observed in a variety of woven composites, was believed to be due to the localized debonding of transverse and longitudinal plies at the crossover points in the fabric, which, when linked, promoted interlaminar damage and failure in the composite. This observation is similar to that of Shuler et al. [9] who witnessed similar behavior in a plain weave C/SiC system. For stress levels at which the composite did not fail, debonding at the crossover sites was believed to allow geometric alignment of the weave. On a macroscopic level, these geometric alignment mechanisms seem to explain the recovery in moduli of the composites during the later stages of fatigue. It is interesting to note that the recovery in modulus was more pronounced and occurred at an earlier number of cycles at the higher applied stresses. Failure in Nicalon/C/SiC composites, on a macroscopic level, consisted of localized matrix damage at the points where adjacent lamina were bonded to each other, Fig. 4.

Along with damage in elastic modulus, significant temperature increases were observed during fatigue of the specimens. Figure 5 shows the effect of frequency on the temperature rise of both composites. As hypothesized, at both 100 Hz and 350 Hz, the composite with the thinner coating exhibited much higher frictional heating. The thicker coating seemed provide protection to the fiber against abrasion damage, which resulted in less frictional heating and wear of the fibers during fatigue. Thus, just as oil served as a lubricant in Nicalon/CAS, the thicker C coating in Nicalon/SiC was a more effective lubricant during high frequency fatigue. At higher stresses more significant heating was observed, Fig. 6. A similar trend was reported by Koch and Grathwohl [10] in 100 Hz fatigue of Tyranno/C/SiC composites, although much higher temperatures were observed in the latter study. It should be noted that the higher heat generation (and resulting temperature increase) with increasing frequencies for both composites was simply due to an increase in the energy dissipated per unit time.

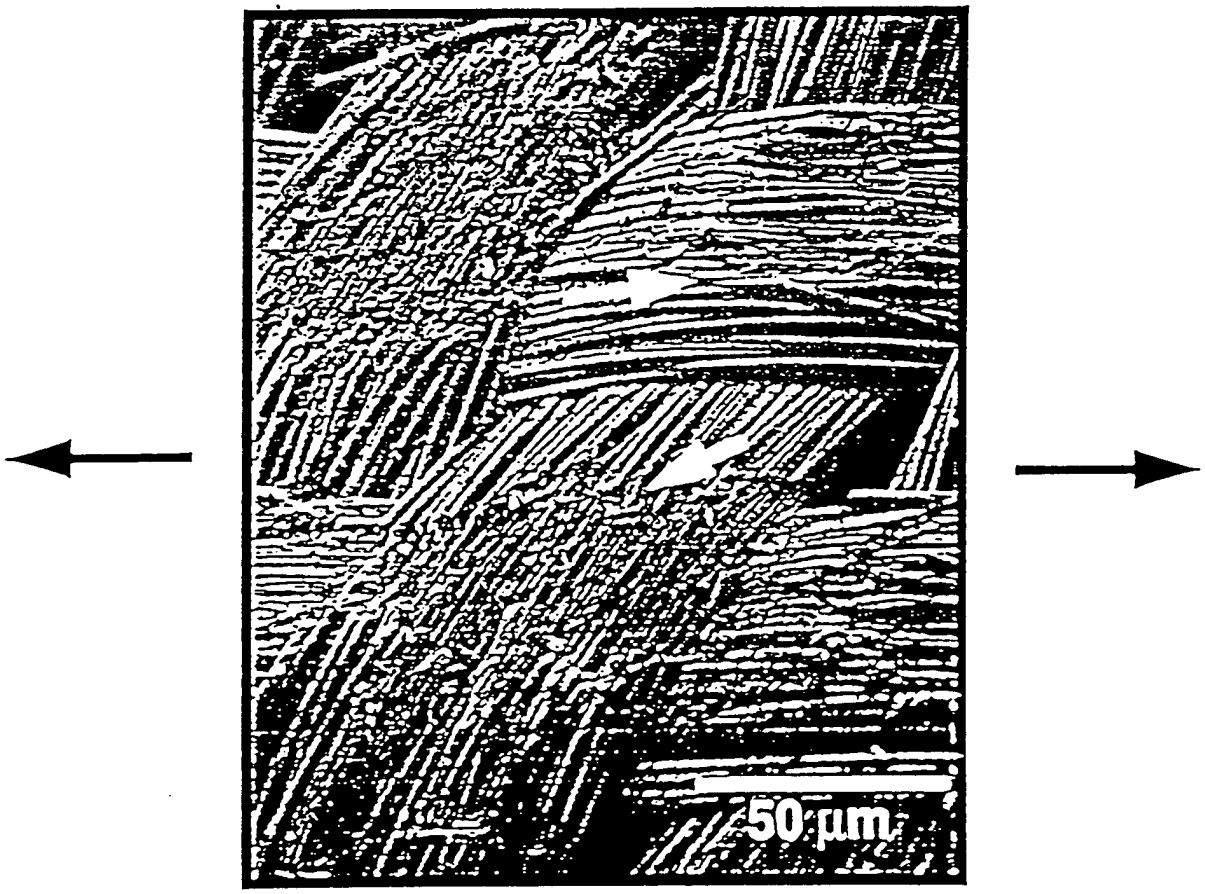

Figure 4. Macroscopic damage around points where lamina were bonded to each other.

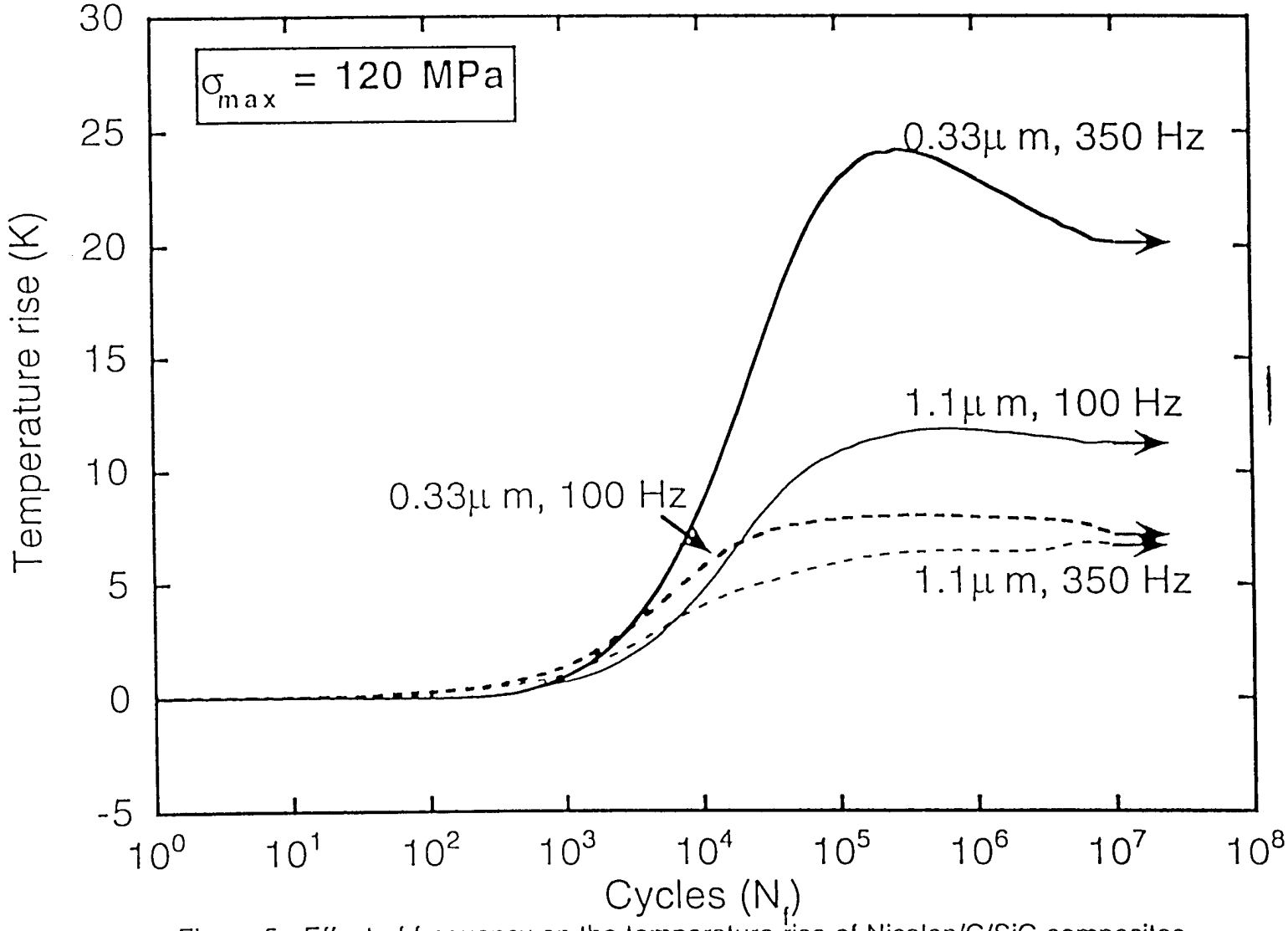

Figure 5. Effect of frequency on the temperature rise of Nicalon/C/SiC composites.

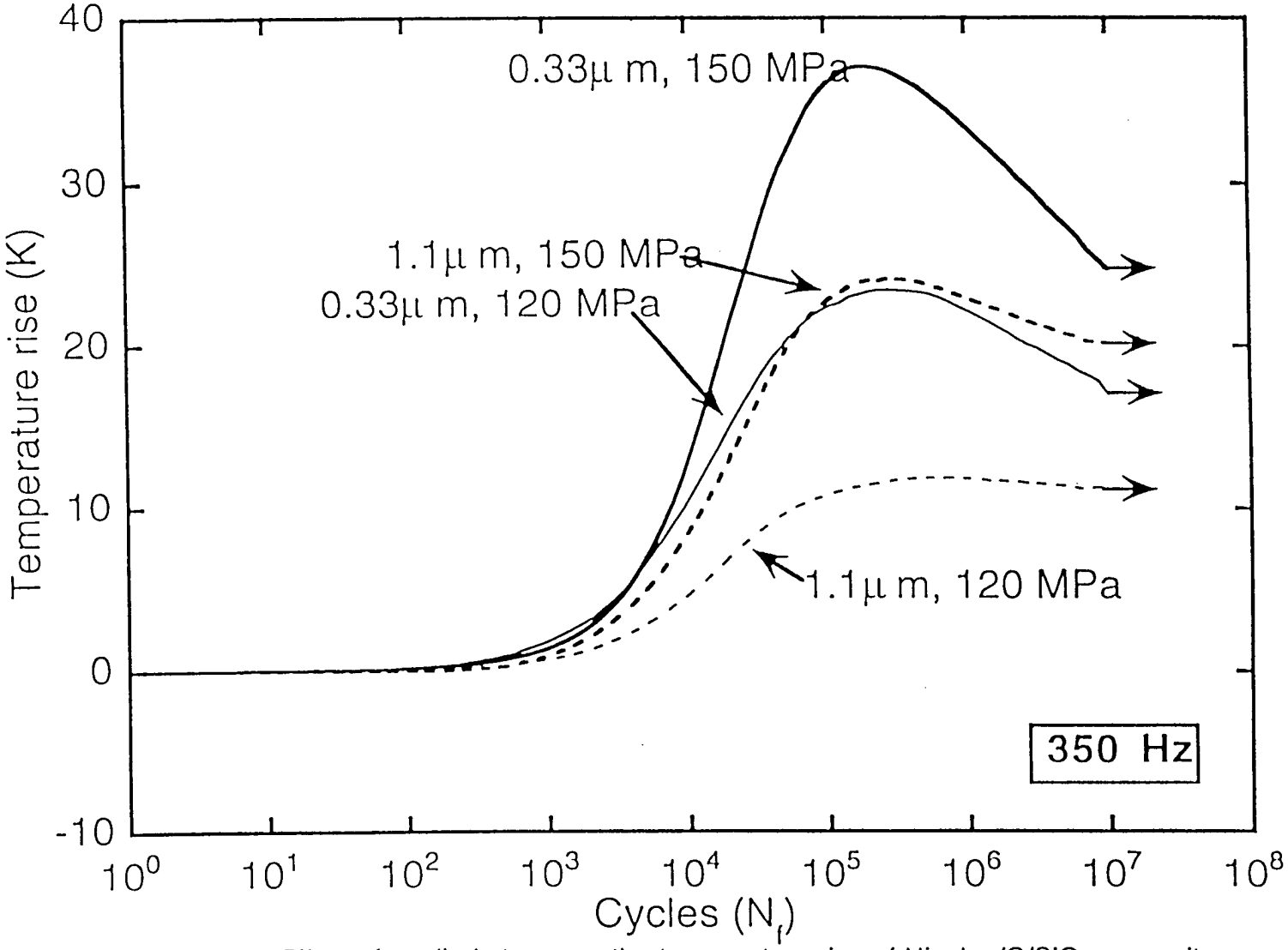

Figure 6. Effect of applied stress on the temperature rise of Nicalon/C/SiC composites.

It is interesting to note that a decrease in temperature was observed after 10^5 cycles, Fig. 5, which paralleled the recovery in modulus. On the microscopic level then, the recovery in modulus may be due to an increase in the interfacial shear stress at the fiber/matrix interface, τ. Such an increase in τ may be caused by the wedging of particles or asperities between fiber/fiber or fiber/matrix interfaces, shown in Fig. 7, which inhibited the sliding of the fibers. While increasing the friction and inhibiting sliding, these asperities serve a detrimental role by acting as stress concentrators that cause increased fiber failure during fatigue. Thus, by having a thicker coating, the fibers can be protected from these stress concentrators for a longer period of time. A schematic of possible wear mechanisms at the fiber/matrix interface, at the microscopic level, is shown in Fig. 7. These include trapping of particles or asperities, sharp points of contact, and embedding of particles or asperities in the fibers - all of which act as stress concentrations and cause fiber failure.

IV. Conclusions

The following conclusions can be made on the high frequency fatigue behavior of Nicalon/C/SiC composites:

- Thicker coatings on the fibers are more effective in reducing the amount of fiber wear and damage which occur during high frequency fatigue. Thicker, more lubricating coatings are more effective in inhibiting frictional heating in these composites.

- On a macroscopic level, geometric alignment of the weave seems to be responsible for the recovery in modulus in the later stages of fatigue.

- On a microscopic level, wear mechanisms at the interface include trapping of particles or asperities, sharp points of contact, and embedding of particles or

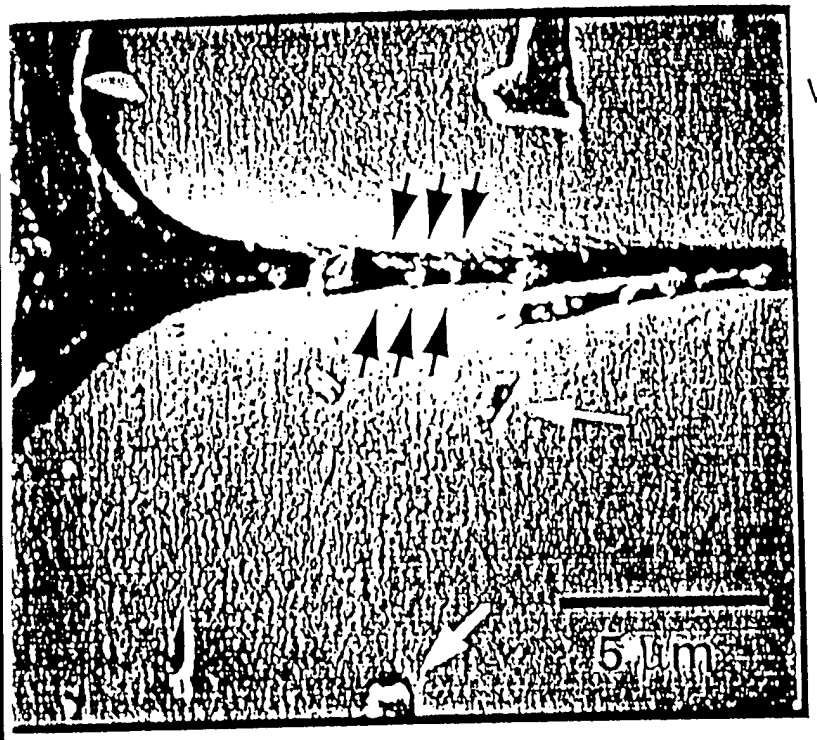

(a)

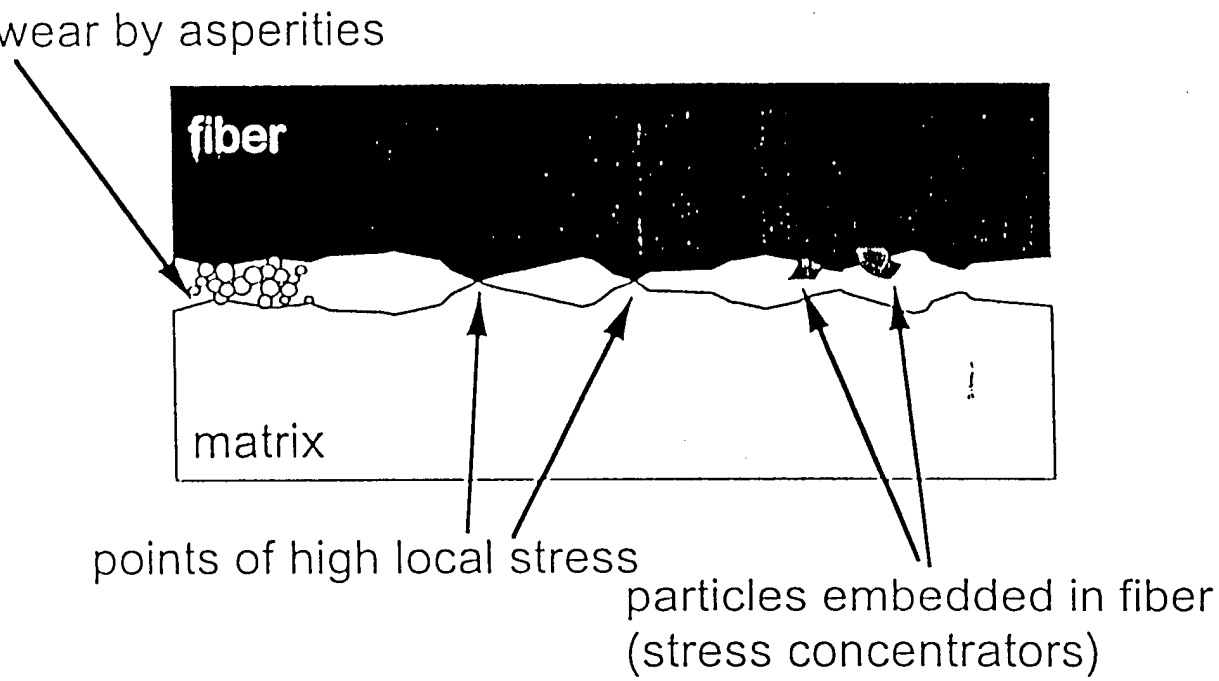

(b)

Figure 7. (a) Wear and trapping of asperities at the fiber/matrix interface and (b) possible wear and damage mechanisms at the fiber/matrix interface.

asperities in the fibers - all of which act as stress concentrations and cause fiber failure.

V. References

1. R.A. Lowden and D.P. Stinton, *Ceram. Eng. Sci. Proc.*, 9, 705 (1988).

2. R.W. Goettler and K.T. Faber, *Comp. Sci. and Tech.*, 37, 129 (1989).

3. K.K. Chawla, M.K. Ferber, Z.R. Xu, .and R. Venkatesh, *Mater. Sci. and Eng.*, A162, 35 (1993).

4. J.W. Holmes and C. Cho, *J. Am. Ceram. Soc.*, 75, 929 (1992).

5. J.W. Holmes, X. Wu, and B.F. Sorensen, *J. Am. Ceram. Soc.*, 77, 3284 (1994).

6. S.F. Shuler, J.W. Holmes, X. Wu, and D. Roach, *J. Am. Ceram. Soc.*, 76, 2327 (1993).

7. B.F. Sorensen and J.W. Holmes, *Scripta Met. et Mater.*, 32, 1393 (1995).

8. T.M. Besmann, B.W. Sheldon, R.A. Lowden, D.P. Stinton, *Science*, 253, 1104 (1991).

9. N. Chawla, Y.K. Tur, J.W. Holmes, J.R. Barber, and A. Szweda, submitted to *J. Am. Ceram. Soc.*

10. D. Koch and G. Grathwohl, Composites Testing and Standardization ECCM-CTS, p. 217, EACM, Bordeaux, France, (1992).

V. Effect of Laminate Stacking Sequence on the High Frequency Fatigue Behavior of SCS-6 Fiber Reinforced Si_3N_4 Composites

N. Chawla

I. Introduction

In this work, the effect of laminate stacking sequence on the frictional heating behavior under high frequency fatigue, was investigated. Two laminated SCS-6 fiber reinforced Si_3N_4 composites with stacking laminate stacking sequences of [0/90] and [±45] were used. Damage in both systems was quantified by stress-strain hysteresis loops and elastic modulus reduction.

II. Materials and experimental procedure

The SCS-6/Si_3N_4 composites used in this study were fabricated by dry-powder layup and hot pressing [1]. SCS-6 fibers are about 140 μm in diameter and have a composite structure Fig. 1. The center of the fiber consists of a carbon mandrel, on which β-SiC is deposited by chemical vapor deposition (CVD). The layer on the carbon core is carbon rich β-SiC, followed by a layer of stoichiometric β-SiC. The surface of the fiber is coated with carbon, which provides an interface conducive to debonding, crack deflection, and fiber pullout in the composite. The matrix powder, consisting of 94% Si_3N_4, 5% Y_2O_3, and 1% MgO (wt. %), had a nominal particle size of 0.5 μm. Fiber volume fraction was 30%. Hot pressing was conducted in vacuum at an applied pressure of 70 MPa and a temperature of 1700°C. The composites had a theoretical density of 98%.

A micrograph of the fiber distribution in the [0/90] composite is shown in Fig. 2(a). While the fiber distribution is fairly homogenous, notice that residual porosity exists between fiber and matrix, in the as-received condition, Fig. 2(b). Double-tapered edge-loaded specimens were machined using diamond tooling. A schematic of the edge-loaded configuration is shown in Fig. 3. The gauge section of the specimens was polished to a 0.25 μm finish using

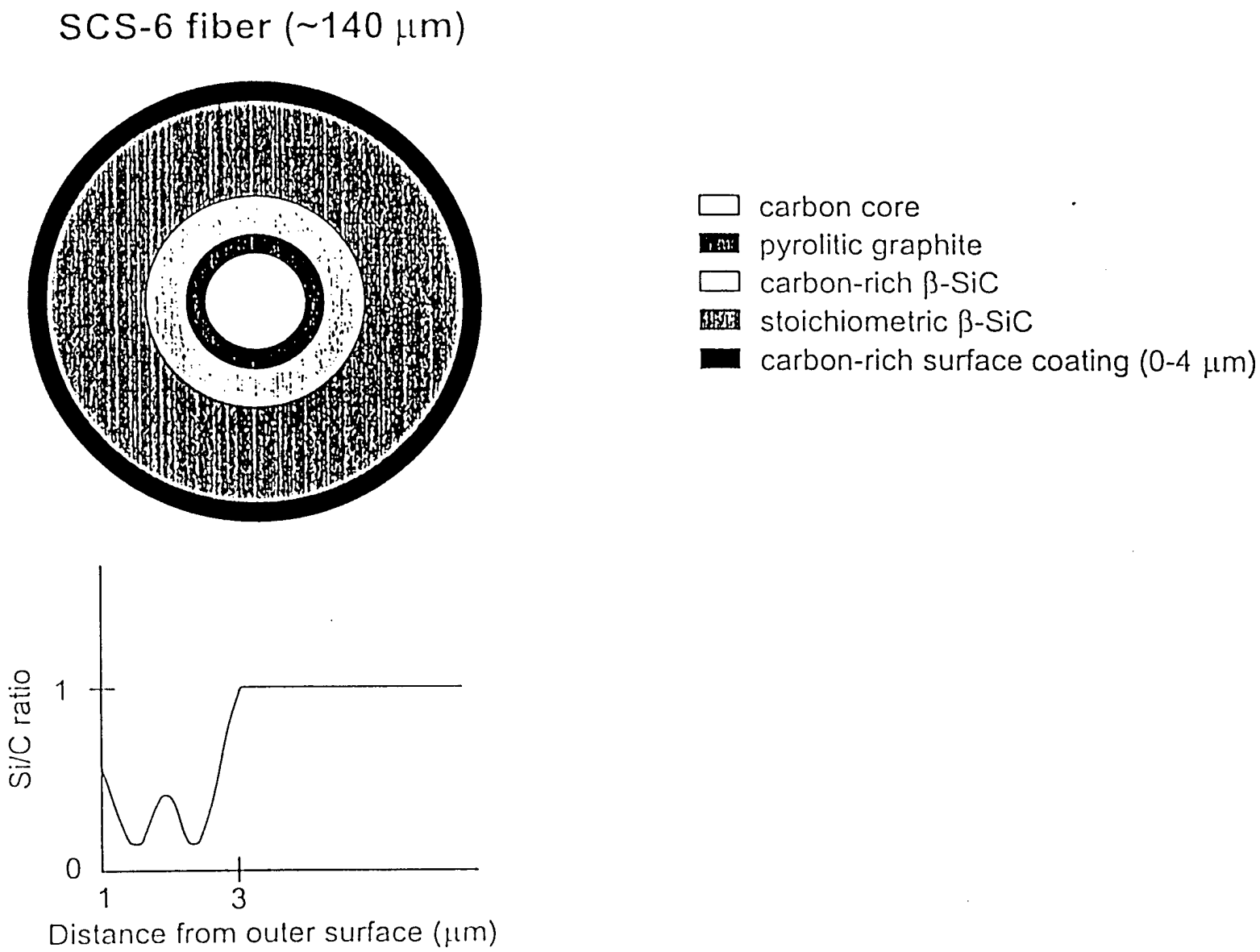

Figure 1. Schematic and compositional profile of an SCS-6 composite fiber.

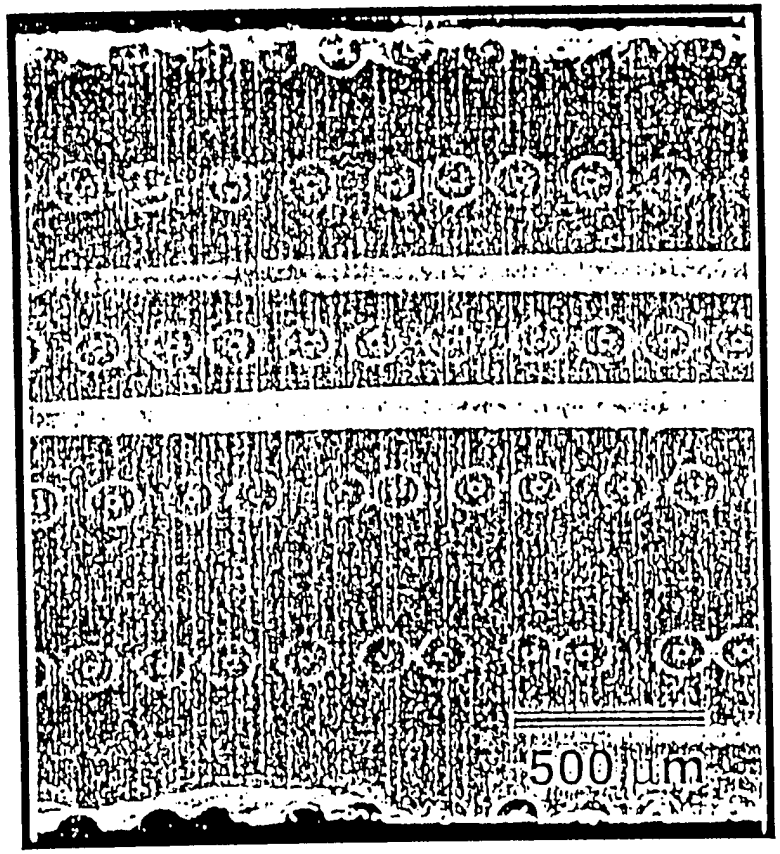

(a)

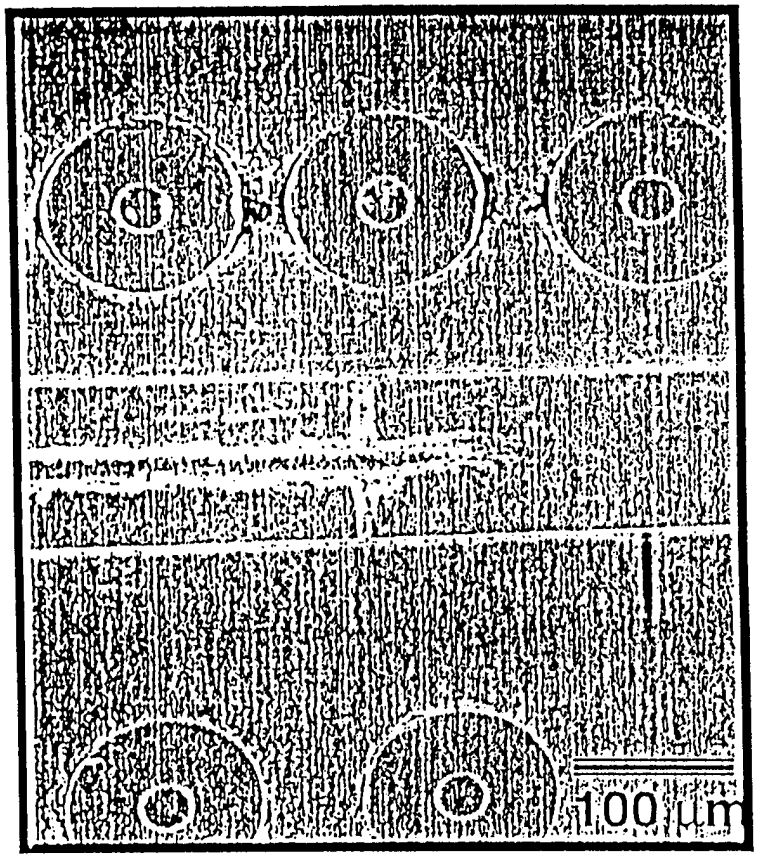

(b)

Figure 2.(a) SEM micrograph of fiber distribution in [0/90] composite in the as-received condition showing homogeneous fiber distribution, and (b) residual porosity between fiber and matrix.

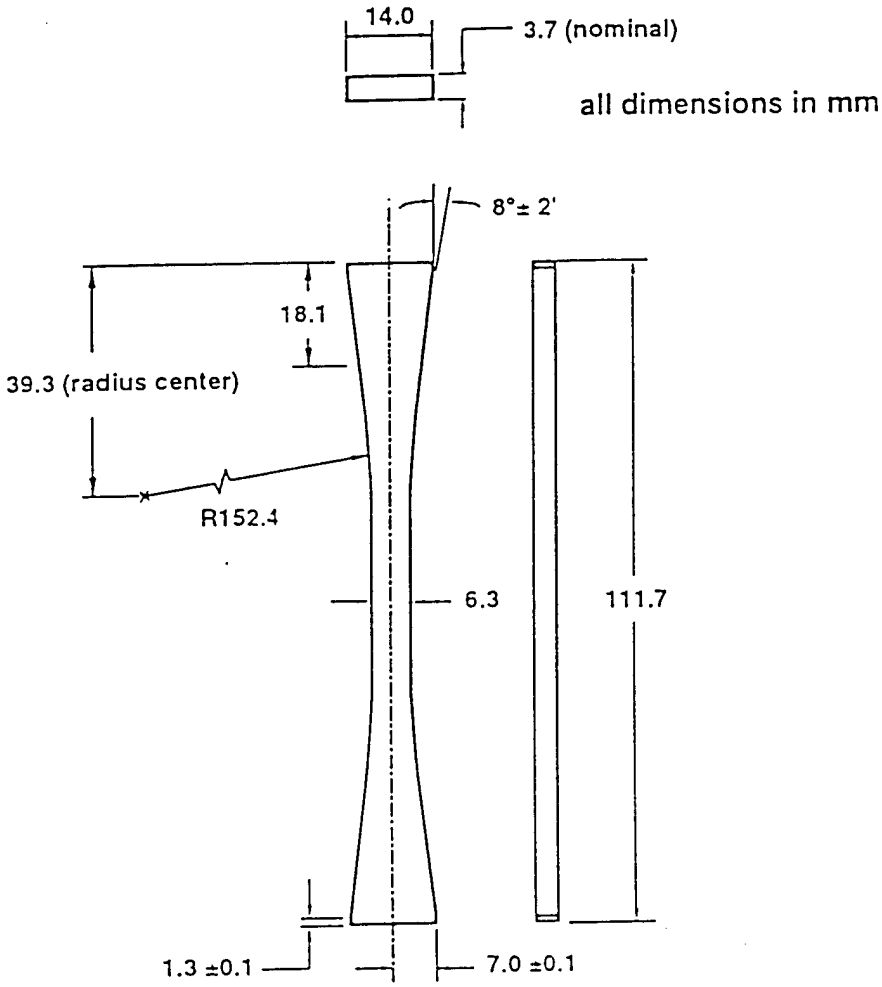

Figure 3. Schematic of the edge-loaded tensile specimen used in high frequency experiments.

diamond paste, and replicas were taken at different stages of the test to observe any cracking.

Specimens of both orientations were fatigued at 100 Hz for 20,000 cycles each at increments of 40, 80, 120 MPa, etc. until failure occurred. Stress-strain loops and temperature data were acquired for each loading increment. After each loading step, the specimen was unloaded to 10 MPa and a replica was taken. Replicas were taken at low stresses to prevent cracking at static loads. Fractured surfaces were examined using scanning electron microscopy.

III. Results and discussion

The laminate stacking sequence had a profound effect on frictional heating and fatigue behavior of the SCS-6/Si_3N_4 composites. Figure 4 shows the stress-strain hysteresis loops for the [0/90] composite. Very little hysteresis is present at lower stresses but at higher stresses, such as 240 MPa, the frictional sliding of the fibers within the matrix causes significant hysteresis. The temperature rise associated with each stress level indicates the extent of frictional heating. At low stresses a change in temperature, ΔT, of only 0.1°C was observed, Fig. 5. At 200 MPa the temperature rise was close to 1°C, before failure at 240 MPa. In all temperature profiles, the temperature increases rapidly and reaches a plateau during cycling. When the 20,000 cycles were over a gradual decay in temperature was observed.

It is interesting to note that frictional heating in this composite system begins at very low stresses (~40 MPa). In other composite systems the onset of frictional heating was correlated to the matrix cracking stress, and occurred at higher stresses. The inherent porosity at the fiber/matrix interface in Fig. 2(b), while slight, is enough for sliding and frictional heating to begin at low stresses, since the fiber is debonded from the matrix before testing.

The decrease in modulus of the composite correlates very well with the observed temperature rise, Fig. 6. The modulus decays with increasing stress amplitude, from 330 to 268 before failure, while temperature increases steadily.

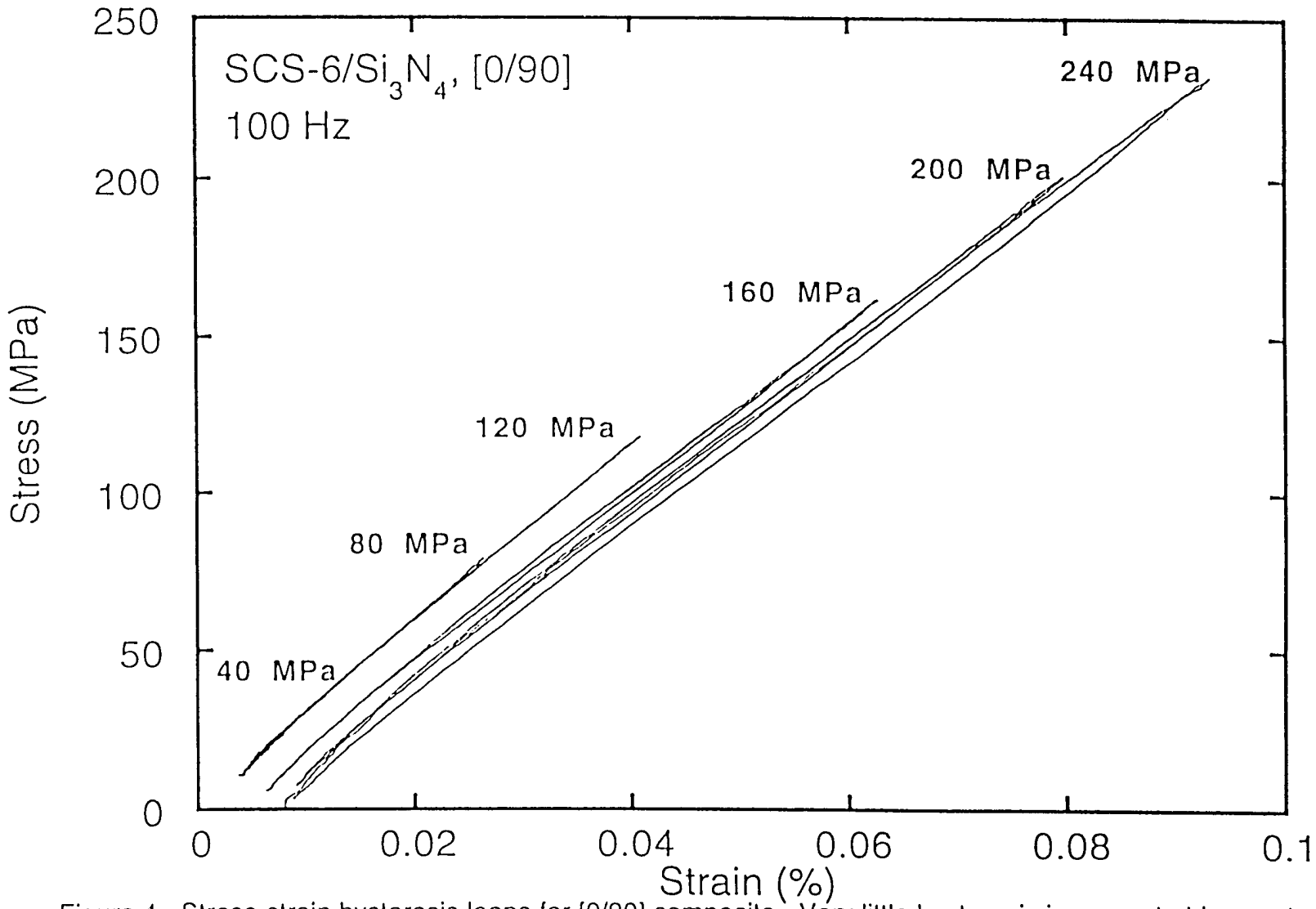

Figure 4. Stress-strain hysteresis loops for [0/90] composite. Very little hysteresis is present at lower stresses, but at higher stresses frictional sliding of the fibers within the matrix causes significant hysteresis.

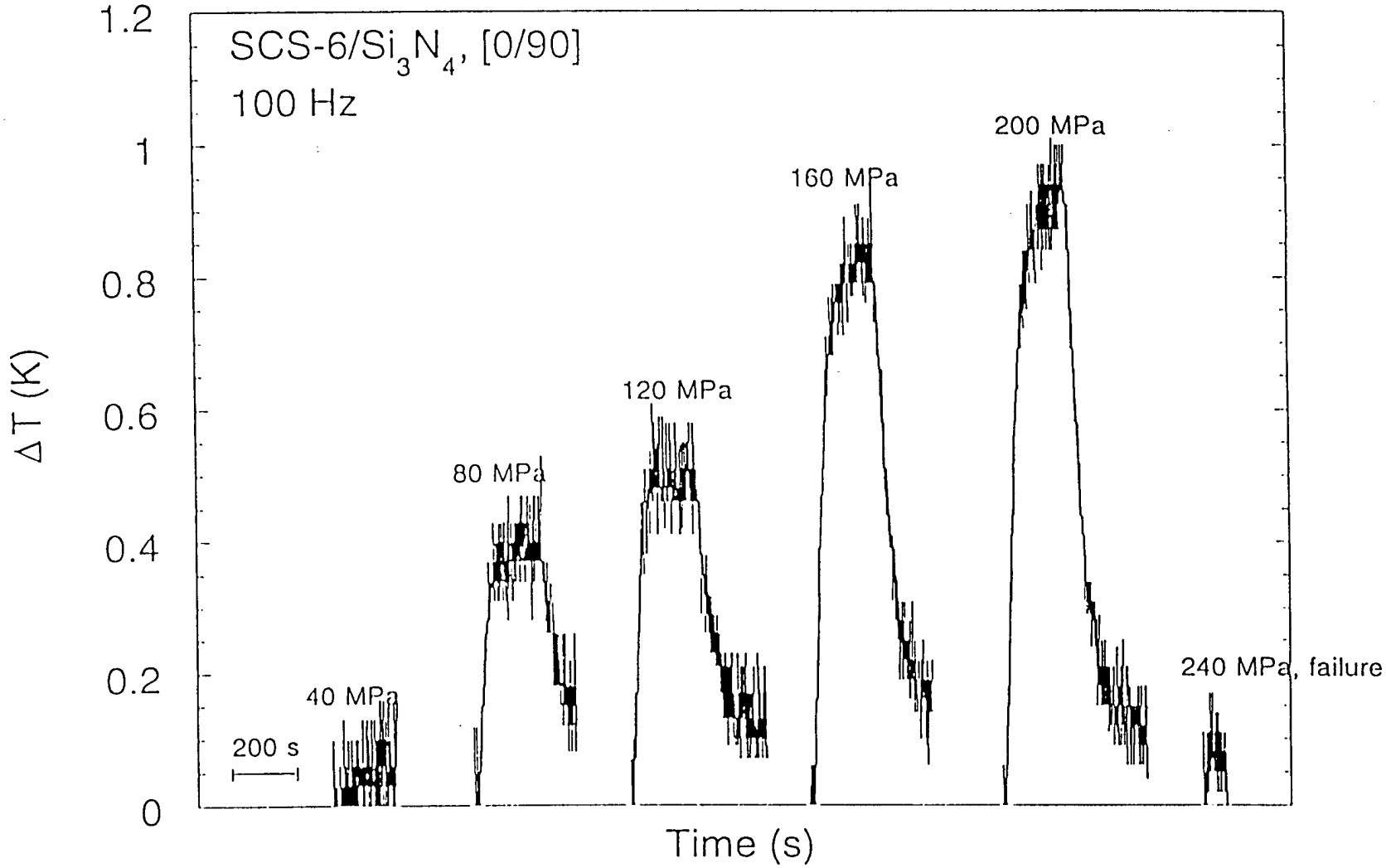

Figure 5. Temperature rise associated with frictional heating in [0/90] composite.

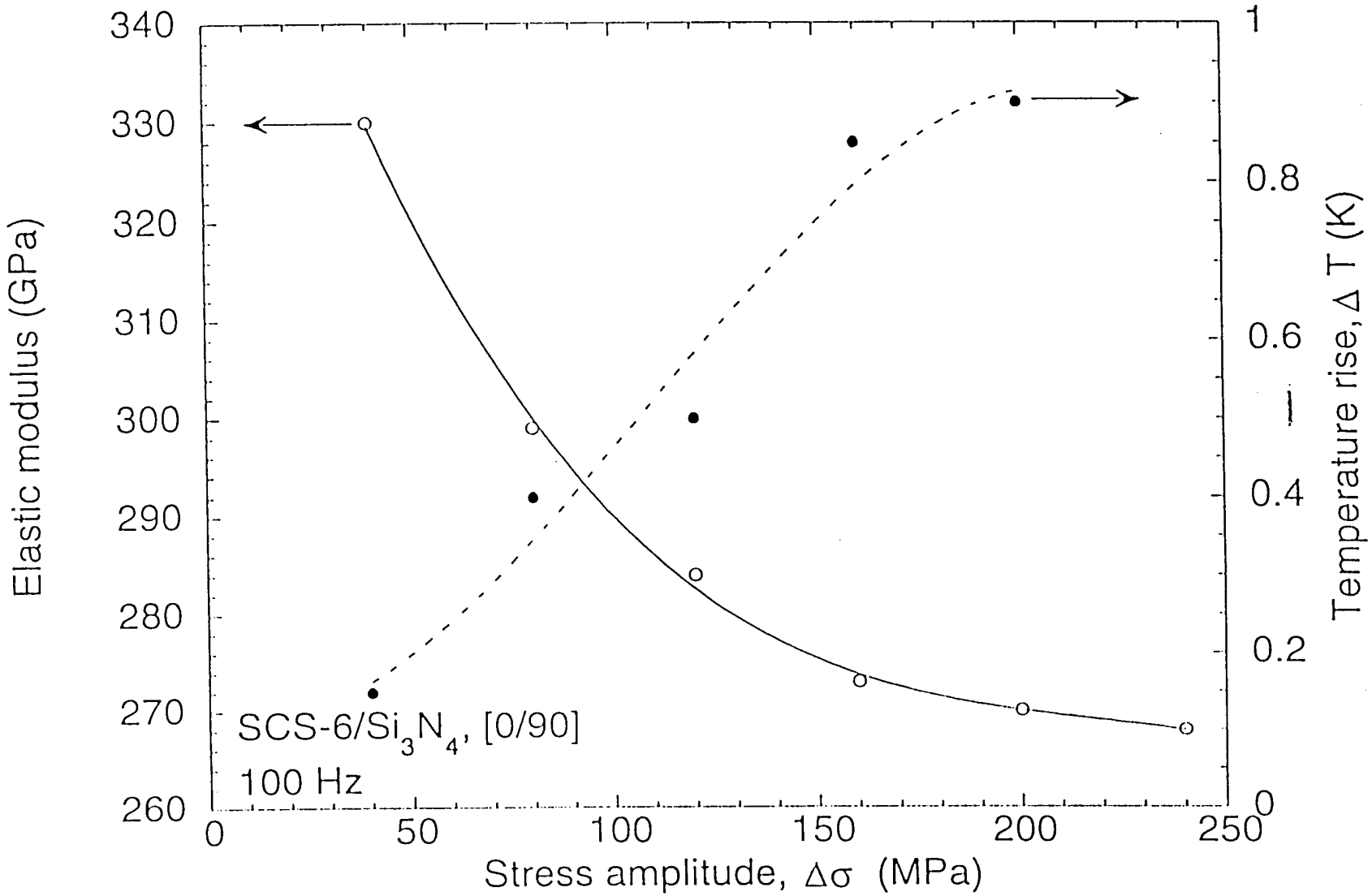

Figure 6. Decrease in modulus of the [0/90] composite during fatigue, correlated with observed temperature rise.

Scanning electron microscopy (SEM) showed very little cracking and fiber pullout in the [0/90] composite. Surface replication showed no significant cracking on the gauge length of the specimen during testing. The small amount of matrix cracks explains the relatively small magnitude in heating (1°C) compared to other systems. Figures 7 (a) and (b) show the limited cracking on within the composite after fatigue. In composites with very small diameter fibers, and therefore more surface area between matrix and fiber, heating was as high as 150 K at similar testing frequencies and applied stresses [2].

It has been reported that SCS-6 fibers are typically cracked because of the hot-pressing pressures and temperatures [3]. Such cracks were observed in this study as well, Fig. 8. The cracks extend from the carbon core to the outer carbon-rich layer, so they are within the SCS-6 fiber and must be caused by processing. Cracking within the fiber may lead to other sites where frictional heating can take place. Since the SCS-6 fiber is a composite itself, sliding can occur at the interface between pyrolitic carbon and carbon core, between pyrolitic carbon and β-SiC, and between β-SiC and the outer carbon-rich layer. Figure 9(a) shows a fractured SCS-6 fiber. Notice debonding between the carbon core and pyrolitic carbon, and between the pyrolitic carbon and the β-SiC. Figure 9(b) shows the damage due to high frequency fatigue in the pyrolitic coating over the carbon core in the form of debonding and flaking.

In the [±45] orientation, significant heating and hysteresis occurred at much lower stresses, Figs. 10 and 11, and failure also occurred at lower stress due to relative orientation of the fibers. The temperature rise in [±45] at 80 MPa was equivalent in magnitude to that in [0/90] at 200 MPa. This phenomenon can be attributed to the shear stresses being largest in [±45] fiber orientation. The modulus of this composite was also lower, decreasing from 233 to 213 when cycled at 40 and 80 MPa, respectively. Substantially more cracking occurred in [±45], Fig. 12(a) , allowing for more debonding and frictional sliding sites at lower stresses. Notice that the cracks are deflected by the large diameter fibers. Once again, the cracking seems to be confined to the interior of

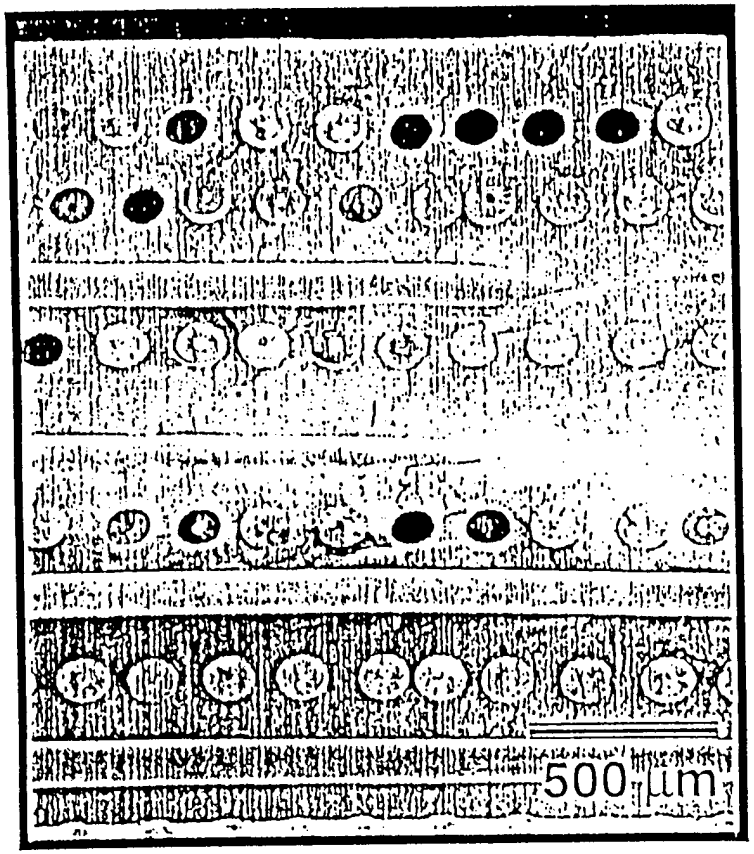

(a)

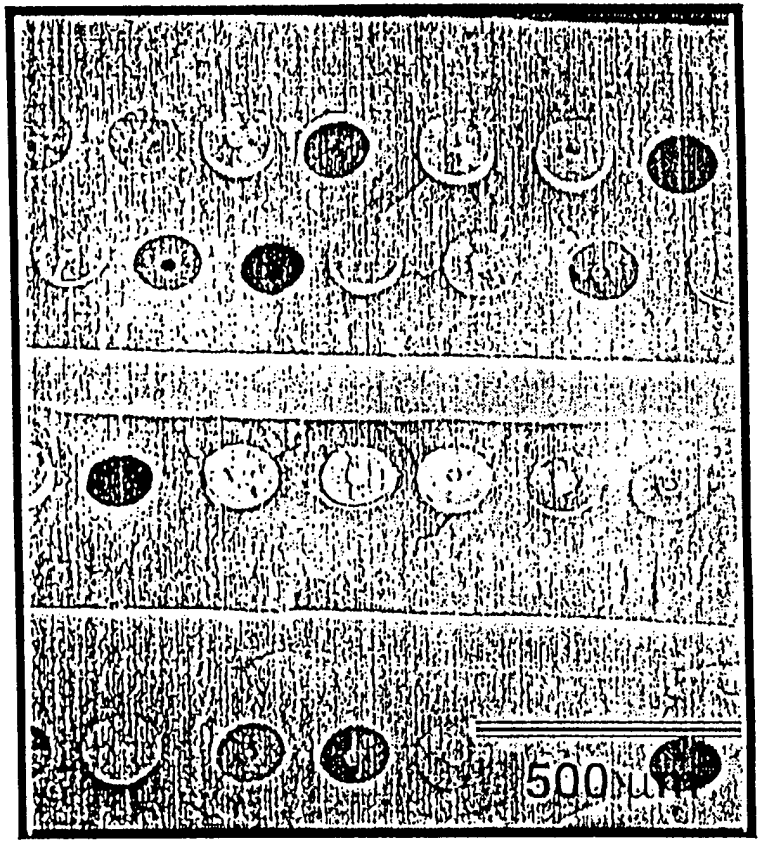

(b)

Figure 7. (a) Low magnification micrograph of [0/90] composite showing limited matrix microcracking after fatigue and (b) higher magnification micrograph of the same area.

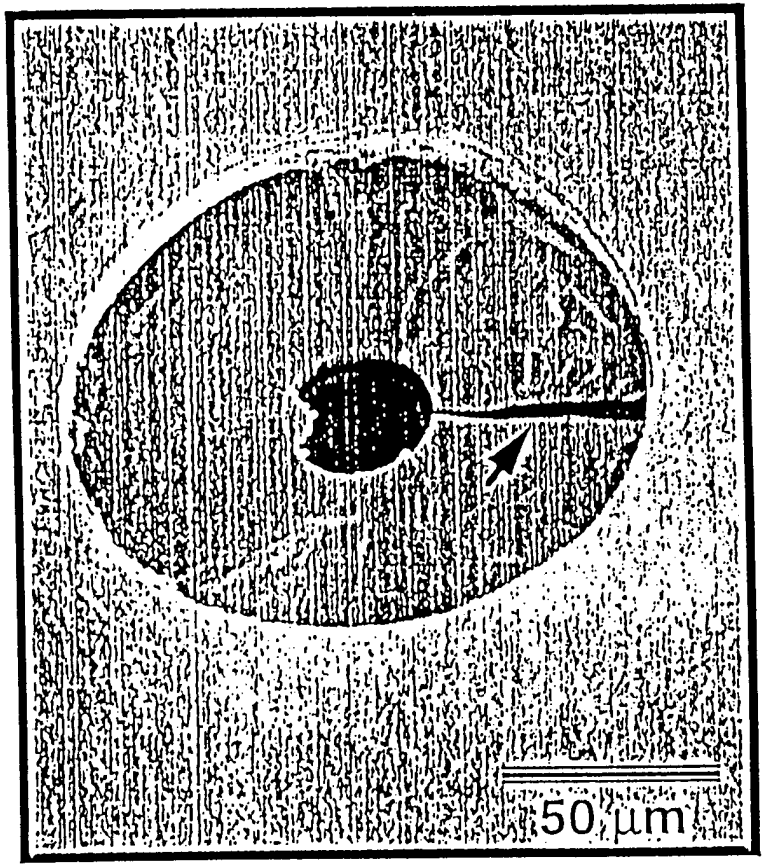

Figure 8. Crack in SCS-6 fiber due to high hot-pressing pressures and temperatures.

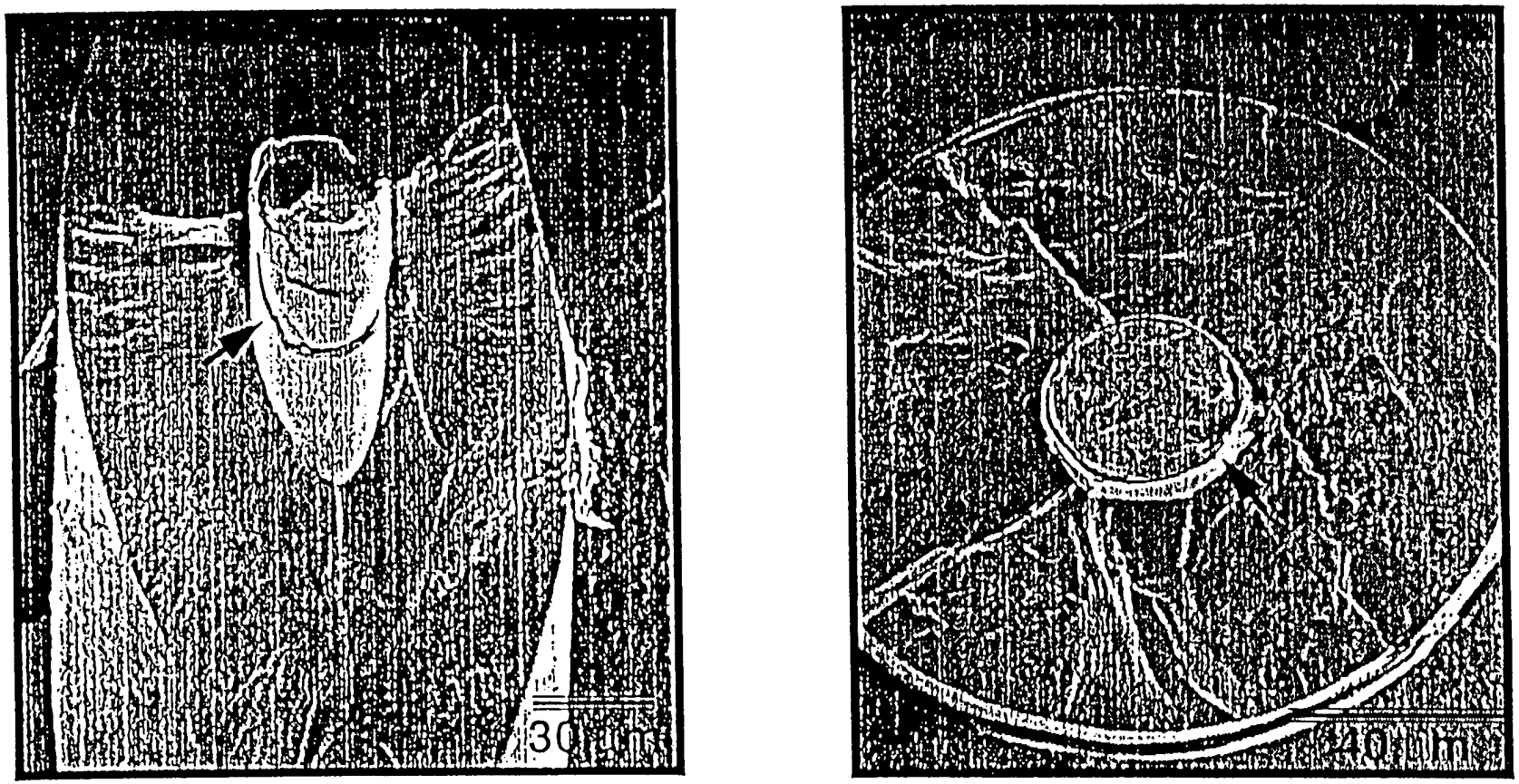

(a) (b)

Figure 9. (a) Fractured SCS-6 fiber that shows debonding between the carbon core and pyrolitic carbon, and between the pyrolitic carbon and the β-SiC, and (b) damage due to high frequency fatigue in the pyrolitic coating over the carbon core in the form of debonding and flaking.

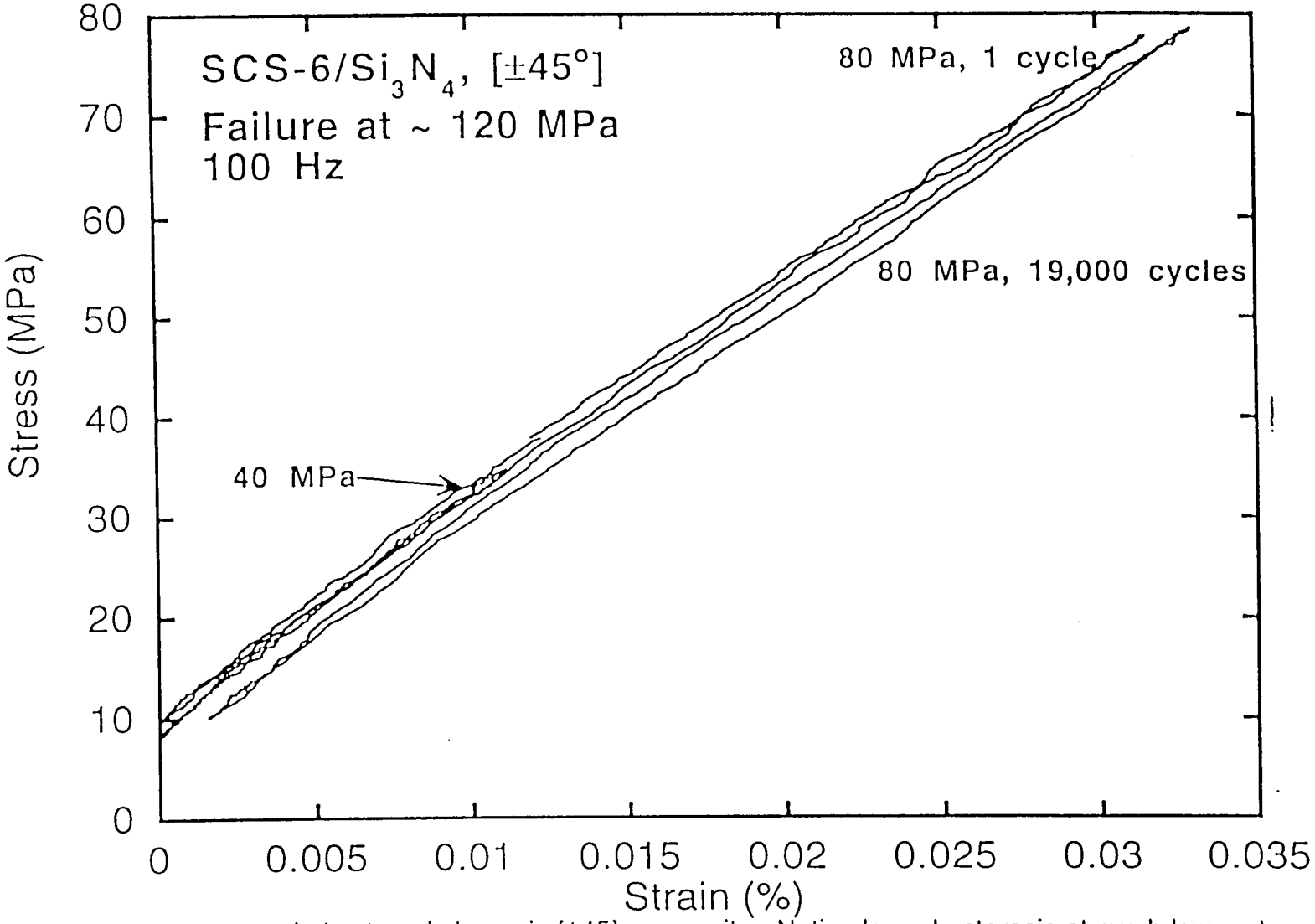

Figure 10. Stress-strain hysteresis loops in [±45] composite. Notice large hysteresis at much lower stresses than that observed in the [0/90] composite.

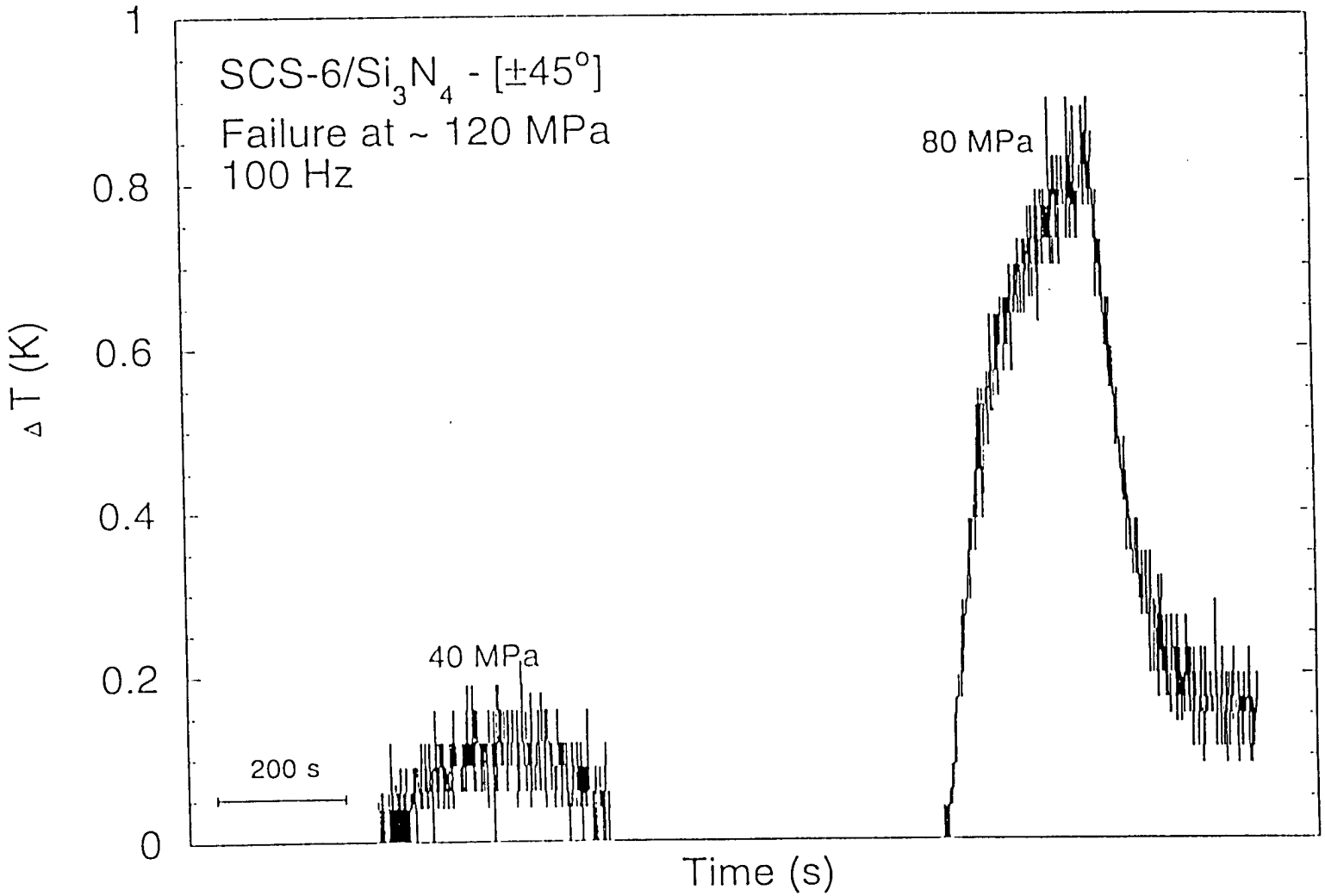

Figure 11. Substantial temperature rise at low stresses in [±45] composite.

the specimen, since surface replicas did not show any change in crack density in the gauge length of the specimen. Fig. 12(b) shows a higher magnification micrograph - as described before, debonding and frictional sliding during fatigue occurred at various interfaces within the composite SCS-6 fiber. Figure 13 shows an SCS-6 fiber fractured at a 45° angle. The crack was deflected and traveled along the carbon-rich layer on the outer surface of the fiber before the fiber fractured. The somewhat lighter, featureless surface extending from the carbon core is the C-rich β-SiC, while the next circumferential layer is stoichiometric β-SiC.

The mechanisms in high frequency fatigue can be summarized as follows. During the initial stages of testing, wear and damage begin, so the temperature of the specimen increases. As more and more sliding occurs, the interfacial shear stresses also decrease. The magnitude of temperature rise scales with the stress amplitude, because with higher stress amplitudes the fibers slide over a greater length and produce more frictional heating. With increased sliding, fibers slowly begin to fail and the composite fractures.

Analysis using classical laminated plate theory. One can calculate the state of stress in a laminated composite by using classical laminated theory [4-6]. For an orthotropic material, the stresses in a given lamina can be related to the strains by the stiffness matrix [Q] [4]:

$$\begin{bmatrix} \sigma_1 \\ \sigma_2 \\ \tau_{12} \end{bmatrix} = \begin{bmatrix} Q_{11} & Q_{12} & 0 \\ Q_{12} & Q_{22} & 0 \\ 0 & 0 & Q_{66} \end{bmatrix} \begin{bmatrix} \varepsilon_1 \\ \varepsilon_2 \\ \gamma_{12} \end{bmatrix}$$

where σ_1 and σ_2 are the principal stresses and ε_1 and ε_2 are the principal strains. τ_{12} and γ_{12} are the shear stresses and strains, respectively. If the fibers are oriented in a direction other than parallel to the applied load, a transformation of coordinates must be undertaken such that [4]:

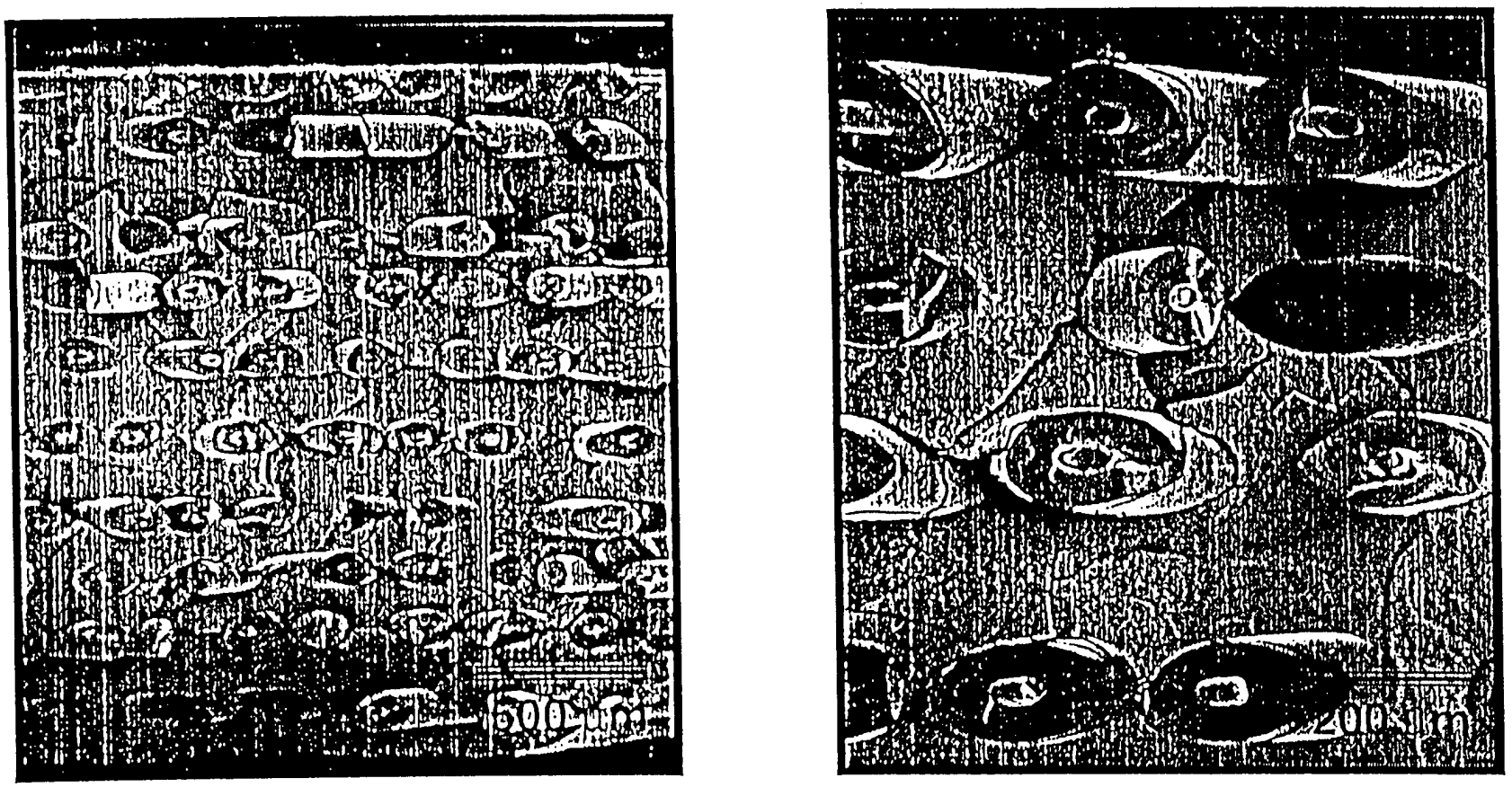

(a) (b)

Figure 12.(a) Substantial matrix cracking in [±45] composite, allowing for more debonding and frictional sliding sites at lower stresses, and (b) higher magnification micrograph showing debonding and frictional sliding at various interfaces within the composite SCS-6 fiber and between fiber and matrix.

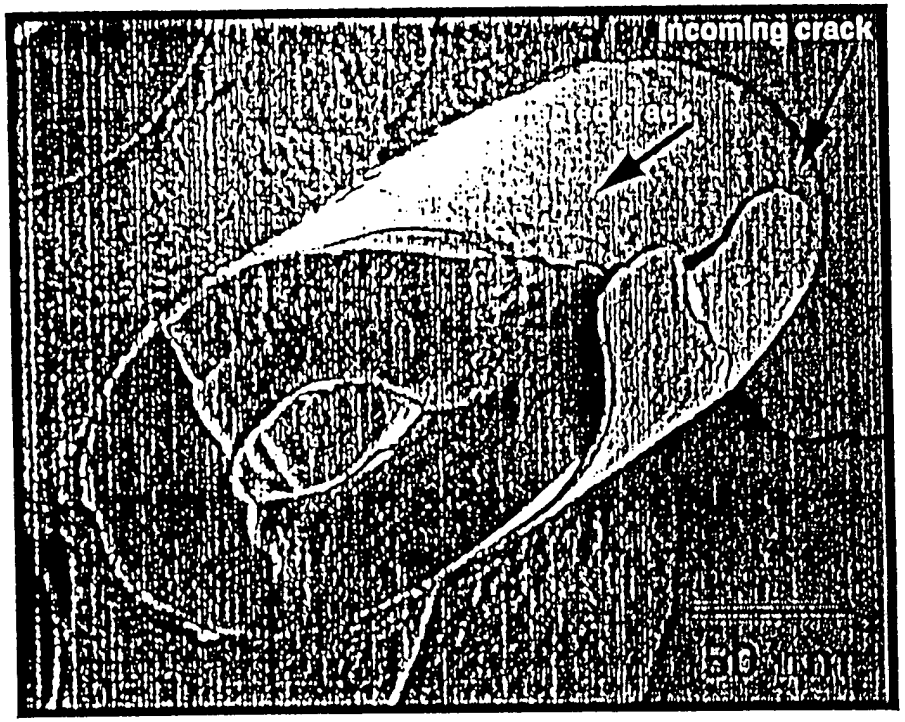

Figure 13. SCS-6 fiber fractured at a 45° angle. The crack was deflected and traveled along the carbon-rich layer on the ou;ter surface of the fiber before the fiber fractured.

$$\begin{bmatrix} \sigma_x \\ \sigma_y \\ \tau_{xy} \end{bmatrix} = \begin{bmatrix} \overline{Q}_{11} & \overline{Q}_{12} & \overline{Q}_{16} \\ \overline{Q}_{12} & \overline{Q}_{22} & \overline{Q}_{26} \\ \overline{Q}_{16} & \overline{Q}_{26} & \overline{Q}_{66} \end{bmatrix} \begin{bmatrix} \varepsilon_x \\ \varepsilon_y \\ \gamma_{xy} \end{bmatrix}$$

where the subscripts x and y denote the new coordinate system. [Q] and [Q] are related by the angle between the orientation of the fibers and that of the applied load. The exact formulations relating [Q] and [Q] may be found elsewhere [4,5].

The force per unit length matrix, [N], and the moment per unit length [M], can be related to the stiffness matrix [Q] and the bending curvature of the laminate [κ] [4]:

$$\begin{bmatrix} N_x \\ N_y \\ N_{xy} \end{bmatrix} = \begin{bmatrix} A_{11} & A_{12} & A_{16} \\ A_{12} & A_{22} & A_{26} \\ A_{16} & A_{26} & A_{66} \end{bmatrix} \begin{bmatrix} \varepsilon_x \\ \varepsilon_y \\ \gamma_{xy} \end{bmatrix} + \begin{bmatrix} B_{11} & B_{12} & B_{16} \\ B_{12} & B_{22} & B_{26} \\ B_{16} & B_{26} & B_{66} \end{bmatrix} \begin{bmatrix} \kappa_x \\ \kappa_y \\ \kappa_{xy} \end{bmatrix}$$

$$\begin{bmatrix} M_x \\ M_y \\ M_{xy} \end{bmatrix} = \begin{bmatrix} B_{11} & B_{12} & B_{16} \\ B_{12} & B_{22} & B_{26} \\ B_{16} & B_{26} & B_{66} \end{bmatrix} \begin{bmatrix} \varepsilon_x \\ \varepsilon_y \\ \gamma_{xy} \end{bmatrix} + \begin{bmatrix} D_{11} & D_{12} & D_{16} \\ D_{12} & D_{22} & D_{26} \\ D_{16} & D_{26} & D_{66} \end{bmatrix} \begin{bmatrix} \kappa_x \\ \kappa_y \\ \kappa_{xy} \end{bmatrix}$$

where

$$A_{ij} = \sum_{k=1}^{n} \left(\overline{Q}_{ij}\right)_k \left(z_k - z_{k-1}\right), \quad B_{ij} = \frac{1}{2}\sum_{k=1}^{n} \left(\overline{Q}_{ij}\right)_k \left(z_k^2 - z_{k-1}^2\right), \text{ and } D_{ij} = \frac{1}{3}\sum_{k=1}^{n} \left(\overline{Q}_{ij}\right)_k \left(z_k^3 - z_{k-1}^3\right)$$

A_{ij} is termed the extensional stiffness, B_{ij} the coupling stiffness, and D_{ij} the bending stiffness. If the B_{ij} terms are not zero, this means that a coupling between bending and extension is present; that is, extension of the laminate cannot occur without bending or twisting.

From these equations, if an antisymmetric balanced cross-ply laminate is used ([0/90]), or an antisymmetric balanced angle-ply laminate is used (e.g., [±45]), then $A_{16} = A_{26} = 0$, and $D_{16} = D_{26} = 0$, because [5]:

$$\left(\overline{Q}_{16}\right)_{+\theta} = \left(\overline{Q}_{16}\right)_{-\theta} \text{ and } \left(\overline{Q}_{26}\right)_{+\theta} = \left(\overline{Q}_{26}\right)_{-\theta}$$

By taking advantage of the canceling effect in the B matrix, it can be shown that for a cross-ply laminate [4]:

$$\begin{bmatrix} N_x \\ N_y \\ N_{xy} \end{bmatrix} = \begin{bmatrix} A_{11} & A_{12} & 0 \\ A_{12} & A_{22} & 0 \\ 0 & 0 & A_{66} \end{bmatrix} \begin{bmatrix} \varepsilon_x \\ \varepsilon_y \\ \gamma_{xy} \end{bmatrix} + \begin{bmatrix} B_{11} & 0 & 0 \\ 0 & -B_{11} & 0 \\ 0 & 0 & 0 \end{bmatrix} \begin{bmatrix} \kappa_x \\ \kappa_y \\ \kappa_{xy} \end{bmatrix}$$

$$\begin{bmatrix} M_x \\ M_y \\ M_{xy} \end{bmatrix} = \begin{bmatrix} B_{11} & 0 & 0 \\ 0 & -B_{11} & 0 \\ 0 & 0 & 0 \end{bmatrix} \begin{bmatrix} \varepsilon_x \\ \varepsilon_y \\ \gamma_{xy} \end{bmatrix} + \begin{bmatrix} D_{11} & D_{12} & 0 \\ D_{12} & D_{22} & 0 \\ 0 & 0 & D_{66} \end{bmatrix} \begin{bmatrix} \kappa_x \\ \kappa_y \\ \kappa_{xy} \end{bmatrix}$$

Similarly, for the angle-ply laminate [4]:

$$\begin{bmatrix} N_x \\ N_y \\ N_{xy} \end{bmatrix} = \begin{bmatrix} A_{11} & A_{12} & 0 \\ A_{12} & A_{22} & 0 \\ 0 & 0 & A_{66} \end{bmatrix} \begin{bmatrix} \varepsilon_x \\ \varepsilon_y \\ \gamma_{xy} \end{bmatrix} + \begin{bmatrix} 0 & 0 & B_{16} \\ 0 & 0 & B_{26} \\ B_{16} & B_{26} & 0 \end{bmatrix} \begin{bmatrix} \kappa_x \\ \kappa_y \\ \kappa_{xy} \end{bmatrix}$$

$$\begin{bmatrix} M_x \\ M_y \\ M_{xy} \end{bmatrix} = \begin{bmatrix} 0 & 0 & B_{16} \\ 0 & 0 & B_{26} \\ B_{16} & B_{26} & 0 \end{bmatrix} \begin{bmatrix} \varepsilon_x \\ \varepsilon_y \\ \gamma_{xy} \end{bmatrix} + \begin{bmatrix} D_{11} & D_{12} & 0 \\ D_{12} & D_{22} & 0 \\ 0 & 0 & D_{66} \end{bmatrix} \begin{bmatrix} \kappa_x \\ \kappa_y \\ \kappa_{xy} \end{bmatrix}$$

Finally, it can be demonstrated that as the thickness of each individual lamina in the composite decreases, the B matrix goes to zero, so for both composites, [0/90] and [±45], the force per unit length can be written as [4]:

$$\begin{bmatrix} N_x \\ N_y \\ N_{xy} \end{bmatrix} = \begin{bmatrix} A_{11} & A_{12} & 0 \\ A_{12} & A_{22} & 0 \\ 0 & 0 & A_{66} \end{bmatrix} \begin{bmatrix} \varepsilon_x \\ \varepsilon_y \\ \gamma_{xy} \end{bmatrix}$$

The [Q] matrix that determines, [A], however, is different for cross-ply and angle-ply laminates. If we use a model composite such that E_{11} = 400 GPa, E_{22} = 200 GPa, G_{12} = 50 GPa, ν_{12} = 0.3 , then:

$$\nu_{21} = \nu_{12}\frac{E_{22}}{E_{11}} = 0.15 \text{ and}$$

$$Q_{[0°]} = \begin{bmatrix} \frac{E_{11}}{1-\nu_{12}\nu_{21}} & \frac{\nu_{21}E_{11}}{1-\nu_{12}\nu_{21}} & 0 \\ \frac{\nu_{12}E_{11}}{1-\nu_{12}\nu_{21}} & \frac{E_{22}}{1-\nu_{12}\nu_{21}} & 0 \\ 0 & 0 & \frac{1}{G_{12}} \end{bmatrix}$$

Now, using the [Q] transformation equations the [A] matrix for three two-ply laminates, $[0]_2$, [0/90], and [±45], is calculated:

$$[A]_{[0]_2} = \begin{bmatrix} 837.6 & 125.6 & 0 \\ 125.6 & 418.8 & 0 \\ 0 & 0 & 0.04 \end{bmatrix} \text{kN/mm}, \quad [A]_{[0/90]} = \begin{bmatrix} 628.2 & 125.6 & 0 \\ 125.6 & 628.2 & 0 \\ 0 & 0 & 0.04 \end{bmatrix} \text{kN/mm},$$

$$\text{and } [A]_{[\pm 45]} = \begin{bmatrix} 376.6 & 376.6 & 0 \\ 376.6 & 376.6 & 0 \\ 0 & 0 & 251.2 \end{bmatrix} \text{kN/mm}$$

From the above [A] matrices one can see that the [0] laminate has the highest stiffness in the longitudinal direction (A_{11}). The [0/90] laminate has the same stiffness, although lower that the [0] laminate, in both longitudinal and transverse directions (A_{11} and A_{22}). The term relating shear modulus, A_{66}, in both [0] and [0/90] is quite low. This term is much higher in the [±45] laminate, although the stiffness in A_{11} and A_{22} are substantially lower. Thus, with applied

load in the longitudinal direction of both [0/90] and [±45], the former laminate is stiffer and therefore has a higher modulus and undergoes less heating during high frequency fatigue. Had the load been applied at a 45° angle, the angle-ply laminate would have showed better properties.

IV. Conclusions

Several conclusions can be drawn from this study on the effect of laminate stacking sequence on the high frequency behavior of SCS-6 fiber reinforced Si_3N_4 composites:

- Angle-ply laminates show the same extent of heating as cross-ply laminates, but at much lower stress levels. From classical laminated theory, it was shown that angle-ply laminates have considerable lower stiffness in the loading direction than cross-ply laminates, which resulted in higher fatigue resistance and strength in the latter composite.

- Substantial cracking was observed in the angle-ply composite compared to the cross-ply composite, although the angle-ply composite failed at much lower stresses. This is due, once again, to the much lower stiffness of the angle-ply composite in the longitudinal loading direction.

- Frictional heating correlates very well with decrease in modulus as a function of fatigue cycles in the composites.

- Frictional heating stems from sliding at a variety of interfaces. It is believed that frictional sliding not only occurs at the fiber/matrix interface, but within the composite fiber itself.

V. References

1. K.K. Chawla, **Ceramic Matrix Composites**, Chapman & Hall, London, 1993, p. 4-10, 176, 314,

2. S.F. Shuler, J.W. Holmes, X. Wu, and D. Roach, "Influence of Loading Frequency on the Room-Temperature Fatigue of a Carbon-Fiber/SiC-Matrix Composite," (1993) *J. Am. Ceram. Soc.*, **76** [9] 2327.

3. D.K. Shetty, M.R. Pascucci, B.C. Mutsuddy, and R.R. Wills, "SiC Monofilament-Reinforced Si_3N_4 Matrix Composites," *Ceram. Eng. Sci. Proc.*, (1985) 632.

4. R.M. Jones, Mechanics of Composite Materials, Scripta Book Company, New York, 1975, p. 168.

5. K.K. Chawla, **Composite Materials: Science and Engineering**, Springer-Verlag, New York, 1987, p. 100.

6. F.L. Matthews and R.D. Rawlings, **Composite Materials: Engineering and Science**, Chapman and Hall, London, 1994, p.244.

VI. Surface Roughness Characterization of Continuous Ceramic Fibers by Atomic Force Microscopy (AFM).

N. Chawla, J.W. Holmes, and J.F. Mansfield

I. Introduction

Several important factors control the fiber/matrix behavior. For example, thermal residual stresses from processing will induce radial stresses at the interface (which, for most composites are compressive) and axial stresses between the matrix and fibers [1,2]. Fiber surface roughness can also contribute a mechanical component to the radial clamping stresses between the fibers and matrix, because the matrix becomes mechanically keyed to the fiber [3-5]. A roughness-induced strain arises because of this mechanical keying. This strain can be estimated by the roughness amplitude between the fiber and matrix. Figure 1 shows schematically the qualitative effect of fiber roughness on the sliding behavior at the fiber/matrix interface of a composite.

An adequate technique for the measurement of surface roughness in ceramic fibers is not available. Conventional profilometry techniques are accurate only to 1 mm, while the roughness in ceramic fibers may be as low as 1 nm. With the commercial availability of Atomic Force Microscopy (AFM), several surface studies have been conducted in the areas of polymers, semiconductors, and biology [6-9]. AFM has a distinct advantage over Scanning Tunneling Microscopy (STM) because the technique does not require a conductive surface. Chawla et. al were the first to use AFM as a technique to measure surface roughness of ceramic fibers [10]. They examined three different continuous Al_2O_3 fibers and quantitatively described the extent of roughness and its effect on properties of the composite.

In this study we have used AFM to examine and quantify the surface roughness of two polymer-derived ceramic fibers, Nicalon™ and Hi-Nicalon™ (Nippon Carbon Co., Tokyo, Japan). The composition of the two fibers is given in Table 1. Nicalon is used extensively in ceramic composites because of its

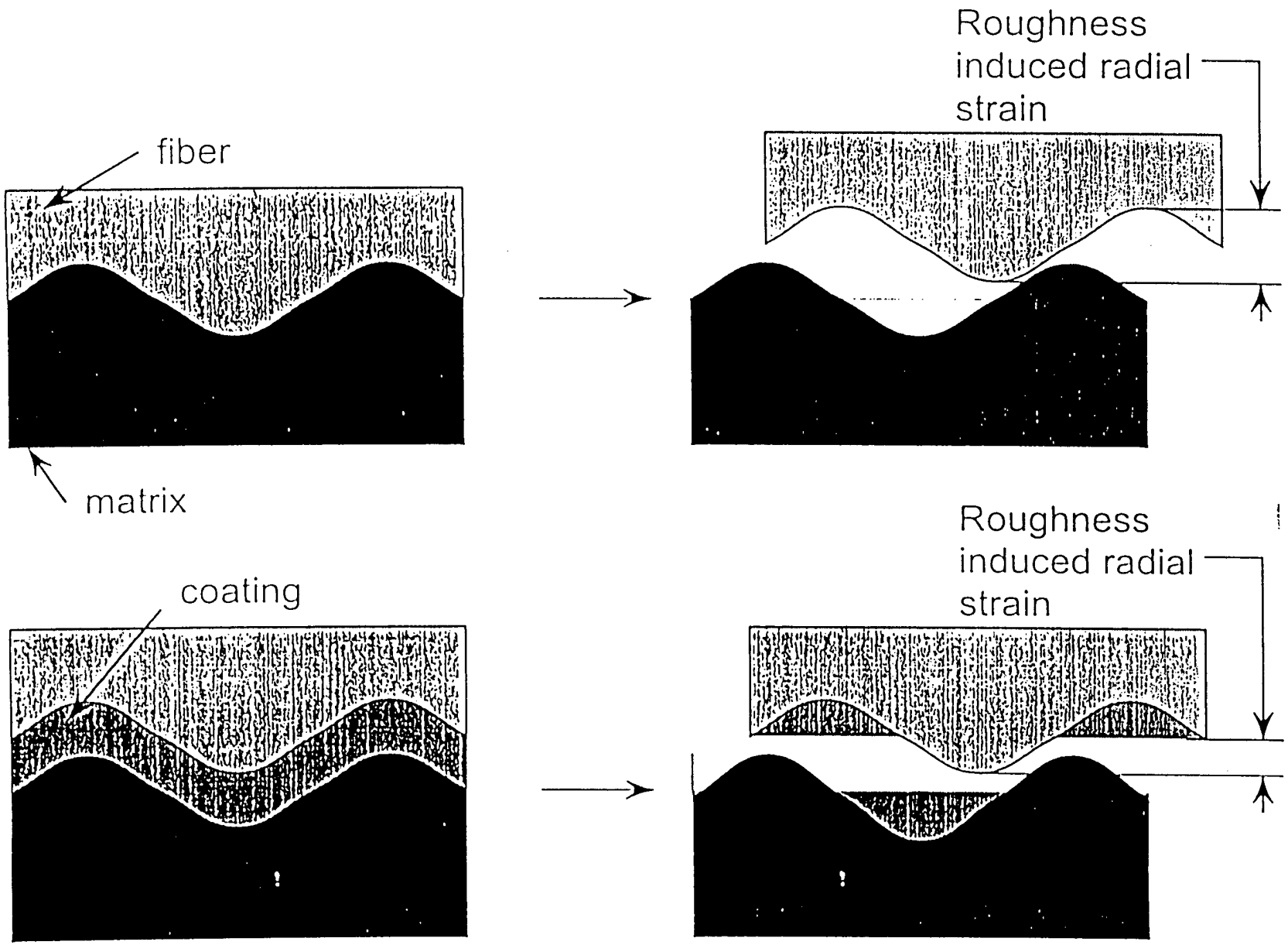

Figure 1. Qualitative effect of roughness on the sliding behavior at the fiber/matrixinterface in a composite.

Table 1: Properties of Nicalon and HI-Nicalon fibers
(Manufacturer's reported data, Dow Corning Corp., 1995)

	Nicalon	HI-Nicalon
Composition (wt. %)	58% Si, 31% C, 11% O	63.7% Si, 35.8% C, 0.5% O
Fiber diameter, μm	12-18	12-18
Elastic Modulus (GPa)	193	269
Tensile strength (GPa)	2.96	2.80
Coefficient of thermal expansion (10^{-6} K^{-1})	3.9	-------

high strength, low cost, and small diameter [11,12]. Unfortunately, it contains a substantial amount of free oxygen so at high temperatures the oxygen combines with free silicon to form a glassy phase, SiO_2, that forms a strong bond between the fiber and matrix, and is therefore detrimental to the properties of the composite [13]. HI-Nicalon (recently developed by Nippon Carbon) contains substantially less free oxygen, so it is very attractive as a reinforcement for ceramic matrices at high temperatures.

II. Experimental procedure

In AFM, a very sharp gold coated Si_3N_4 tip few microns in diameter is attached to a cantilever probe and placed a few angstroms away from the specimen surface, see Fig. 2. In this study, the AFM (Digital Instruments Nanoscope III, Santa Barbara, CA) was used in contact mode, where the tip was in actual contact with the specimen surface. It should be noted that the sharper the AFM tip, the higher the resolution in tracing contours of a given surface. The interatomic repulsion that exists between the surface and the tip causes a deflection of the cantilever. A laser is used to measure the deflection and the signal is processed to obtain images as well as profiles of surface roughness.

To prepare the specimen for AFM, the fibers were placed in an acetone bath in an ultrasonic cleaner to remove the protective sizing on the surface. Next, a thin layer of hot wax was placed on a steel magnetic disk. Using an optical microscope, dry single fibers were placed on the wax and allowed to cool down. Care was taken to ensure that no wax was present on the surface of the fiber and the fiber was completely flat (bowing or movement of the fiber during AFM scanning would yield erroneous results), Fig. 3. The magnetic disk was positioned in the AFM and the cantilever tip was lowered close to the fiber. When the cantilever was close enough, the controlling computer descended until the cantilever touched the fiber surface. Several locations were scanned

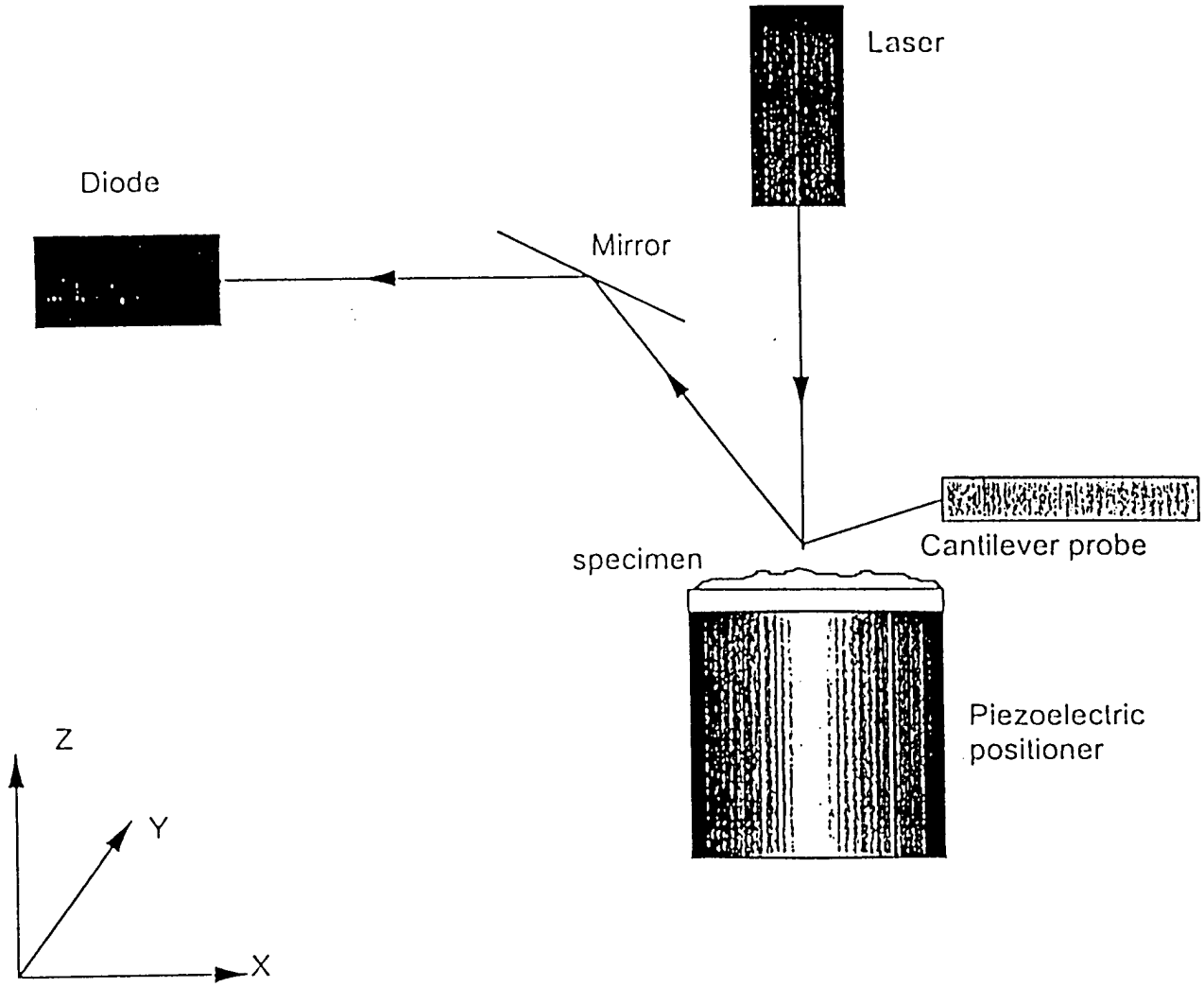

Figure 2. Schematic of the atomic force microscope (AFM).

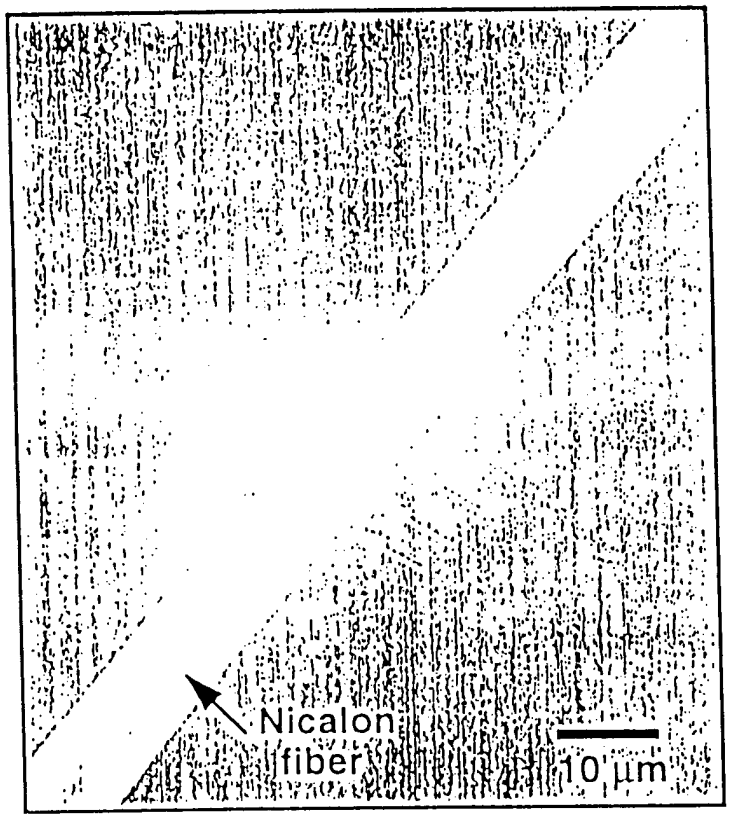

Figure 3. Scanning electron microscope (SEM) micrograph of Nicalon fiber on the magnetic stub before AFM.

at the top of the fiber surface, and the scan direction was varied to ensure that a given image was not an artifact of the AFM tip.

After capturing the images, polynomial fits were applied to "flatten" the curved surface obtained from the AFM. Three-dimensional and section profiles of the fiber surface were obtained and a variety of quantitative roughness values were calculated, such as the mean roughness, R_a, which is defined as:

$$R_a = \frac{1}{L}\int_0^L f(x)dx \qquad (1)$$

where L is the length of the roughness profile and f(x) is the roughness curve. Additional roughness parameters that were calculated are R_{max}, the difference between highest and lowest point in a given image, and R_{rms}, the root-mean squared roughness.

III. Results and discussion

Figures 4 and 5 show height mode images of Nicalon and HI-Nicalon fibers respectively. Topographic views of the profiles are shown in Figs. 6 and 7. Notice the nodular surface profile in both fibers. It is speculated that these nodules form during processing. Melt spinning processes are used to manufacture Nicalon and HI-Nicalon fibers, Fig. 8. Polycarbosilane is spun and a green fiber, ready for sintering, is obtained. The difference in processing between fibers lies the next steps. In Nicalon the green fiber is cured by oxidation and pyrolyzed. HI-Nicalon, on the other hand, is cured by an electron beam and then pyrolyzed; this procedure lowers the oxygen content.

Averaged roughness profiles were taken from the areas scanned in both images, Table 2. HI-Nicalon has a somewhat higher roughness than Nicalon, but the roughness amplitude of both fibers is quite low, on the order of 4-5 nm. Taking into the consideration such factors as the radius of the tip, type of scanner, size of features being imaged, and number of pixels in the image the

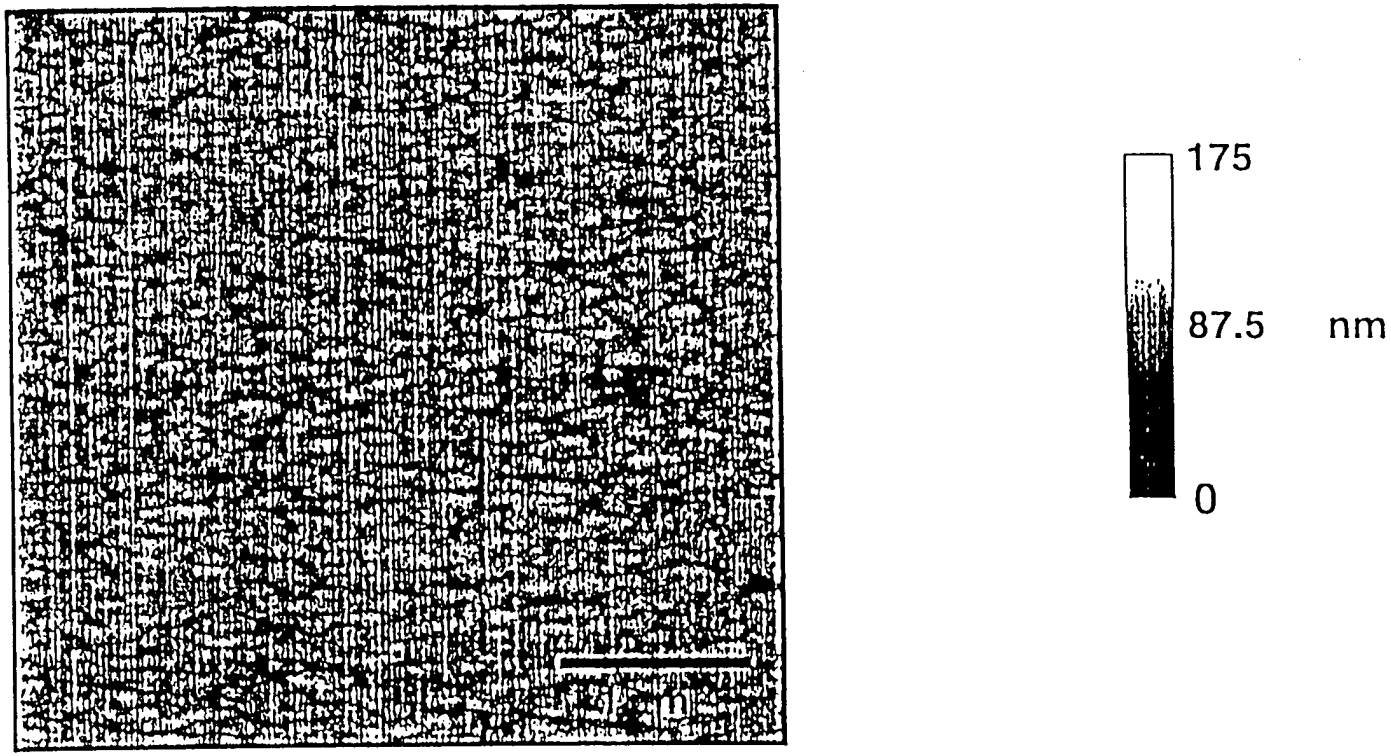

Figure 4. Height mode image of the surface of a Nicalon fiber.

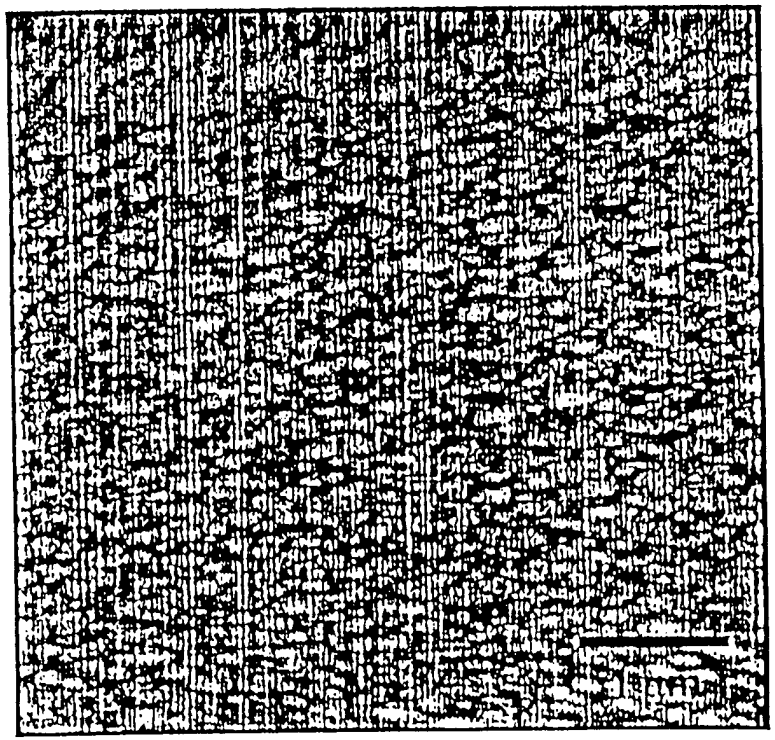

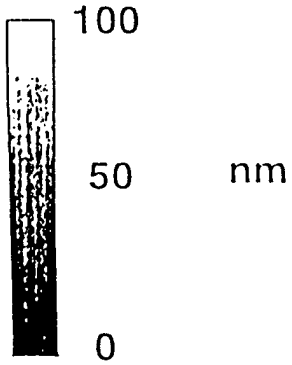

Figure 5. Height mode image of the surface of a HI-Nicalon fiber.

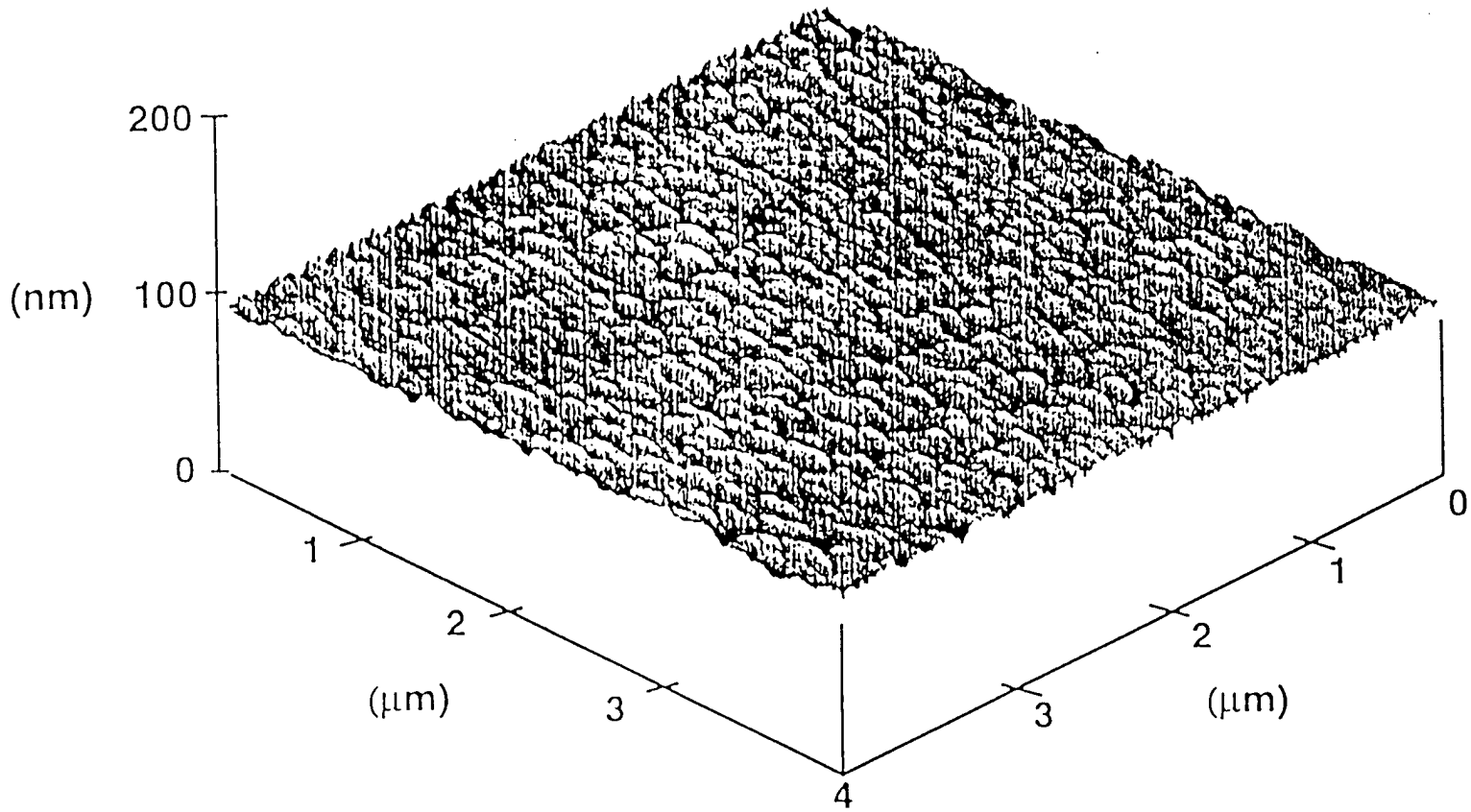

Figure 6. Topographic view of the surface of a Nicalon fiber.

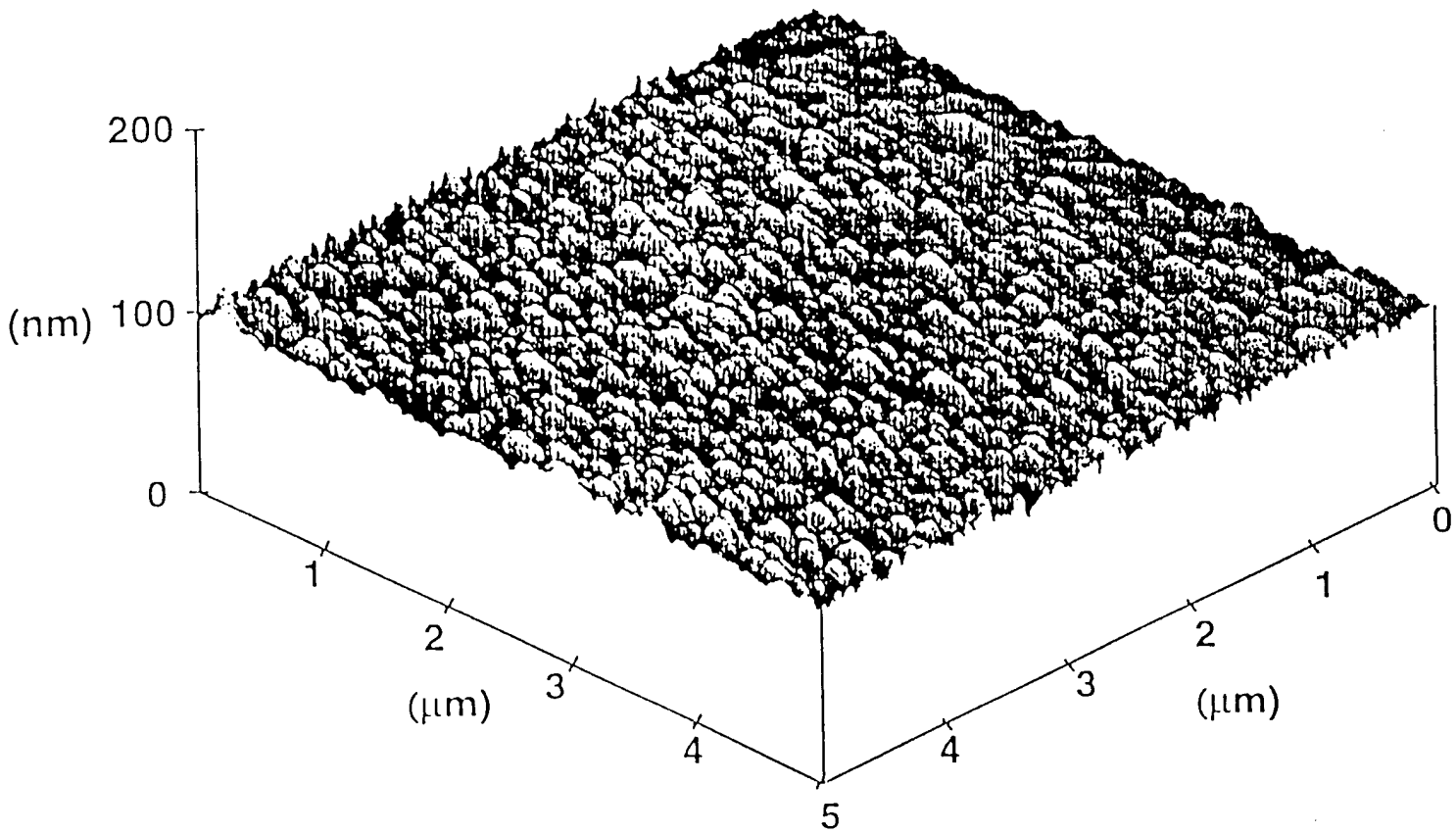

Figure 7. Topographic view of the surface of a HI-Nicalon fiber.

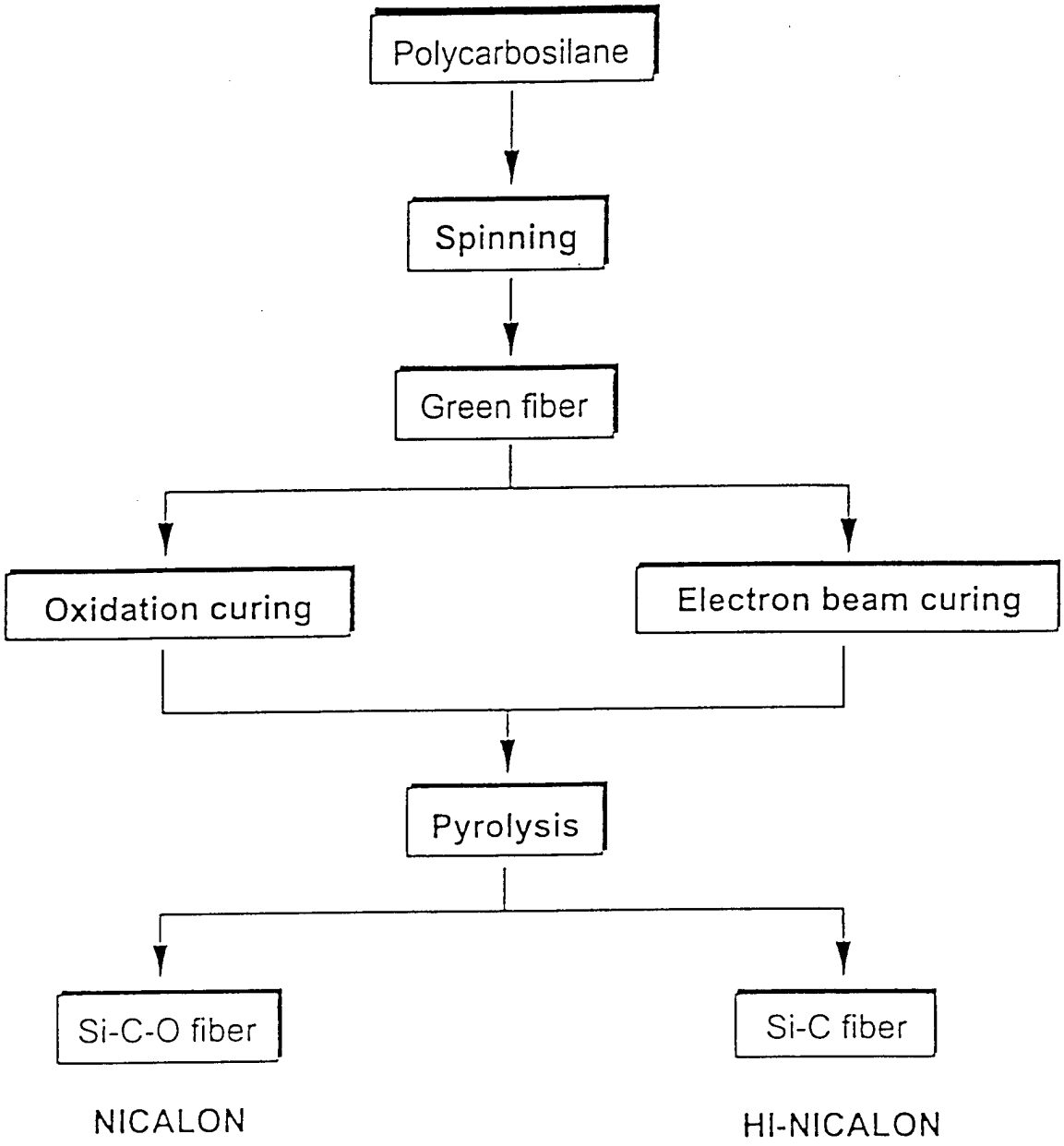

Figure 8. Melt-spinning process used to manufacture Nicalon and HI-Nicalon fibers, which may influence surface roughness of fibers.

Table 2: Roughness values of Nicalon and HI-Nicalon fibers

(uncertainty in roughness values is ±0.67 nm)

	Nicalon	HI-Nicalon
Mean roughness (R_a), nm	3.29	4.28
Root-mean square roughness (R_{rms}), nm	4.08	5.42
Max height (R_{max}), nm	30.84	43.14

uncertainty in the roughness measurements was calculated as ±0.67 nm. From Figs. 6 and 7, section analyses were also conducted to provide a graphic profile of the roughness, Fig. 9. A line was drawn on the image and the corresponding roughness profiles are plotted. Notice that both fibers have similar profiles. Notice, however, that the roughness is more uniform in Nicalon than HI-Nicalon. This may be critical during fiber sliding, as a large amplitude between a given peak and valley may serve as an obstacle to sliding.

It should be noted that with conventional techniques such as scanning electron microscopy (SEM), coating of the specimen would obliterate any desired features. Using low voltage microscopy, one can view images without coating the specimen, but height information would not be possible without some kind of stereo microscopy which may not be nearly as accurate as AFM.

The surface roughness information obtained from AFM can be used to determine the roughness-induced contribution to the radial stress on the fiber σ_{rough}, from the matrix. Kerans and Parthasarathy showed that the radial stress is a combination of the roughness-induced radial stress and the residual normal stress that arises from the mismatch in coefficient of thermal expansion (CTE), $\Delta\alpha$, between fiber and matrix [14,15]. The roughness-induced radial stress, σ_{rough}, in their model is given by:

$$\sigma_{rough} = \frac{E_m E_f}{E_f(1+\nu_m) + E_m(1-\nu_f)}\left(\frac{-A}{r}\right) \qquad (2)$$

where , A is the characteristic roughness amplitude, r is the radius of the fiber, and E_m, E_f, ν_m, and ν_f are the elastic moduli and Poisson ratios of fiber and matrix, respectively. This term is added to the residual normal stress contribution from CTE mismatch. The total residual normal stress, σ_N, is then given by [14, 15]:

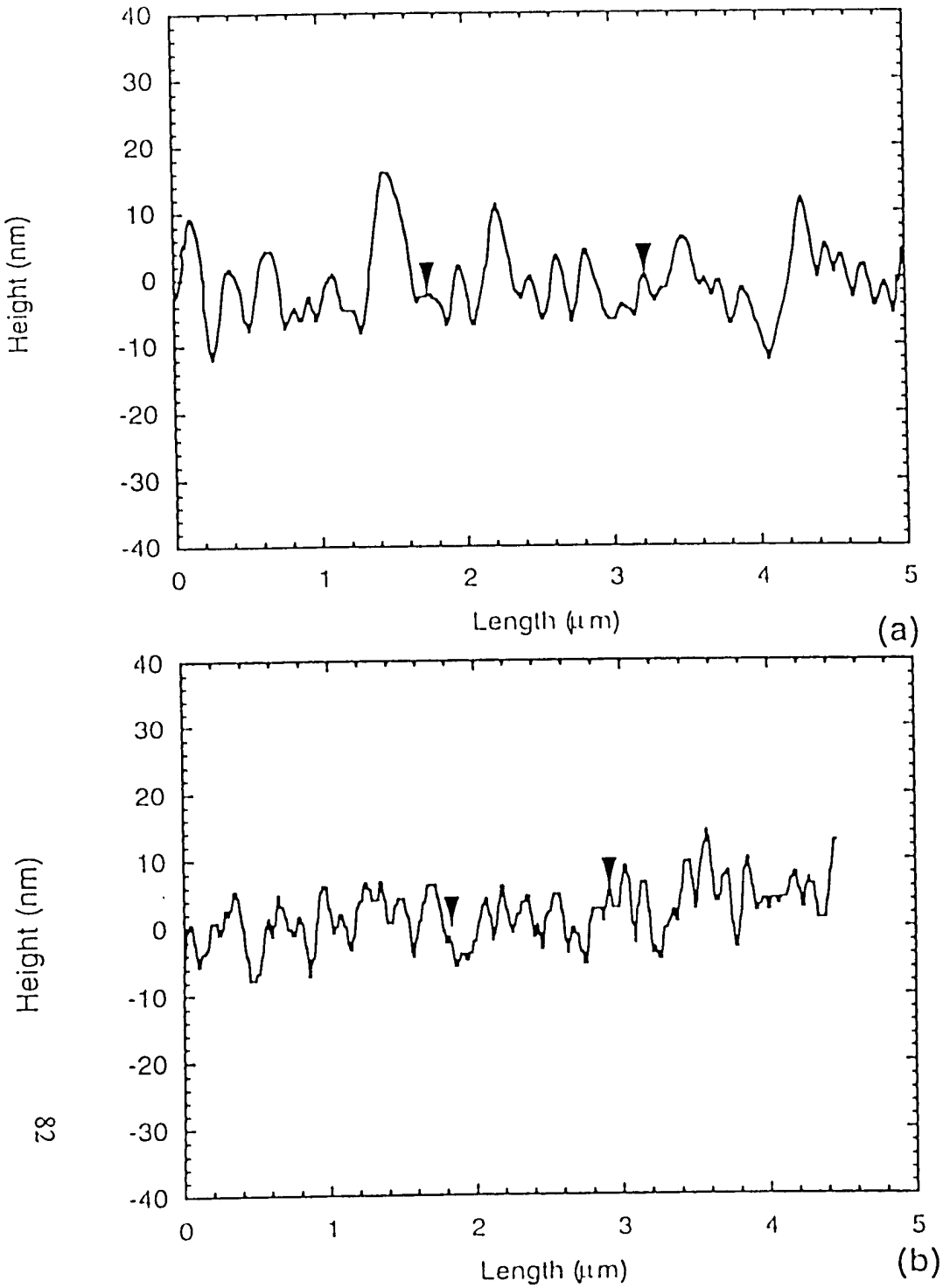

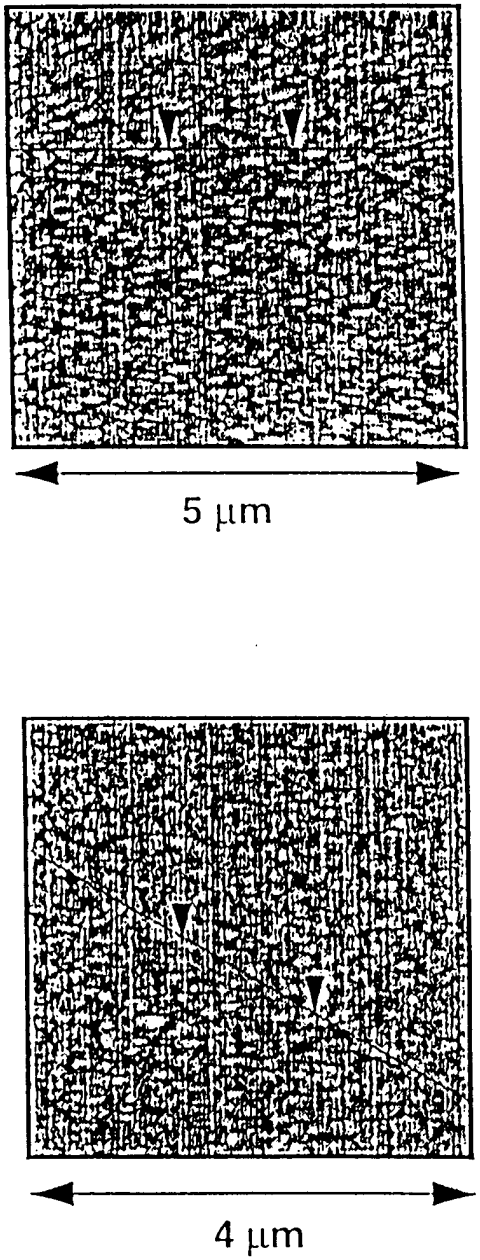

Figure 9. Section analyses of the surface roughness in (a) HI-Nicalon fiber and (b) Nicalon fiber.

$$\sigma_N = \frac{-E_m E_f}{E_f(1+\nu_m)+E_m(1-\nu_f)}\left(\Delta\alpha\Delta T + \frac{A}{r}\right) \qquad (3)$$

where $\Delta\alpha = \alpha_m - \alpha_f$ and ΔT is the temperature gradient due to processing.

In a model ceramic composite, Nicalon or HI-Nicalon fibers would be coated with a material such as pyrolitic carbon to promote a weak bond at the fiber/matrix interface and interfacial sliding. It is well known that debonding and crack deflection take place at the fiber/coating interface. Furthermore, in this model the pyrolitic carbon coating is assumed to be compliant enough to relieve thermal and roughness induced stresses at the coating/matrix interface. Thus, the stresses at the matrix/coating interface are ignored, and the stresses in eqs. 2 and 3 can be considered as the stresses at the fiber/coating interface, so all matrix terms (subscript m) correspond to fiber coating terms. The roughness-induced strain, -A/r, was calculated by using the maximum roughness, R_{max}, as a conservative estimate of the characteristic roughness amplitude, A. The thermally-induced strain component, $\Delta\sigma\Delta T$ was assumed to be the same in both fibers, and was calculated by taking $\alpha_m=\alpha_{carbon}=28.3\times10^{-6}$ K^{-1} (pyrolitic carbon, perpendicular to the graphitic layers, [16]), $\alpha_f=\alpha_{Nicalon}=\alpha_{HI\text{-}Nicalon}=3.9\times10^{-6}$ K^{-1}, and for conventional chemical vapor deposition (CVD) of the coating, ΔT= 1400 K [17]. Due to the large CTE difference between coating and fiber, the thermally-induced strains are larger than the roughness-induced strains, but due to higher roughness in HI-Nicalon, the net strain in the composite is higher with HI-Nicalon fibers, Table 3.

The radial clamping stresses were also calculated using eqs. 2 and 3, using $E_{Nicalon}$=193 GPa, $E_{HI\text{-}Nicalon}$=269 GPa, $\nu_{Nicalon}=\nu_{HI\text{-}Nicalon}$=0.12, $E_m=E_{carbon}$=12 GPa (perpendicular to graphitic layers), and ν_{carbon} = 0.4 (perpendicular to graphitic layers), [17,18]. Notice that due solely to moduli differences in the fiber, the thermally-induced stresses are greater with Hi-Nicalon fibers, Table 3. Coupled with the higher roughness-induced stresses in the latter fiber, the net

Table 3. Roughness and thermally-induced strains and stresses in composites with Nicalon and HI-Nicalon fibers

	Nicalon	HI-Nicalon
Roughness-induced strain, R_{max}/r	**-0.0051**	**-0.0071**
Thermally-induced strain, $\Delta\alpha\Delta T$	-0.0341	-0.0341
Net radial strain	**-0.0392**	**-0.0412**
Roughness-induced stress, σ_{rough}, (MPa)	**-42.4**	**-59.9**
Thermally-induced stress, $\sigma_{thermal}$, (MPa)	-281	-284
Net radial normal stress, σ_N (MPa)	**-323**	**-344**

radial clamping stress will be about 20 MPa higher in a composite with Hi-Nicalon fibers. With both fibers, however, it is important to note that the net radial stress is quite high and compressive, so that a substantial clamping stress is applied to the fiber. Future studies will include the use of AFM to examine wear damage to the fibers during cyclic fatigue of ceramic matrix composites.

IV. Conclusions

Several conclusions can be drawn from the quantification of surface roughness of Nicalon and Hi-Nicalon ceramic fibers using atomic force microscopy:

- AFM is a simple and effective technique to measure surface roughness, if used carefully and consistently, with an uncertainty in measurements of 1 nm.
- Roughness profiles and analysis show that HI-Nicalon fibers have a higher roughness amplitude than Nicalon fibers. This difference may be attributed to differences in processing.
- Higher roughness in HI-Nicalon induces greater roughness-induced strains and stresses which contributes to even higher clamping stresses than are observed with Nicalon fibers.

V. References

1. Y. Mikata and M. Taya, Stress Field in a Coated Continuous Fiber Composite Subjected to Thermo-Mechanical Loadings, *J. Comp. Mater.* 19:554 (1985).

2. Z.R. Xu, K.K. Chawla, A. Neuman, A. Wolfenden, G.M. Liggett, and N. Chawla, Stiffness loss and density decrease due to thermal cycling in an alumina fiber/magnesium alloy composite, *Mater. Sci. & Eng.*. in press (1995).

3. R.W. Goettler and K.T. Faber, Interfacial shear stresses in SiC and alumina fiber reinforced glasses, *Comp. Sci. and Tech.* 37:129 (1989).

4. P.D. Jero and R.J. Kerans, The contribution of interfacial roughness to sliding friction of ceramic fibers in a glass matrix, *Scripta Met. et. Mater.* 24:2315 (1990).

5. P.D. Warren, T.J. Mackin, and A.G. Evans, Design, analysis and application of an improved push-through test for the measurement of interface properties in composites, *Acta. metall. mater.* 40:1243 (1992).

6. G. Binning, C.F. Quate, and Ch. Gerber, Atomic force microscope, *Phys. Rev. Lett.* 56:930 (1986).

7. T.R. Albrecth, M.M. Dovek, C.A. lang, L.P. Grutter, C.F. Quate, S.W.J. Kuan, C.W. Frank, and R.F.W. Pease, Imaging and modification of polymers by scanning tunneling microscopy and atomic force microscopy, *J. Appl. Phys.* 64:1178 (1988).

8. S. Alexander, L. Hellemans, O. Marti, J. Schneir, V. Elings, P.K. Hansma, M. Longmire, and J. Gurley, An atomic-resolution atomic-force microscope implemented using an optical lever, *J. Appl. Phys.* 65:164 (1989).

9. H.B. Butt, K.H. Downing, and P.K. Hansma, Imaging the membrane protein bacteriorhodopsin with the atomic force microscope, *J. Byophys. Soc.* 58:1473 (1990).

10. K.K. Chawla, Z.R. Xu, A. Hlinak, and Y.-W. Chung, *Surface roughness characterization of three alumina-type fibers by atomic force microscopy*, Proc. of Conf. on Advances in Ceramic Matrix Composites, Indianapolis, IN (April, 1993).

11. S. Yajima, K. Okamura, J. Hayashi, and F.E. Wawner, Synthesis of continuous SiC fiber with high tensile strength, *J. Am. Ceram. Soc.* 59:324 (1976).

12. T. Ishikawa, Silicon carbide continuous fiber (Nicalon), in *Silicon Carbide Ceramics - 2*, S. Somiya and Y. Inomata, eds., Elsevier Press, New Tork, p. 81 (1991).

13. E. Bischoff, M. Ruhle, O. Sbaizero, and A.G. Evans, Microstructural studies of the interface zone of a SiC-fiber-reinforced lithium aluminum silicate glass-ceramic, *J. Am. Ceram. Soc.* 72:741 (1989).

14. R.J. Kerans and T.A. Parthasarathy, Theoretical analysis of the fiber pullout and pushout tests, *J. Am. Ceram. Soc.* 74 :1585 (1991).

15. T.A. Parthasarathy, P.D. Jero, and R.J. Kerans, Extraction of interface properties from a fiber push-out test, *Scripta Met. et Mater.* 25:2457 (1991).

16. *Thermophysical properties of matter-Vol. 13*, Y.S. Toloukian and C.Y. Ho, eds., Plenum Press, New York p. 79 (1977).

17. S. Shanmugham, D.P. Stinton, F. Rebillat, A. Bleier, T.M. Besmann, E. Lara-Curzio, and P.K. Liaw, Oxidation-resistant interfacial coatings for continuous fiber ceramic composites, *Ceram. Eng. Sci. Proc.* in press (1995).

18. *Engineered Materials Handbook-Vol. 4*, ASM International, Materials Park, OH (1991).